AD NUMBER

AD404303

NEW LIMITATION CHANGE

TO

Approved for public release, distribution unlimited

FROM

Distribution authorized to U.S. Gov't. agencies and their contractors; Administrative/Operational Use; APR 1963. Other requests shall be referred to Office of Naval Research, Arlington, VA 22203-1995.

AUTHORITY

ONR ltr, 28 Jul 1973

SEL-63-019

Round-the-World High-Frequency Propagation

by
R. B. Fenwick

April 1963

Technical Report No. 71

Prepared under
Office of Naval Research Contract
Nonr-225(64), NR 008-003 and
Advanced Research Projects Agency ARPA Order 196-62

RADIOSCIENCE LABORATORY

STANFORD ELECTRONICS LABORATORIES

STANFORD UNIVERSITY · STANFORD, CALIFORNIA

SEL-63-019

ROUND-THE-WORLD HIGH-FREQUENCY PROPAGATION

by

R. B. Fenwick

April 1963

Technical Report No. 71

Prepared under
Office of Naval Research Contract
Nonr-225(64), Nr 088-003 and
Advanced Research Projects Agency ARPA Order 196-62

Radioscience Laboratory
Stanford Electronics Laboratories
Stanford University Stanford, California

ABSTRACT

Many features of round-the-world (RTW) high-frequency (hf) propagation have in the past defied explanation in terms of simple models consistent with known characteristics of the ionosphere. During 1961 and 1962, theoretical and experimental studies were carried out for the purpose of defining the mechanism of hf RTW propagation, and deriving prediction procedures for RTW signal characteristics. The theoretical work indicated that D-layer absorption, the global distribution of F2-layer critical frequencies, and the magnitude, location, and orientation of F2-layer gradients of horizontal electron density, or "tilts," should be of fundamental importance in determining such characteristics as maximum usable frequency (MUF), lowest usable frequency (LUF), absorption, and optimum azimuth. Extensive experimental measurements--with the transmitter and receiver at the same location--of the time variations of MUF, LUF, optimum azimuth, time delay, pulse dispersion, and other features of RTW signals, have generally confirmed the theoretical predictions, showing that the anomalous features of RTW propagation can be readily explained.

The experimental measurements showed that RTW pulse dispersion varies inversely with frequency, while minimum time delays vary directly with frequency, as was expected from theory. It was demonstrated that RTW propagation is not confined to the "twilight zone," as was previously widely believed, and that propagation orthogonally to this zone is frequently possible. All of the RTW propagation characteristics noted experimentally appear to be explainable and to be qualitatively predictable by use of world maps of f_oF2 and absorption, and by proper consideration of the effects of ionospheric tilts.

From comparison of the experimental data with the theoretical predictions, it is concluded that the dominant propagation mode is a low-angle earth-ionosphere-earth hop mode, primarily in the sunlit hemisphere, plus an ionosphere-ionosphere "tilt mode" in a portion of the dark hemisphere. The latter mode is possible when the transmission point is in the daylight hemisphere. The relative placement of the hop modes and tilt-supported modes appears determinable from world maps of f_oF2.

TABLE OF CONTENTS

Chapter		Page
I.	INTRODUCTION	1
II.	THEORY	3
	A. Factors Affecting RTW Propagation	3
	B. The Effects of Absorption on LUF and Optimum Azimuth	3
	C. The Effects of f_oF2 Variations on MUF and Optimum Azimuth	10
	D. The Effects of Ionospheric Tilts on MUF and LUF	15
	1. Qualitative Discussion	15
	2. Calculated Effects of Ionospheric Tilts from an Idealized Model	22
	E. Theoretical Time Delays and Pulse Dispersions	32
III.	EXPERIMENTAL ARRANGEMENTS AND OBJECTIVES	34
	A. Manual Experiments	34
	B. Automatic Experiments	36
IV.	EXPERIMENTAL RESULTS AND COMPARISON WITH PREDICTIONS	38
	A. The Observed Frequency of Occurrence of RTW Propagation	38
	B. The Variation of the Optimum Azimuth with Time and Frequency	43
	1. Winter Measurements	43
	2. Summer Measurements	45
	3. Spring Measurements	47
	4. An Explanation for Multiple Optimum Azimuths and "Echo of the Second Kind"	54
	5. Autumn Measurements	56
	C. The Propagating Frequency Range	58
	1. Experimental Results	58
	2. LUF and Path Loss Prediction	63
	3. MUF Prediction	72
	D. The Effects of Geomagnetic Storms	78
	E. Time delays and Pulse Dispersions	86
	F. Backscatter and Vertical-Incidence Measurements and Their Implications	92
V.	DISCUSSION AND CONCLUSIONS	96
	A. The Propagation Modes	96
	B. Implications for Long-Distance hf Paths	99
	C. Recommendations for Further Study	99
APPENDIX		
A.	METHOD FOR CALCULATING IONOSPHERIC TILT EFFECTS	101
REFERENCES		104

LIST OF ILLUSTRATIONS

Figure		Page
1.	Examples of minimum-absorption great-circle paths assuming that absorption is a function only of sun's zenith angle . .	4
2.	Geometry used in determination of the minimum-absorption great-circle path through point T	4
3.	Theoretical circular approximations to global constant-absorption curves	5
4.	Theoretical variation of RTW-signal optimum azimuth vs time, based on minimum absorption	7
5.	Theoretical attenuation of the minimum-absorption RTW path relative to absorption of path through subsolar point . . .	8
6.	Predicted RTW-signal D-layer attenuations for paths through twilight zone and subsolar point	9
7.	World map of f_oF2, with six great circles through Stanford	12
8.	Curves used in predicting optimum f_oF2 azimuth at Stanford, using three-point method	13
9.	Predicted optimum RTW azimuths for Stanford, from absorption and f_oF2 standpoints	14
10.	Examples of curves derived from world maps used to obtain predicted curves of Fig. 11	16
11.	Predicted curves of maximum RTW-signal frequency vs time, assuming 4000-km "hop" modes	17
12.	Ground and 300-km-height twilight lines for time of equinox ground sunrise at San Francisco	19
13.	Predicted twilight-line curves of $h_{max}F2$ and $h(f_c = 4.0$ Mc) derived from world maps for June, RASSN 50, 0400 GMT	20
14.	World map of f_oF2 at RASSN 50, June, 0400 GMT, showing twilight-line great circle	21
15.	Geometry used to determine the effects of ionospheric tilts on ray paths that do not miss the earth	23
16.	Geometry used to determine the effects of ionospheric tilts on ray paths that do miss the earth	24

LIST OF ILLUSTRATIONS (Cont)

Figure		Page
17.	Computed effects of ionospheric tilts from idealized model for various H and D_T	25
18.	Ray-path plots in a model ionosphere exhibiting a horizontal gradient of electron density	32
19.	Typical A-scope displays used during manual RTW-propagation experiments	35
20.	Times data were available (shaded) and when RTW propagation was observed (solid) at Stanford, 24 March - 21 May 1962	39
21.	Percent of records showing presence of RTW propagation vs time during automatic tests	42
22.	A-scope displays showing variation of RTW-signal propagation characteristics with time	44
23.	Predicted curves and experimental points for optimum RTW-propagation azimuth vs time for winter day	45
24.	Predicted curves and experimental points for optimum RTW-propagation azimuth vs time for summer night	46
25.	Intensity-modulated displays showing RTW signal strength vs azimuth at two frequencies, 28 April 1962, Stanford	48
26.	Intensity-modulated displays showing RTW signal strength vs azimuth at three frequencies, 28 April 1962, Stanford	49
27.	Step-frequency records showing RTW signal strength vs frequency and azimuth at Stanford	51
28.	Theoretical and experimental curves of RTW-signal optimum azimuth vs time	52
29.	Experimental average RTW-signal optimum azimuths vs time at Stanford	53
30.	Predicted three-point average f_oF2 vs azimuth at Stanford, April, RASSN 50, 0730 PST	53
31.	World map of f_oF2 with twilight-zone and subsolar-point great circles through Stanford	55
32.	Optimum RTW-signal azimuths observed in October 1961, with curves of theoretical minimum absorption azimuth and azimuth of constant f_oF2 contours at Stanford	57

LIST OF ILLUSTRATIONS (Cont)

Figure		Page
33.	Average maximum frequencies propagated around the world vs time for quiet days in 1961 at Stanford	59
34.	Average maximum and minimum frequencies propagated around the world vs time at Stanford	61
35.	Idealized and corrected curves of α/α_{ss} vs time for 7 April at 37°25' N latitude	67
36.	Curves of experimental and predicted LUF for RTW propagation vs time	69
37.	Daily experimental RTW-signal LUF measured in the period 24 March - 22 April 1962 at Stanford	70
38.	Experimental and predicted curves of RTW-signal average MUF vs time	73
39.	Predicted 4000-km MUF in two directions corresponding with experimental optimum-azimuth great circle vs time together with average experimental MUF's at Stanford	75
40.	World map of f_oF2 showing twilight line and observed optimum RTW path through Stanford	77
41.	Correlation of evening duration of RTW propagation with preceding 12-hr ΣK_p during period 14 April - 16 May 1962 at Stanford	79
42.	Correlation of evening LUF and MUF with magnetic activity, 24 March - 20 May 1962 at Stanford	80
43.	Correlation of evening RTW propagation MUF with K_p	81
44.	Correlation of evening RTW propagation LUF with K_p	82
45.	Correlation of morning and evening RTW-propagation MUF with K_p for July and August 1961, at Stanford	83
46.	Maximum observed frequencies propagating around the world vs date in the period May - September 1961	85
47.	Received, detected RTW pulses, log-amplitude vs time delay, for 1-msec transmitted pulses	87
48.	Minimum time delay and received-pulse width of RTW signals vs frequency	88

LIST OF ILLUSTRATIONS (Cont)

Figure		Page
49.	Apparent minimum-time-delay measurements vs frequency for RTW transmission, July - September 1961	89
50.	Apparent received-pulse widths vs frequency for 1-msec transmitted pulses after RTW propagation in the period July - September 1961	90
51.	Apparent time delay of maximum amplitude vs frequency for RTW pulses received in the period July - September 1961 . .	91
52.	A-scope display showing presence of RTW signal at 25.0 Mc .	93
53.	Curves of virtual height vs distance from Stanford, determined from ionograms on 15 June 1961	94
54.	Long-range backscatter observations made at times and in azimuths of RTW propagation	95
55.	Estimates of regions in which tilt modes were required at RTW-signal MUF for various times on paths through Stanford .	96
56.	Steps in derivation of ionospheric tilt plots	102

ACKNOWLEDGMENT

The suggestions of Prof. O. G. Villard, Jr. throughout the progress of the work were invaluable, and are gratefully acknowledged. Thanks also are due the staff of the Radioscience Laboratory for their continued helpfulness, and to my wife, Jan, for her unlimited patience.

I. INTRODUCTION

It has been known for many years that hf radio waves can often propagate around the world one or more times. The phenomenon was first reported by Quaeck [Refs. 1 and 2], and further investigations were reported by Eckersley [Ref. 3], Taylor and Young [Ref. 4], and Quaeck and Moegel [Ref. 5]. These early investigators found the time taken for signals to travel completely around the earth to be about 138 msec, and found that these so-called circulating signals were most likely to occur in the "twilight belt" around the earth.

Later work by Hess [Ref. 6] showed that successive earth circulations of round-the-world signals sometimes had attenuations of as little as 5 db per circulation. This finding was later substantiated by Luscombe [Ref. 7] and Isted [Ref. 8], who noted the existence of circulating signals at 37 Mc during a solar activity maximum. Hess [Ref. 6] further found that a pulse that had passed around the world as much as three or four times suffered very little distortion (no quantitative measure was given), apparently not exhibiting the multipath distortion that is well known for signals propagated by the usual ionosphere-ground hop modes. Isted [Ref. 8] found this same characteristic at 37 Mc, and hence concluded that the usual earth-ionosphere-earth hop modes were not involved. However, he also noted that the onset of the RTW, or "circulating," signal was coincident with the commencement of F2 backscatter (as observed in the vicinity of the transmitter) and that, when there was no F2 backscatter at 37 Mc, there was no RTW signal.

Extensive measurements of time delays between successive earth circulations were made by Hess [Ref. 6] during World War II. This work was motivated by the fact that the distance to a transmitter of unknown location can be measured by noting the difference in time delays between the "direct" (shorter path) and the "indirect" (longer path) signals. The accuracy of such a determination depends on knowledge of the effect of the ionosphere on these time delays.

In the work by Hess, it was suspected (and hoped) that the time delay was highly constant, 0.137788 sec, and independent of time of day, frequency, or season. It later appeared [Ref. 9] that this was not the

case. A range of time delays between 0.1376 and 0.1384 sec was determined in measurements at 20 Mc. Later measurements by de Voogt [Ref. 10] showed time intervals between 0.137 and 0.139 sec for an unspecified number of measurements in the 10- to 22-Mc range. More recently, Ortner [Ref. 11] has reported time-delay variations from 0.138 to 0.1395 sec on a trans-polar transmission path at 18 Mc.

Hess [Ref. 12] appears to have made the only measurements of doppler shift on RTW signals, finding shifts of 5 to 30 cps for paths passing through the auroral zones, and less than 5 cps for other paths. These measurements do not appear to have been made very frequently.

Bailey [Ref. 13] has pointed out that RTW propagation can also occur through the subsolar point region, as well as through the twilight region. He has referred to the twilight-zone RTW propagation as causing "echo of the first kind" and to the subsolar point propagation as causing "echo of the second kind." Such nomenclature arises from the fact that RTW propagation has been particularly troublesome to hf radiotelegraph circuits because of the relatively long time delay.

Although RTW propagation has thus been observed for many years, there does not appear to be general agreement concerning the modes of propagation; further, prediction procedures for the characteristics of RTW signals, such as attenuation, MUF, and so on, have not been available. This situation is likely due to the fact that major attention has been focused on time delay, while very little systematic experimental data regarding the frequency and azimuthal dependence of the characteristics of RTW signals have appeared.

It is the purpose of this report to present a theoretical discussion of RTW propagation, supported by experimental data such as frequency and azimuthal dependence. It appears that most of the features of RTW propagation can be predicted, and that the postulated propagation mechanisms can account for the observed characteristics of round-the-world hf propagation.

II. THEORY

A. FACTORS AFFECTING RTW PROPAGATION

From basic theory, it should be expected that the overall characteristics of hf RTW propagation will be most affected by three factors: 1) global distribution of nondeviative (D-layer) absorption, 2) global distribution of F2-layer critical frequencies, and 3) global distribution and orientation of effective F2 layer tilts. The effect of these factors on RTW propagation will be considered in the order mentioned.

B. THE EFFECTS OF ABSORPTION ON LUF AND OPTIMUM AZIMUTH

If the absorption due to the lower layers of the ionosphere is assumed to vary in a simple manner proportional to $(\cos \chi)^n$, where χ is the sun's zenith angle and n is determined from data [Ref. 14], and if magnetic-field effects are neglected (a reasonable assumption), the attenuation due to absorption of a high-frequency signal propagated around the world by successive great-circle earth-ionosphere-earth hops (as is normally presumed for shorter paths) would be expected to be minimum when the signal path "misses" the subsolar point by the greatest distance [Ref. 15].

Let us say, for illustration, that the sun stands above the equator as shown in Fig. 1. There exists only one path which virtually avoids absorption, and that is the path on the twilight line which, in this instance, passes through the poles.

Consider transmitting from point P somewhere on the sunlit hemisphere, as shown in Fig. 1. Minimum absorption occurs when the RTW path traverses as little of the densely absorbing region as possible. This is satisfied when the ray path is at right angles to the direction from the transmitter to the subsolar point, as shown. Figure 1 shows qualitatively that this conclusion is reasonable. Paths through points P and Q with azimuths other than those shown will enter circular regions of higher absorption (nearer the subsolar point) and will accordingly suffer greater attenuation.

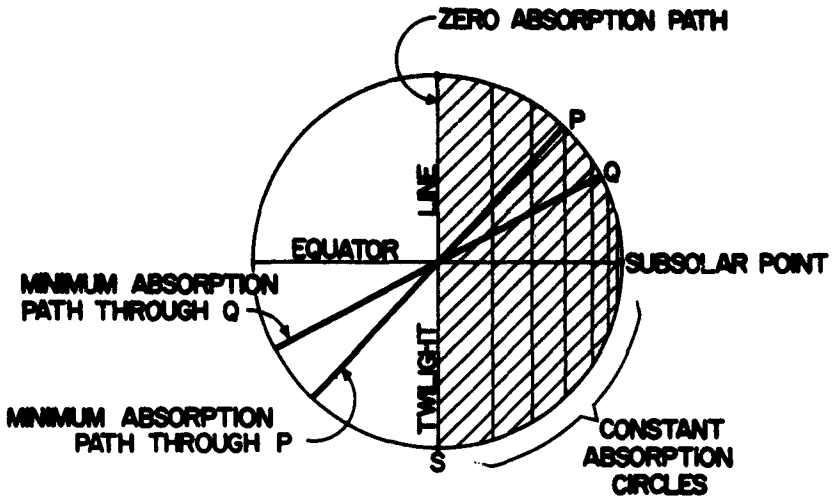

FIG. 1. EXAMPLES OF MINIMUM-ABSORPTION GREAT-CIRCLE PATHS ASSUMING THAT ABSORPTION IS A FUNCTION ONLY OF SUN'S ZENITH ANGLE.

A proof of this assertion is given in the following discussion, with reference to the coordinate system and designations in Figs. 2 and 3.

Let the subsolar point be at point SS, coordinates (R, θ, 0). Let point P(R, θ_2, $\pi/2$) be a point on the earth's surface, and in the yz plane, for which the sun's zenith angle χ_1 is desired. R is the earth's radius. Let point T be the transmission point and, for

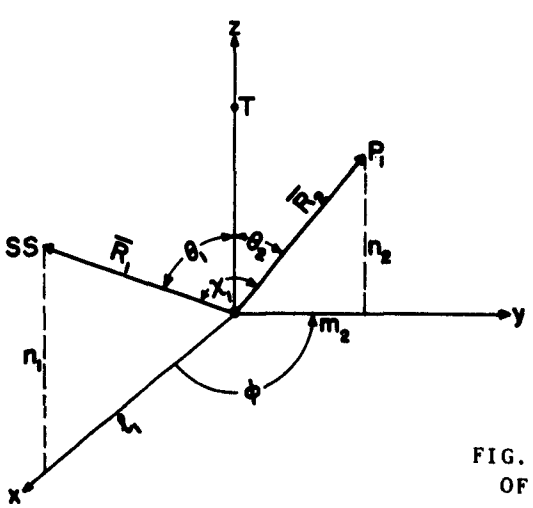

FIG. 2. GEOMETRY USED IN DETERMINATION OF THE MINIMUM-ABSORPTION GREAT-CIRCLE PATH THROUGH POINT T.

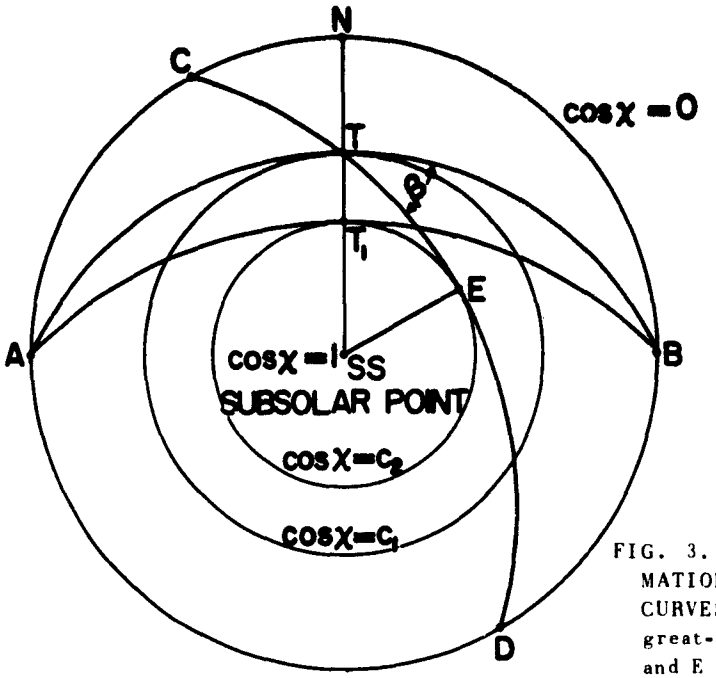

FIG. 3. THEORETICAL CIRCULAR APPROXIMATIONS TO GLOBAL CONSTANT-ABSORPTION CURVES. These determine minimum-absorption great-circle paths through T (ATB), T_1 (AT_1B), and E (CED).

simplicity, let R = 1. Then:

$$\bar{R}_1 \cdot \bar{R}_2 = l_1 l_2 + m_1 m_2 + n_1 n_2 = \cos \chi = n_1 n_2 = \cos \theta_1 \cos \theta_2 \qquad (1)$$

Hence, for any point P_1 on the great circle through T which is normal to the great circle through T and SS,

$$\cos \chi = \cos \theta_1 \cos \theta_2 \qquad (2)$$

Now, consider Fig. 3. The great circle through T for which the sun's zenith angle is described by Eq. (2) is ATB. If absorption along a path is given by:

$$\alpha = \alpha_o \int_{\text{path}} \cos \lambda \, ds \quad \cos \lambda \geq 0$$

then

$$\alpha_{ATB} = 2\alpha_o \int_0^{\pi/2} \cos \theta_1 \cos \theta_2 \, d\theta_2$$

$$\alpha_{ATB} = 2\alpha_o \cos \theta_1 \qquad (3)$$

Equation (3) shows that the total absorption of any path normal to line SS-N at T in Fig. 3 is proportional to $\cos \theta_1$, where θ_1 is the angle subtended at the center of the earth by SS and T. Hence, the absorption of path AT_1B is greater than the absorption of ATB.

Now consider a great-circle path CTD through T making some angle β with ATB. This path enters the circle $\cos \chi = c_1$ and is tangent to some other circle $\cos \chi = c_2$ at E. By symmetry, $\alpha_{CED} = \alpha_{AT_1B} > \alpha_{ATB}$, and the assertion is proved.

The azimuth normal to the direction of the subsolar point from a specified transmission point T is given by:

$$A = 90 - \cot^{-1} \left(\frac{\tan \delta \cos \phi}{\sin h} - \sin \phi \cot h \right) \qquad (4)$$

where A is the desired azimuth

δ is the sun's declination

ϕ is the latitude of the point T

h is the sun's hour angle relative to the point T

This azimuth is plotted in Fig. 4 for $\delta = \pm 23^\circ 26'$ and $\delta = 0^\circ$, for Stanford, California ($\phi = +37^\circ 25'$).

The curves of Fig. 4 would be expected to be an accurate estimate of the variation of optimum RTW-signal azimuth with local time, provided that:

1. D-layer absorption is important in RTW propagation,
2. The azimuth of highest mean F2-layer critical frequency does not vary in a greatly different manner with time than does the minimum-absorption azimuth, and
3. Transverse ionospheric layer tilts are not so great as to prevent propagation in these paths.

The absorption that will be experienced on this theoretical minimum-absorption path relative to that of the path through the subsolar point is given by

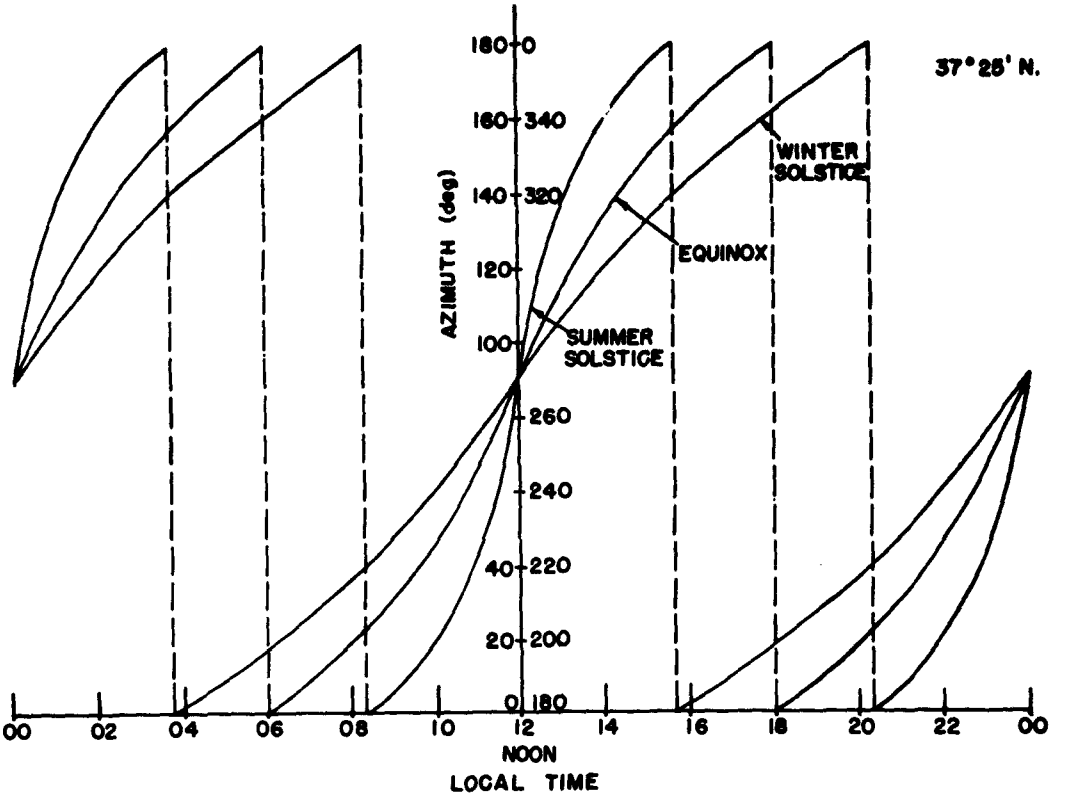

FIG. 4. THEORETICAL VARIATION OF RTW-SIGNAL OPTIMUM AZIMUTH VS TIME, BASED ON MINIMUM ABSORPTION.

$$\frac{\alpha}{\alpha_{ss}} = \cos\theta_1 = \cos\left\{2\tan^{-1}\left[\tan\frac{\phi-\zeta}{2}\;\frac{\sin\left[\tan^{-1}\left(\cot\frac{h}{2}\,\frac{\cos(\phi-\zeta)/2}{\sin(\phi+\zeta)/2}\right)\right]}{\sin\left[\tan^{-1}\left(\cot\frac{h}{2}\,\frac{\sin(\phi-\zeta)/2}{\cos(\phi+\zeta)/2}\right)\right]}\right]\right\} \qquad (5)$$

This function is plotted in Fig. 5 for $\zeta = \pm 23^{\circ}26'$ and $\zeta = 0^{\circ}$, for Stanford, California ($\phi = +37^{\circ}25'$). To the extent that D-layer absorption determines the field strength of RTW signals, and to the extent that the simplifying assumptions given at the beginning of this section are valid,

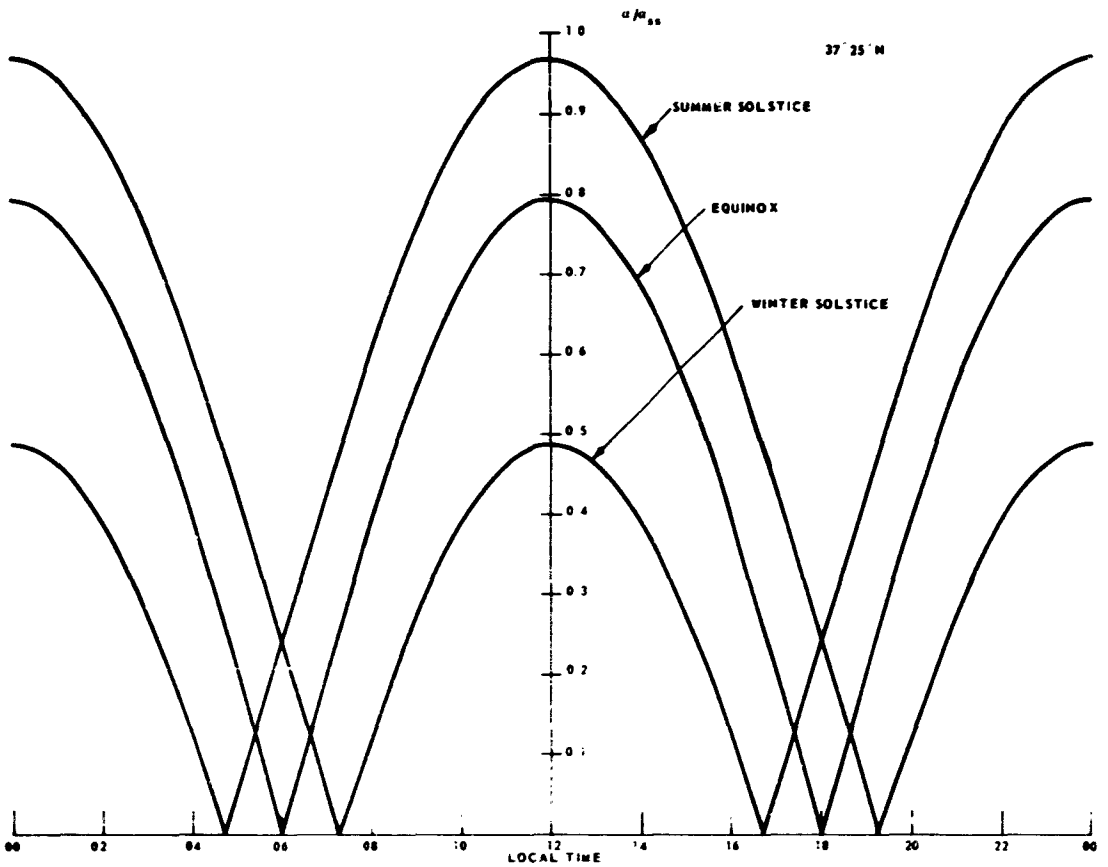

FIG. 5. THEORETICAL ATTENUATION OF THE MINIMUM-ABSORPTION RTW PATH RELATIVE TO ABSORPTION OF PATH THROUGH SUBSOLAR POINT.

these curves would be expected to give relative strength of RTW signals as a function of time of day and season.

Since actual D-layer ionization is never zero at sunrise or sunset, the absorption nulls shown in Fig. 5 actually cannot exist. An estimate of the depth of these absorption minima, α_{min}, may be made from consideration of the lower curves of Fig. 6, which show results of calculations of RTW absorption on certain north-south paths, based on empirical data [Ref. 14], for sunrise at times approximating equinox. To the extent that absorption along the twilight line does not vary seasonally, these curves may be expected to be applicable in months other than those shown.

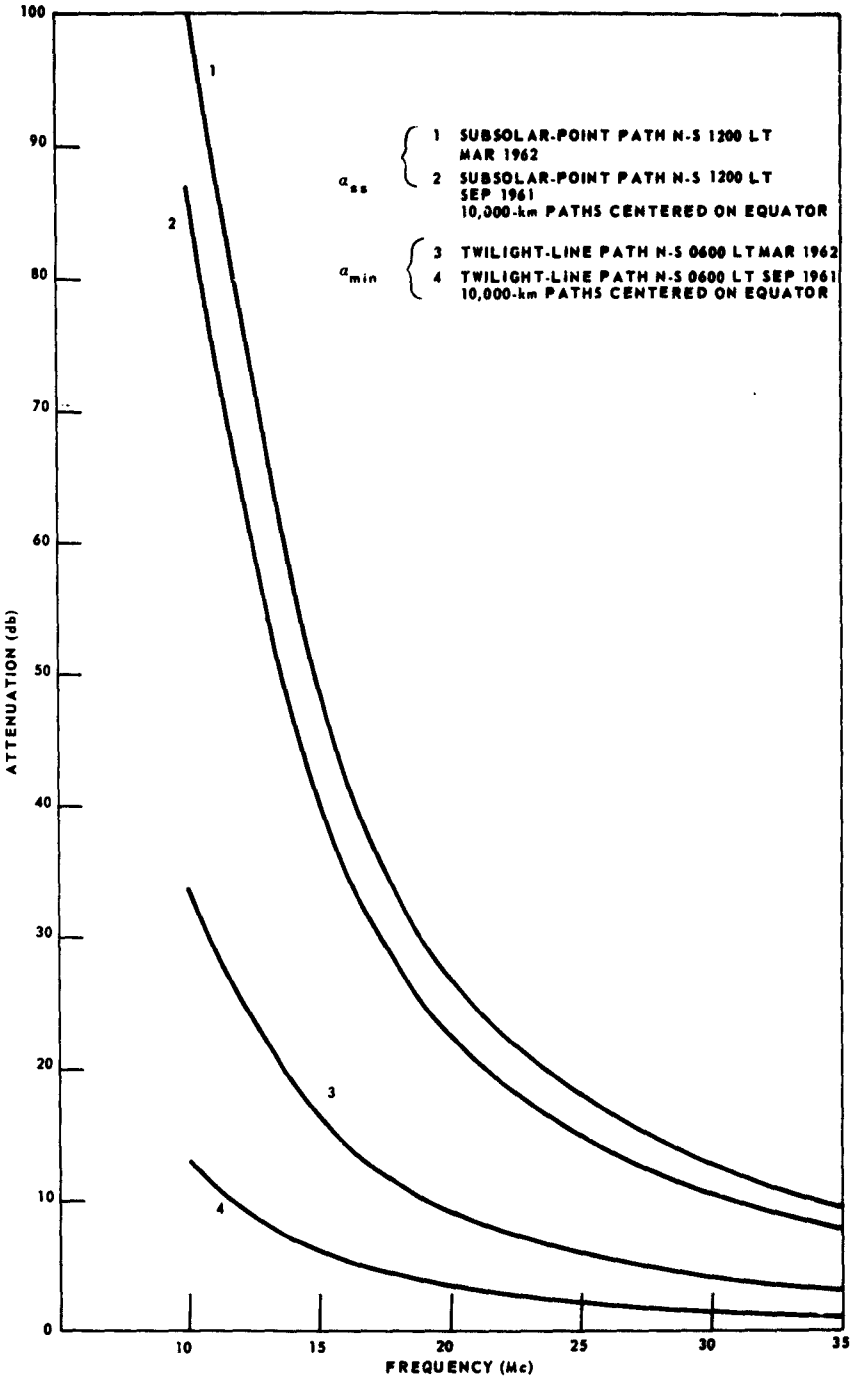

FIG. 6. PREDICTED RTW-SIGNAL D-LAYER ATTENUATIONS FOR PATHS THROUGH TWILIGHT ZONE AND SUBSOLAR POINT.

Curve 3 of Fig. 6 was calculated for the entire 40,000-km path along the twilight line for March 1962. Curve 4 was calculated for two 10,000-km paths (centered on the equator) along the twilight line for September 1961. (The year is an indication of sunspot number only.) The situation required for the validity of curve 3 would be earth-ionosphere-earth hop modes along the entire path. The situation required for the validity of curve 4 would be such modes over half of the path, assuming 10,000-km tilt modes (missing the D layer) centered on the poles (or, for other months, moved in accordance with the change in the sun's declination). The term "tilt mode" will be used throughout this report to mean an ionosphere-ionosphere hop mode, the launching of which is made possible by an appropriately oriented horizonal gradient of electron density in the ionosphere. A later section will discuss such modes in greater detail.

Curves 3 and 4 of Fig. 6 may be considered estimates of the upper and lower bounds of the minimum D-layer absorption which should be expected on RTW propagation. The attenuations shown for 1200 LT (curves 1 and 2) should provide a rough estimate of the scale factor appropriate for the curves of Fig. 5. (This is α_{ss} for vernal equinox.)

The fact that the second circulating signal has been occasionally noted by others to have as little as 5- to 10-db attenuation over the first circuit has been used as evidence that the dominant mode does not involve ionosphere-ground hops (which would presumably have high D-layer attenuation). The curves of Fig. 6, which are approximate at best, indicate that average total path attenuation due to absorption can, for instance, be less than 10 db at 20 Mc even if an ionosphere-ground hop mode is assumed for the entire 40,000-km path. Hence there does not appear to be adequate reason to conclude from past attenuation measurements that the ionosphere-ground hop mode is not significantly involved in normal RTW propagation.

C. THE EFFECT OF f_oF2 VARIATIONS ON MUF AND OPTIMUM AZIMUTH

Considering the magnitude of the RTW time delays, the observed radio frequencies, and many other characteristics, it is clear that the F2 layer of the ionosphere is very significantly involved in normal hf RTW propagation. The global distribution of F2-layer electron-density

profiles thus should be very important in determining the optimum azimuth as well as the MUF for RTW propagation.

If an average electron-density profile and its variation with time, N(h,t), were available for the ionosphere above any specified point on the earth's surface, it should be possible, with present computer ray-tracing techniques, to trace a ray entirely around the world, and the problem of RTW propagation modes would be solved. Not having such detailed information concerning the structure of the ionosphere, it is still possible to gain much insight into the effect of N(h) variations through usage of world maps of f_oF2 [Refs. 16, 17].

The map for 2200 GMT, December, RASSN 50 (running average sunspot number) is shown in Fig. 7. On this map are shown various great-circle paths through the point 37° N latitude, 120° W longitude. It is quite obvious that some paths have a greater average f_oF2 than others (paths having azimuths between 67 1/2° and 112 1/2° appear particularly favorable), but it is not clear what would be the most satisfactory practical way to select the "best" path for RTW propagation. Although much more sophisticated techniques could be, and have been, used, it has been found convenient and interesting to determine an optimum azimuth from a simple average of three points on each great-circle path.

Specifically, the minimum f_oF2 between 90° S and 30° S latitude, the minimum between 30° S and 30° N latitude, and the minimum between 30° N and 90° N latitude have been averaged and plotted as a function of azimuth (with respect to an assumed common transmitting/receiving point). An example of such a plot is shown in Fig. 8 for the map of Fig. 7. A smooth curve is then drawn between the points, the maximum of which is designated the "optimum" azimuth. In this case this azimuth is 103°.

It sometimes occurs, particularly at sunrise and sunset times at equinox, as will be seen later, that there is more than one maximum in a curve of average f_oF2 vs azimuth as determined by the three-point method. Also, there are times when the three-point average f_oF2 varies insignificantly between all possible great-circle paths. At these times, it may be concluded that other factors, specifically the existence and orientation of ionospheric tilts and the variations of absorption between paths, will determine the optimum azimuth(s) for RTW propagation.

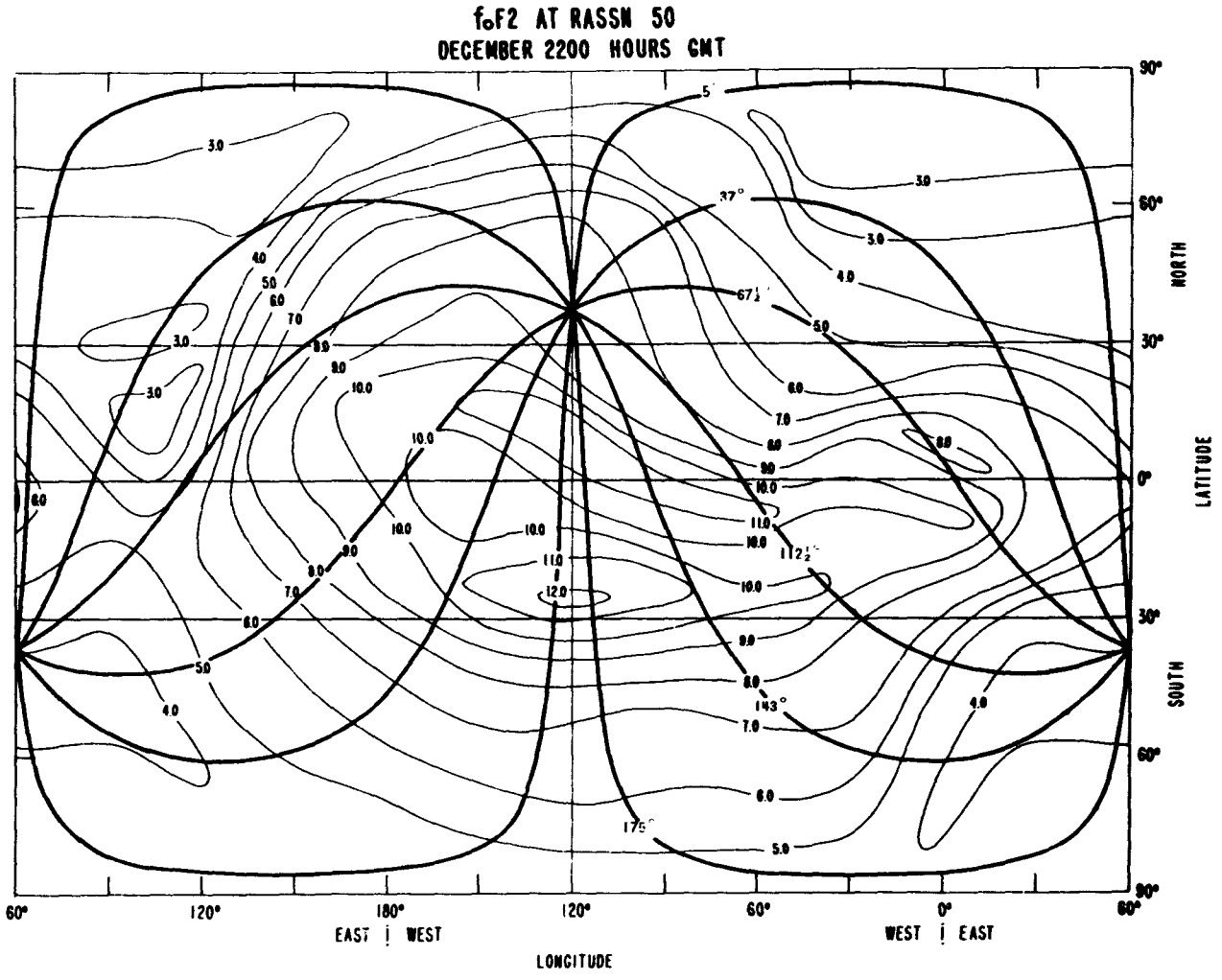

FIG. 7. WORLD MAP OF f_0F2, WITH SIX GREAT CIRCLES THROUGH STANFORD.
(2200 GMT, December, RASSN 50)

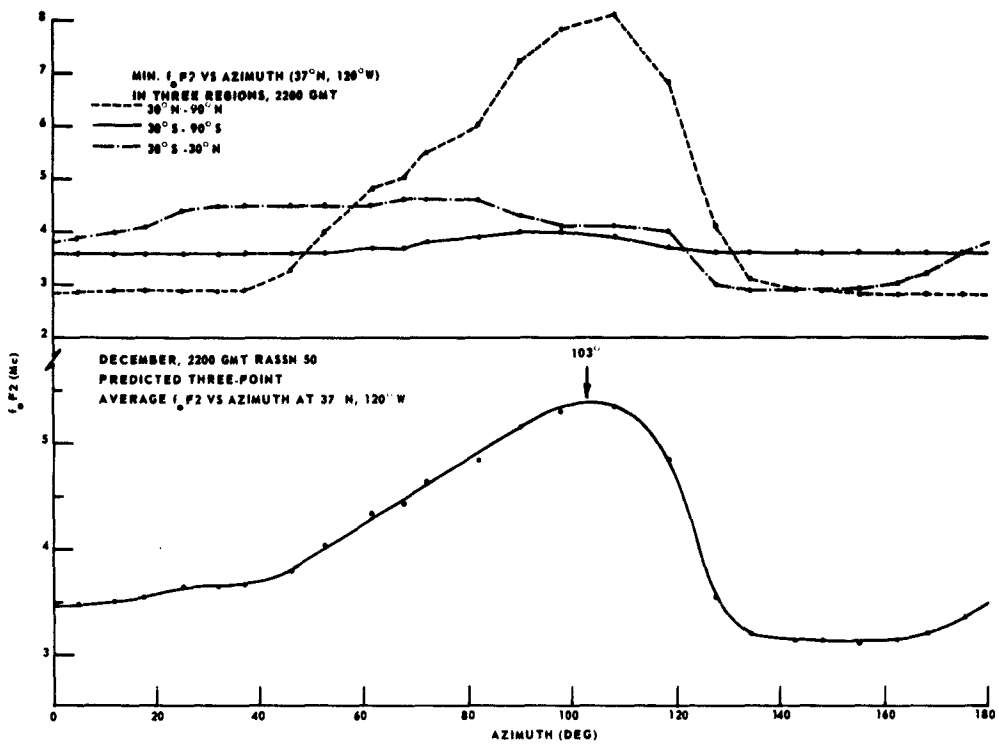

FIG. 8. CURVES USED IN PREDICTING OPTIMUM f_0F2 AZIMUTH AT STANFORD USING THREE-POINT METHOD. (2200 GMT, December, RASSN 50)

Aside from its simplicity, the three-point method described was chosen since it would normally take into account, separately, the three regions where the critical frequencies will be lowest: the regions near the poles, and the mid-latitude predawn region. In Fig. 9 is shown a typical plot of optimum azimuth vs local time obtained by the method described. Also shown is the theoretical minimum-absorption azimuth from Eq. (4). Note the good agreement between the curves for summer night, but the very poor agreement for summer day at the assumed point of transmission (37° N, 120° W). The poor agreement in summer day is due to the fact that the region of the antipodal point is in winter night. The very low critical frequencies associated with this region result in the optimum mean f_0F2 azimuth being nearly $90^\circ/270^\circ$ for the

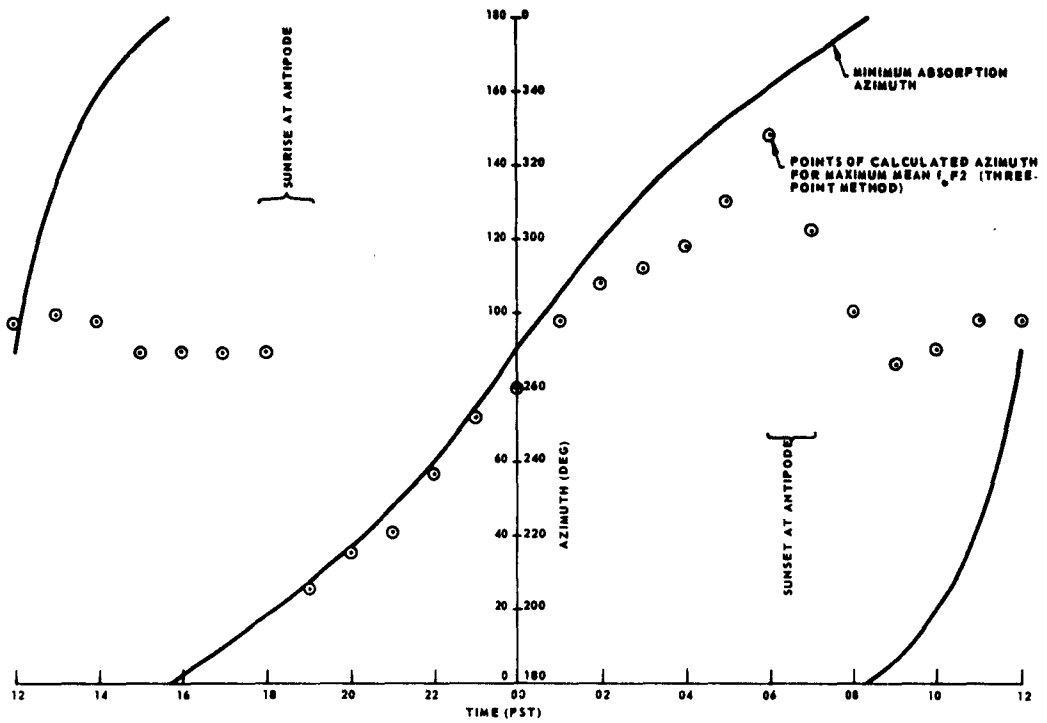

FIG. 9. PREDICTED OPTIMUM RTW AZIMUTHS FOR STANFORD, FROM ABSORPTION AND f_0F2 STANDPOINTS. (June, RASSN 50)

entire day period. This path, incidentally, maintains the shortest distance from the equator and consequently the greatest distance from the poles.

It should immediately be expected that the optimum azimuth for RTW propagation in summer day (and possibly equinox day) might deviate very markedly from the minimum-absorption azimuth, since, as the transmission point nears the subsolar point, the absorption is high no matter what the direction of transmission, as seen in Fig. 5. The December curve of optimum azimuth as determined from Fig. 7 and curves such as those shown in Fig. 8, will be shown later when experimental data are being considered.

Another technique that has been used to determine predicted RTW optimum azimuths and MUF's as a function of time has involved use of world maps of 4000-km MUF factor as well as the f_oF2. These quantities and their product were plotted every 1000 km for a given RTW great-circle path. Examples of such plots are shown in Fig. 10 for 0400 GMT, June, 24° azimuth from 37° N, 120° W, RASSN 50.

The level of the lowest 4000-km line was chosen as the predicted MUF (with the a priori assumption of earth-ionosphere-earth hop modes over the entire 40,000-km path), and the azimuth producing the highest MUF was selected as the "optimum" azimuth. Of course, analogous to the procedure using three points, the average of the curves for each azimuth could be calculated, and the azimuth giving the greatest average could be chosen as a theoretical optimum azimuth. Examples of predicted MUF vs time and azimuth, obtained from curves such as those in Fig. 10, are shown in Fig. 11. It is significant that the results obtained by these methods are normally quite close to those given by the three-point method.

The methods just described are extremely laborious if done by hand, and would be best done by a computer in which is "stored" the world maps. It will be shown later that such calculations actually produce results useful in the prediction of RTW propagation conditions.

D. THE EFFECTS OF IONOSPHERIC TILTS ON MUF AND LUF

1. Qualitative Discussion

In any situation where there are horizontal variations of ionospheric electron density, with or without accompanying changes in the height of maximum ion density, a layer "tilt" may be said to exist [Ref. 18].

Since the very beginning of theoretical studies of RTW propagation it has been found necessary to invoke such tilted ionospheric layers to explain various features of the phenomena. If tilts existed of proper orientation, and the ionosphere were sufficiently smooth along the remainder of the path, it would be possible to launch a wave into the ionosphere which would not touch the earth until its return to the receiving point. This type of mode could conceivably explain features of RTW

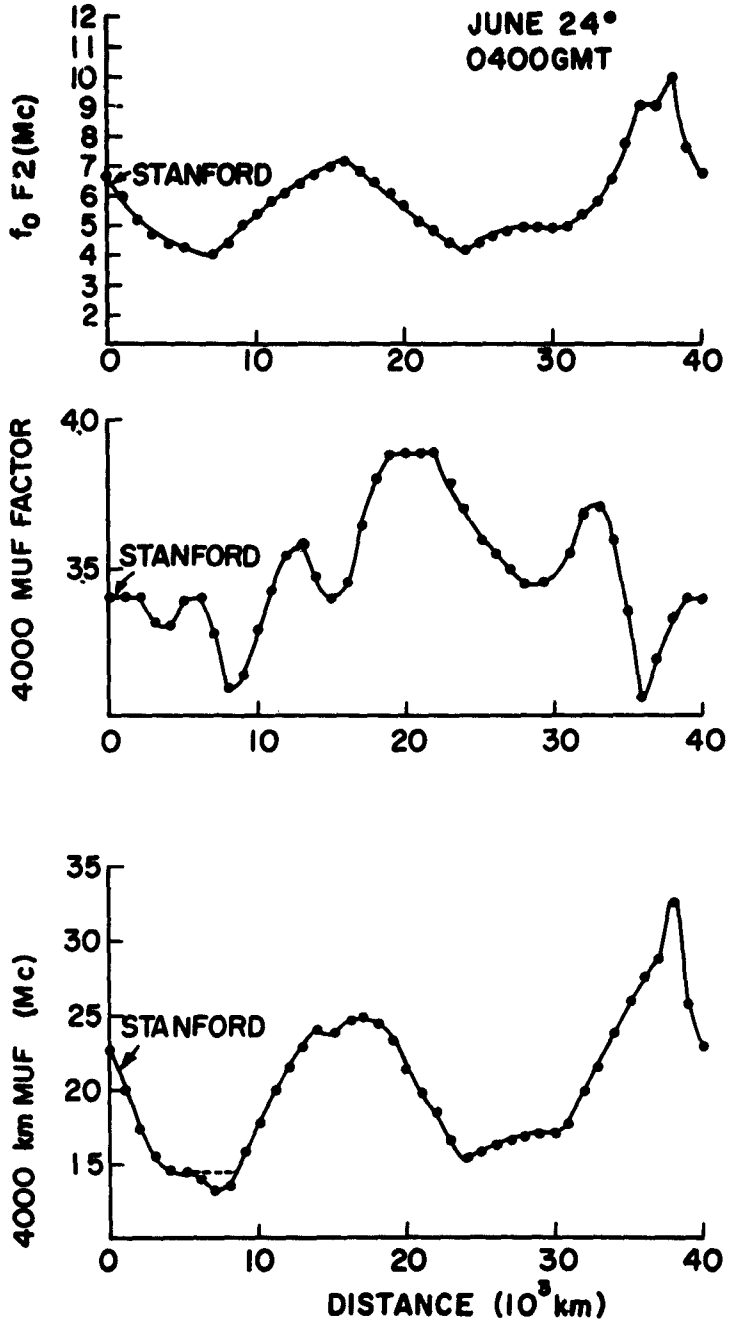

FIG. 10. EXAMPLES OF CURVES DERIVED FROM WORLD MAPS USED TO OBTAIN PREDICTED CURVES OF FIG. 11.

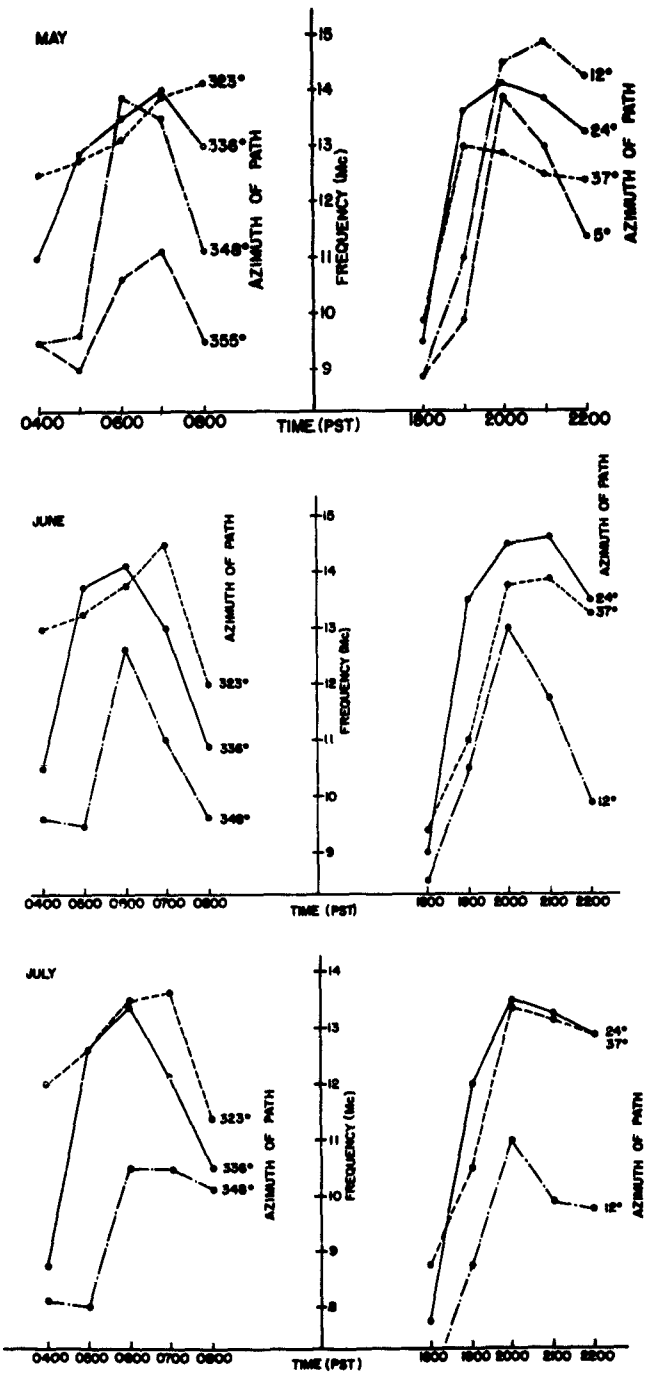

FIG. 11. PREDICTED CURVES OF MAXIMUM RTW-SIGNAL FREQUENCY VS TIME, ASSUMING 4000-km "HOP" MODES. Curves are for May, June, and July, RASSN 50 at Stanford.

propagation such as low attenuation between circulations, the lack of apparent pulse dispersion, apparently constant time delays, and so on.

Unfortunately, such a theory requires characteristics of the ionosphere not known to normally exist (from a great number of observations by other means), and cannot explain why the RTW signal can normally be heard at many points along the path. One theory, the "sliding-wave theory" [Ref. 6] can explain this, but still requires features of the ionosphere that have not been confirmed by other methods. In particular, a constant downward radiation from a "sliding wave" along an ionospheric "limit layer" is needed. The downward radiation presumably would arise from scattering from ionospheric irregularities.

Fundamentally, systematic ionospheric tilts are normally caused by either nonuniform ionizing radiation or magnetic field effects, or both. Neglecting for the moment magnetic field effects, and assuming short time constants in the ionizing and deionizing processes, one would expect the greatest F2-layer electron density (N_{max}) to be above the subsolar point, decreasing uniformly in all directions from this point, as described by the Chapman theory [Ref. 14]. The height of the maximum of the F2 layer (h_{max}) would rise as the distance from the subsolar point is increased.

The above discussion implies that great-circle paths through the subsolar-point region might be expected to encounter predominantly longitudinal layer tilts which could, for instance, cause "tilt modes" [Ref. 18] through the dark hemisphere, allowing higher frequencies to be transmitted through this hemisphere than would normally be thought possible considering the critical frequencies present. (It will be shown later that this phenomenon apparently occurs.)

A continuation of this reasoning, however, leads to the conclusion that only transverse layer tilts should be encountered by a ray path oriented along the twilight line, which is in the region where most RTW propagation has been observed. A study of world maps of f_oF2 immediately shows this not to be the case, as would be expected since the behavior of the F2 layer is most decidedly different from the theoretical Chapman layer [Ref. 14]. Further, the assumptions of short time constants and the neglected magnetic field are very poor indeed.

Finally, there is a very significant difference in location between the ground twilight line and the F2-layer twilight line: the F2-layer twilight line projected to the earth's surface does not even correspond to a great circle, as is seen in the example of Fig. 12.

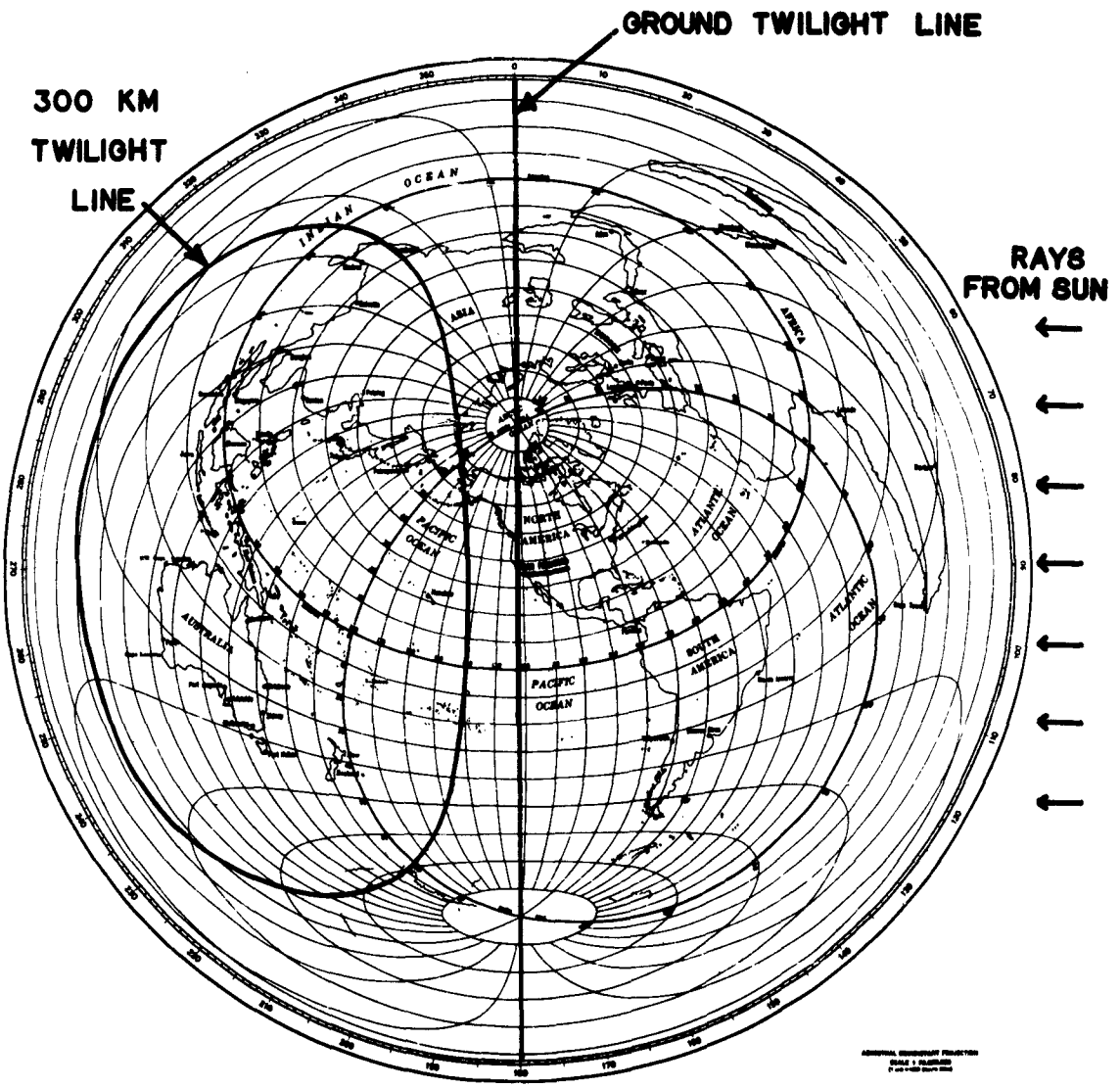

FIG. 12. GROUND AND 300-km-HEIGHT TWILIGHT LINES FOR TIME OF EQUINOX GROUND SUNRISE AT SAN FRANCISCO.

The examples of Fig. 13 well illustrate the nonuniformity of the F2 layer along the ground twilight line both in h_{max} and in the height of a constant electron density. Figure 13a shows $h_{max}F2$ along the twilight line for June, 0400 GMT, RASSN 50, as determined from world maps of f_oF2 and 4000-km MUF factor. Figure 13b shows the height of

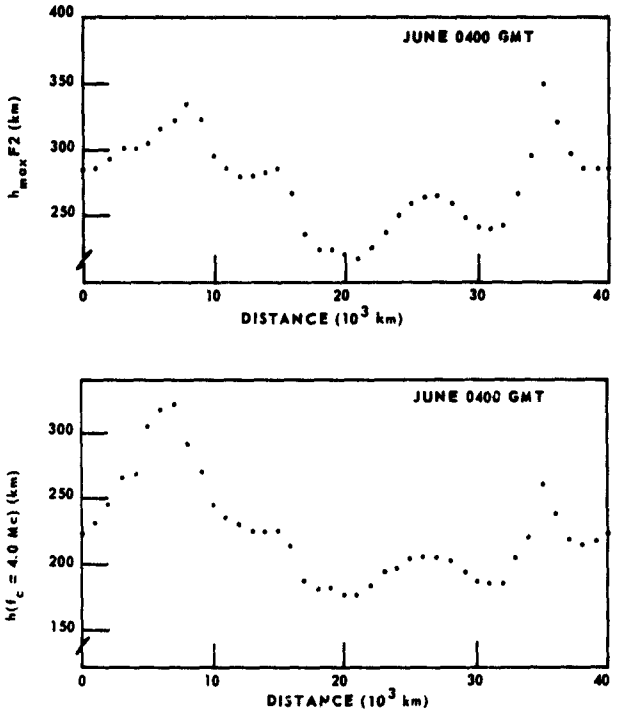

FIG. 13. PREDICTED TWILIGHT-LINE CURVES OF $h_{max}F2$ AND $h(f_c = 4.0$ Mc) DERIVED FROM WORLD MAPS FOR JUNE, RASSN 50, 0400 GMT. A parabolic layer was assumed.

a constant electron-density contour (corresponding to $f_c = 4.0$ Mc) along the twilight line, as determined from the world maps. For these determinations a parabolic F2 layer was assumed, with $y_m/h_o = 0.4$, where y_m is the layer semithickness and h_o is the minimum height of the layer.

The world map of f_oF2 for 0400 GMT, June, RASSN 50, is shown in Fig. 14, together with the twilight-line great circle. It is clear that this great circle by no means corresponds to a constant f_oF2 contour, and indeed, in some areas it is actually orthogonal to these contours.

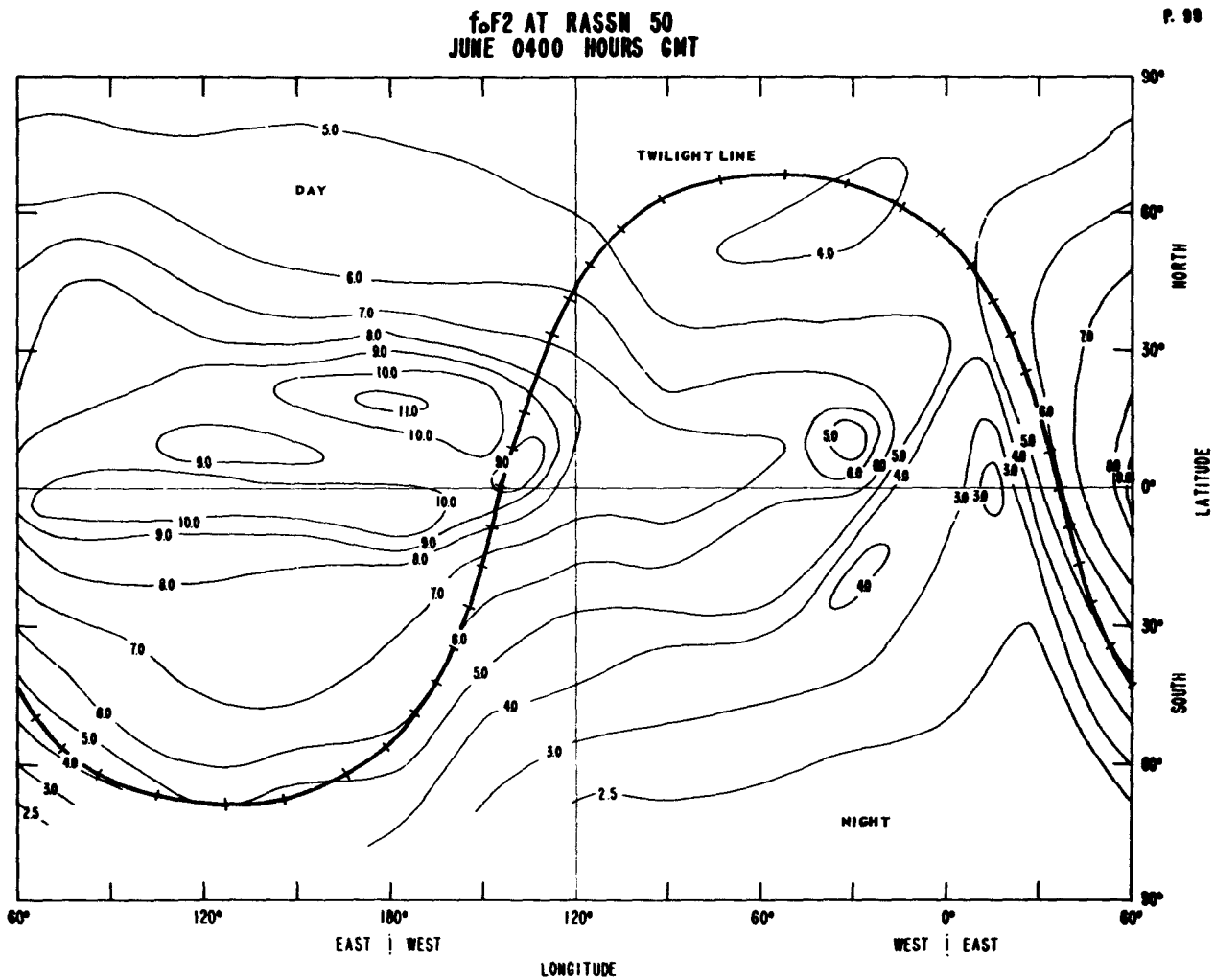

FIG. 14. WORLD MAP OF f_oF2 AT RASSN 50, JUNE, 0400 GMT, SHOWING TWILIGHT-LINE GREAT CIRCLE.

2. Calculated Effects of Ionosphere Tilts from an Idealized Model

It is possible to gain insight into the role of effective ionospheric tilts in determining the ray-path geometry in RTW propagation through use of the simple geometric model shown in Fig. 15. A ray from the transmitter is presumed to be effectively reflected from a mirror at height H, with a tilt angle ϕ and tilt azimuth θ, as shown. If the resultant reflected ray intersects the earth's surface, the point of intersection has coordinates L (the distance from the great circle defined by the ray from the transmitter to the mirror reflection point) and D (the distance from the point on the earth's surface under the mirror reflection point). If the resultant reflected ray misses the earth's surface, as shown in Fig. 16, a miss distance M and path deviation L are defined.

Given the distance from the transmitter to the point on the earth's surface under the mirror reflection point D_T, and given H, it is then possible to calculate D, L, and M as functions of ϕ and θ. This has been derived by T. Croft [Ref. 19], at the suggestion of the author, and the results of six such calculations (for D_T = 1500 and 1750 km and for H = 250, 300 and 350 km) are shown in Figs. 17a through 17f. A description of the derivation and the computer program used to determine the curves of Figs. 17d, e, and f are given in the appendix.

Assuming that a maximum effective ionospheric tilt which may be expected to be encountered normally is on the order of 2 deg [Ref. 18], it is interesting to determine the effect of such a tilt on rays incident from several different aspect angles. Consider Fig. 17b, where H = 300 km and the path length for a nontilted mirror reflection surface is 3000 km (i.e., $2D_T$). Assume ϕ = 2 deg; then,

1. For θ = 0 deg, a purely longitudinal "forward" tilt, the resultant ray path misses the earth (M) by 109 km and is undeviated laterally (L = 0);

2. For θ = 90 deg, a purely transverse tilt, D = 1517 km and L = 33.5 km. Hence the point of intersection of the ray with the earth is 33.5 km off the great-circle path defined by θ, ϕ = 0;

3. For θ = 180 deg, a longitudinal "backward" tilt, D = 922 km and L = 0.

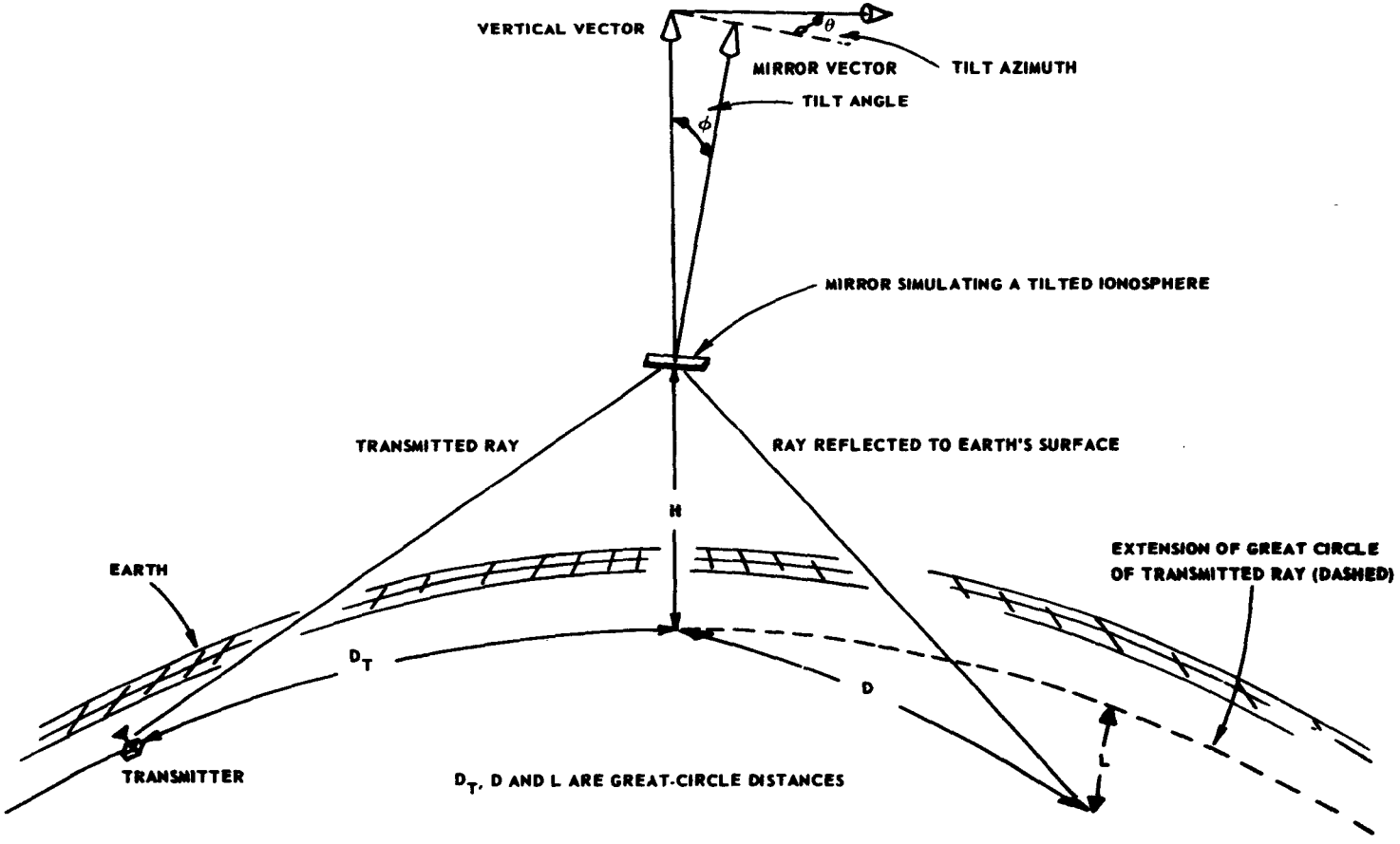

FIG. 15. GEOMETRY USED TO DETERMINE THE EFFECTS OF IONOSPHERIC TILTS ON RAY PATHS THAT DO NOT MISS THE EARTH.

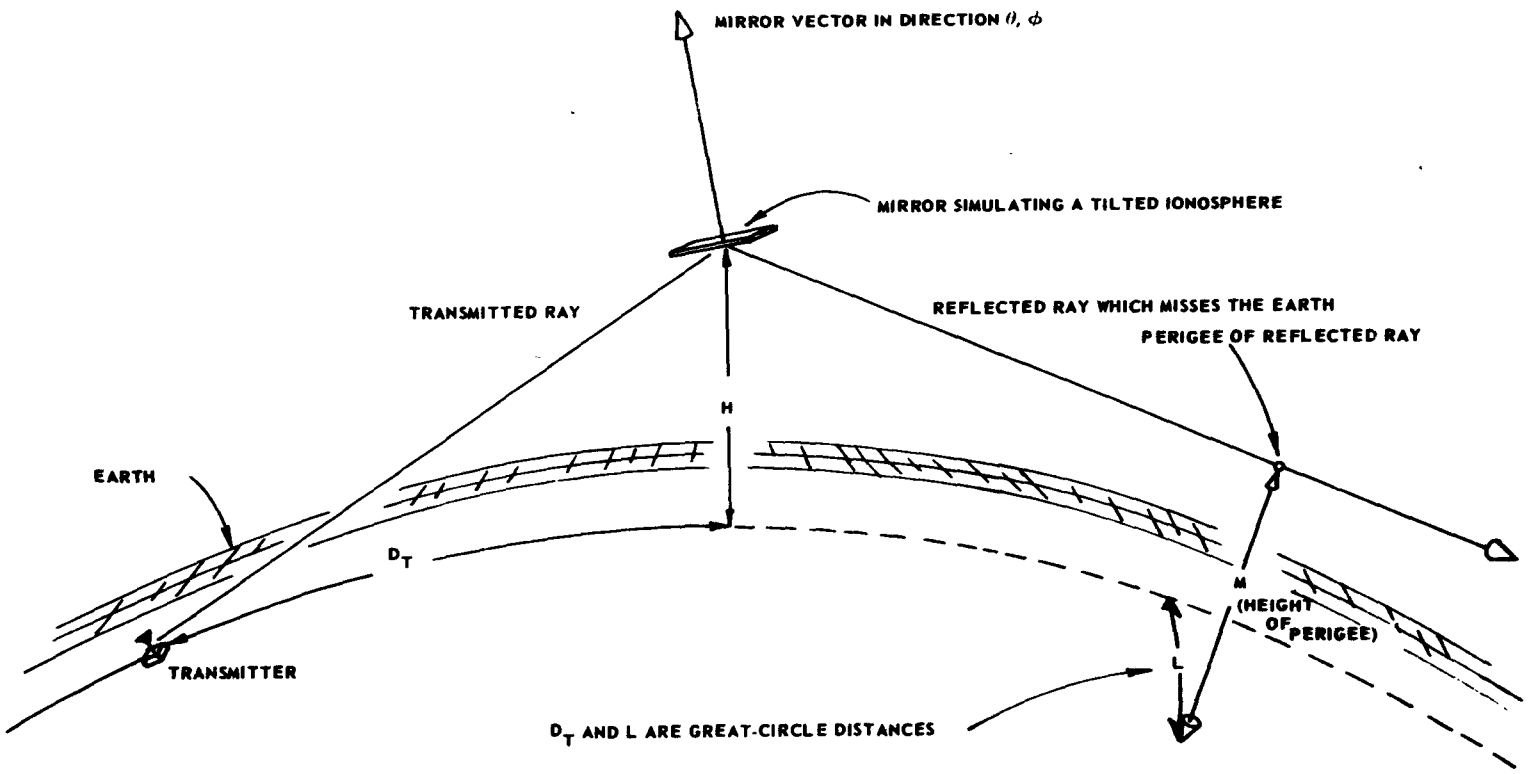

FIG. 16. GEOMETRY USED TO DETERMINE THE EFFECTS OF IONOSPHERIC TILTS ON RAY PATHS THAT DO MISS THE EARTH.

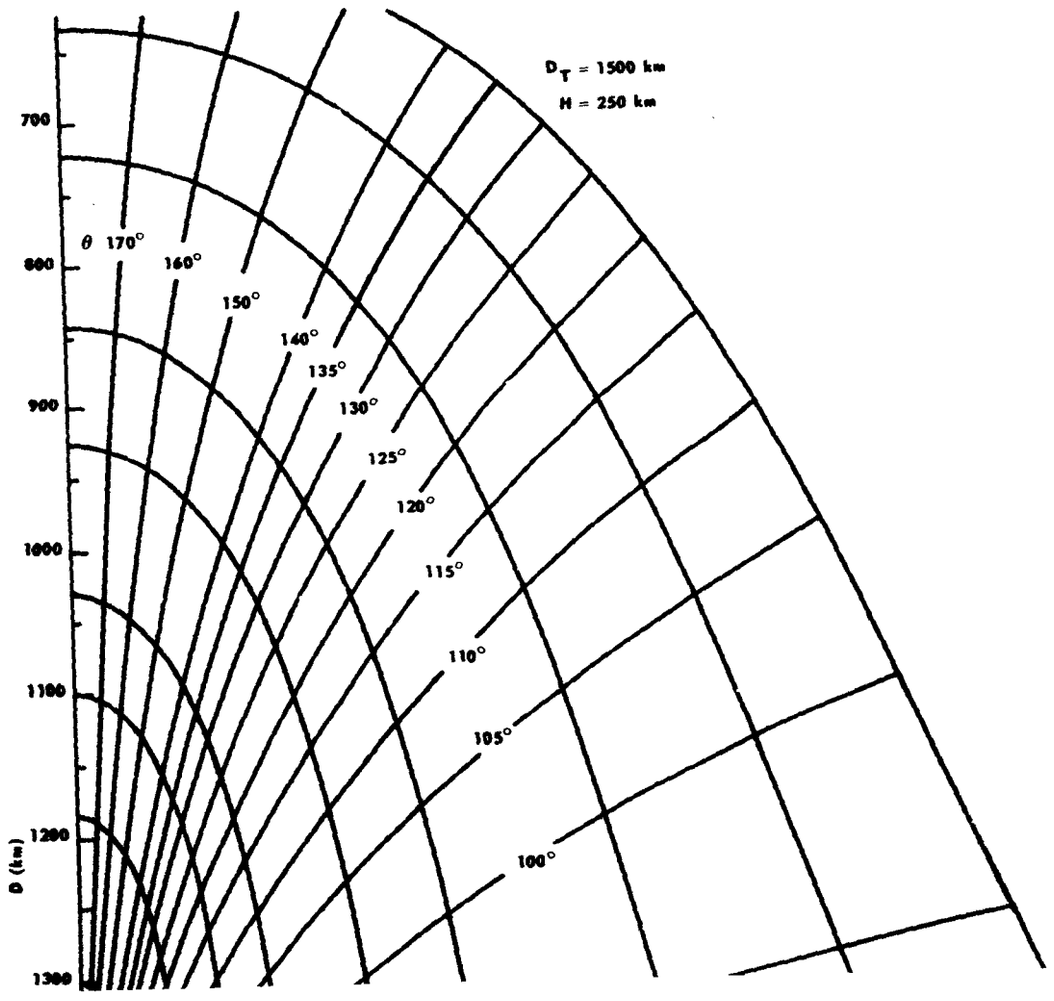
D_T = 1500 km
H = 250 km
θ 170°
160°
150°
140°
135°
130°
125°
120°
115°
110°
105°
100°
700
800
900
1000
1100
1200
1300
D (km)

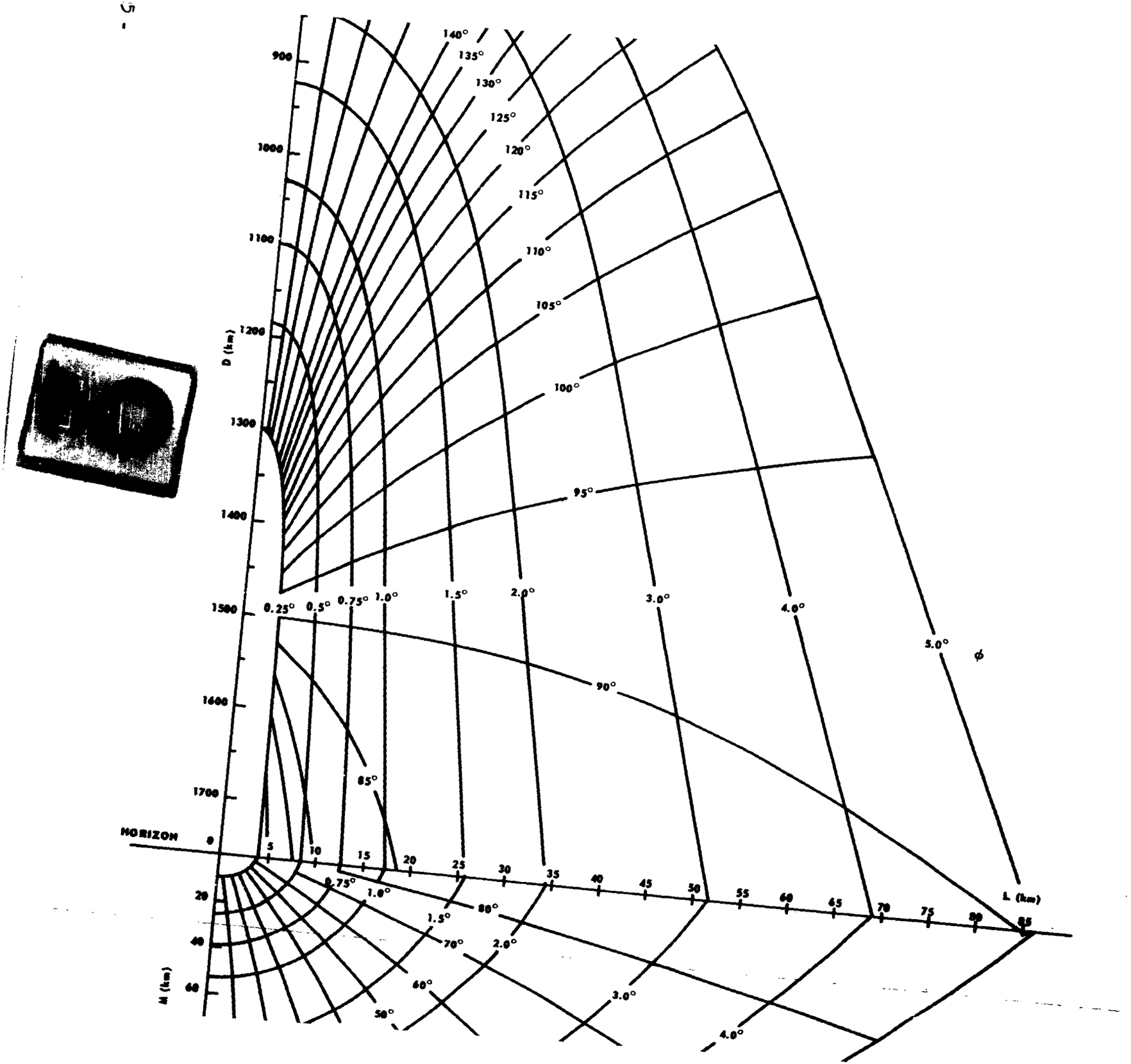
D (km)
900
1000
1100
1200
1300
1400
1500
1600
1700
140°
135°
130°
125°
120°
115°
110°
105°
100°
95°
90°
85°
0.25°
0.5°
0.75°
1.0°
1.5°
2.0°
3.0°
4.0°
5.0°
φ
HORIZON
0
5
10
15
20
25
30
35
40
45
50
55
60
65
70
75
80
85
L (km)
0.75°
1.0°
1.5°
80°
70°
2.0°
60°
3.0°
50°
4.0°
M (km)
20
40
60

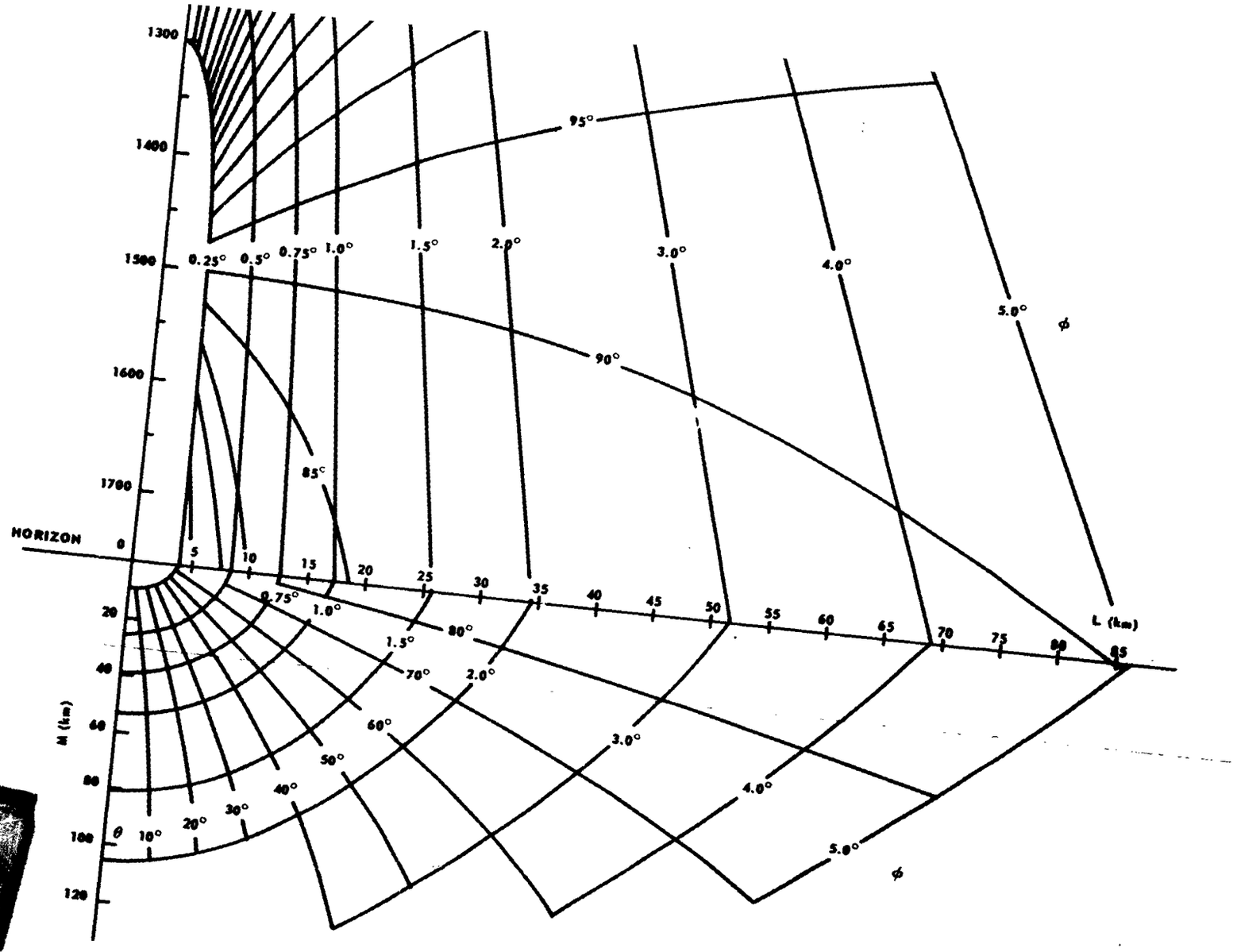

a. H = 250 km, D_T = 1500 km.

FIG. 17. COMPUTED EFFECTS OF IONOSPHERIC TILTS FROM IDEALIZED MODEL FOR VARIOUS H AND D_T.
Parts a. through f. are on pages 25 through 30.

SEL-63-019

SEL-63-019

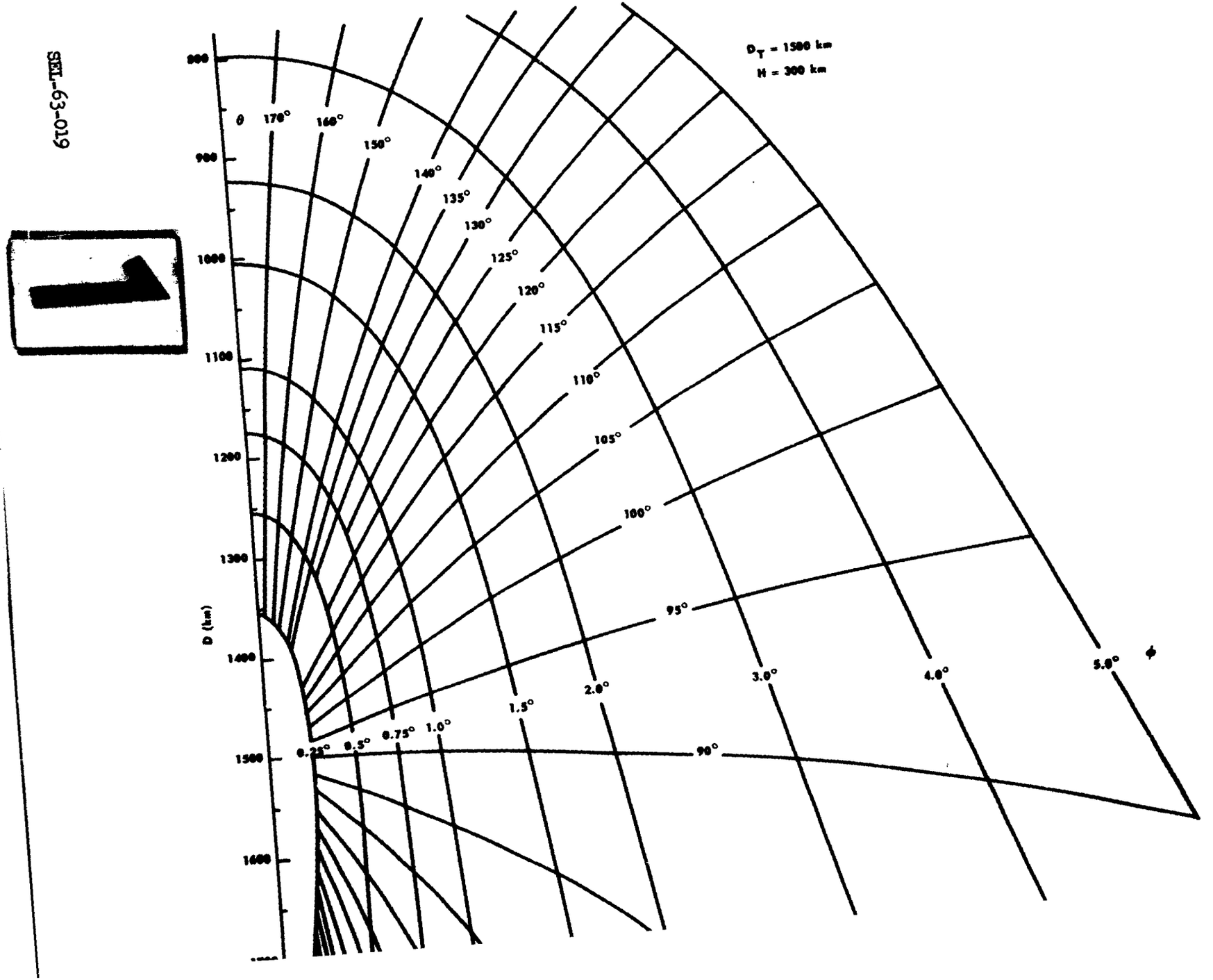
D_T = 1500 km
H = 300 km
θ
170°
160°
150°
140°
135°
130°
125°
120°
115°
110°
105°
100°
95°
90°
0.25°
0.5°
0.75°
1.0°
1.5°
2.0°
3.0°
4.0°
5.0°
φ
D (km)
900
1000
1100
1200
1300
1400
1500
1600

HORIZON
D (ft)
R (ft)
L (ft)
105°
100°
95°
90°
85°
80°
75°
70°
5.0°
4.0°
3.0°
2.5°
2.0°
1.5°
1.0°
0.75°
0.5°
0.25°

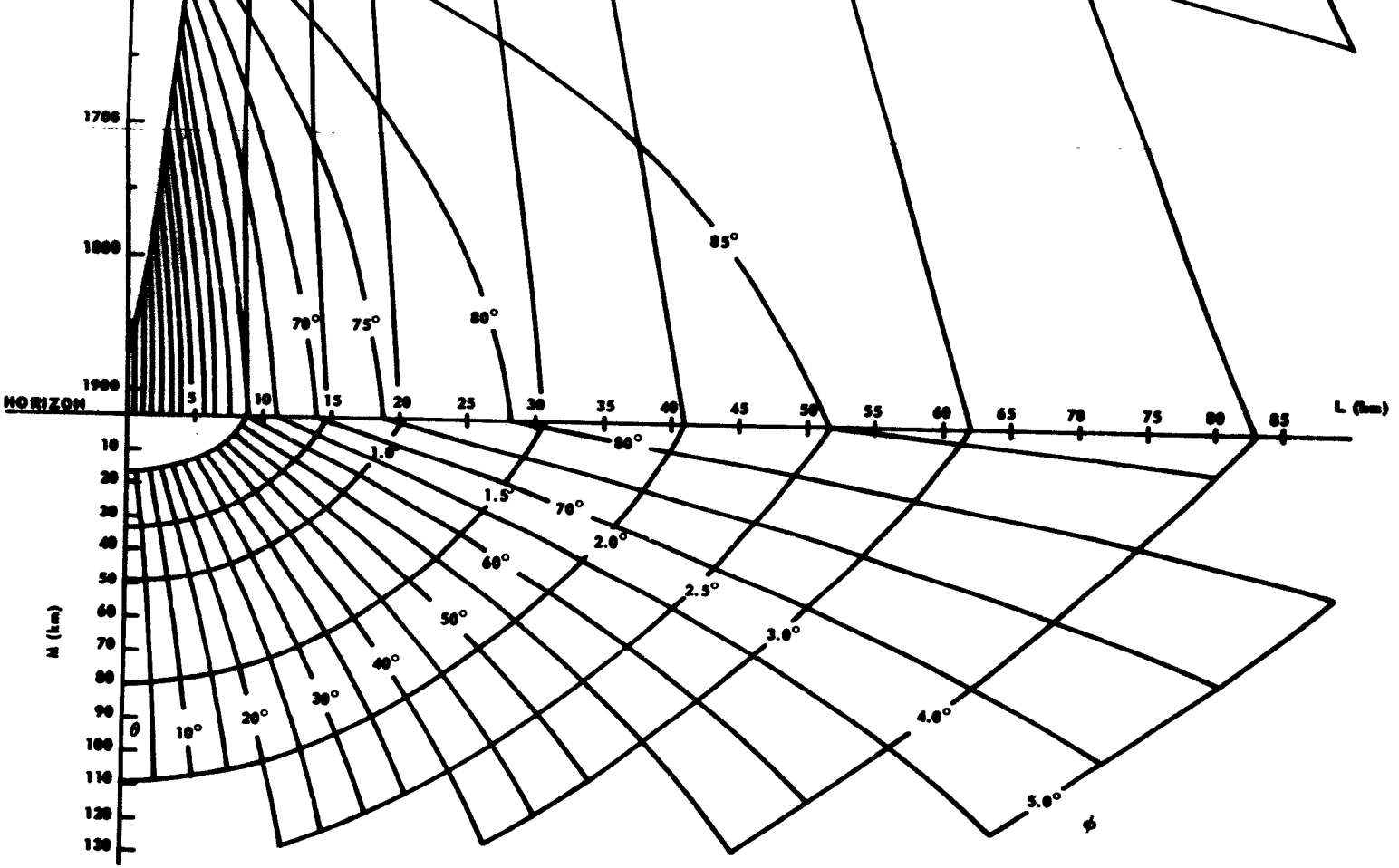

FIG. 17b. H = 300 km, D_T = 1500 km.

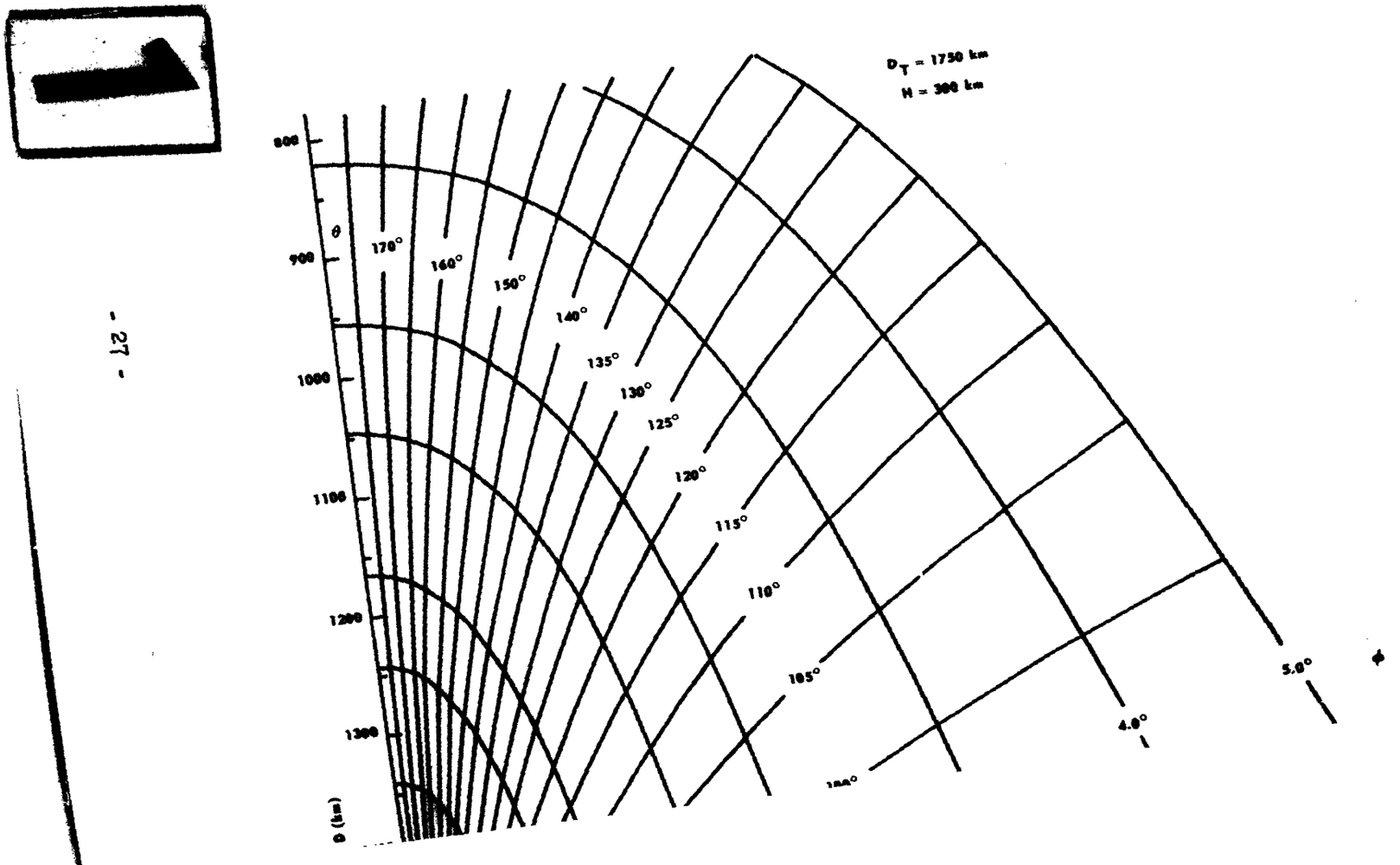
D_T = 1750 km
H = 300 km
800
900
1000
1100
1200
1300
θ
170°
160°
150°
140°
135°
130°
125°
120°
115°
110°
105°
100°
4.0°
5.0°
ϕ
ρ (km)

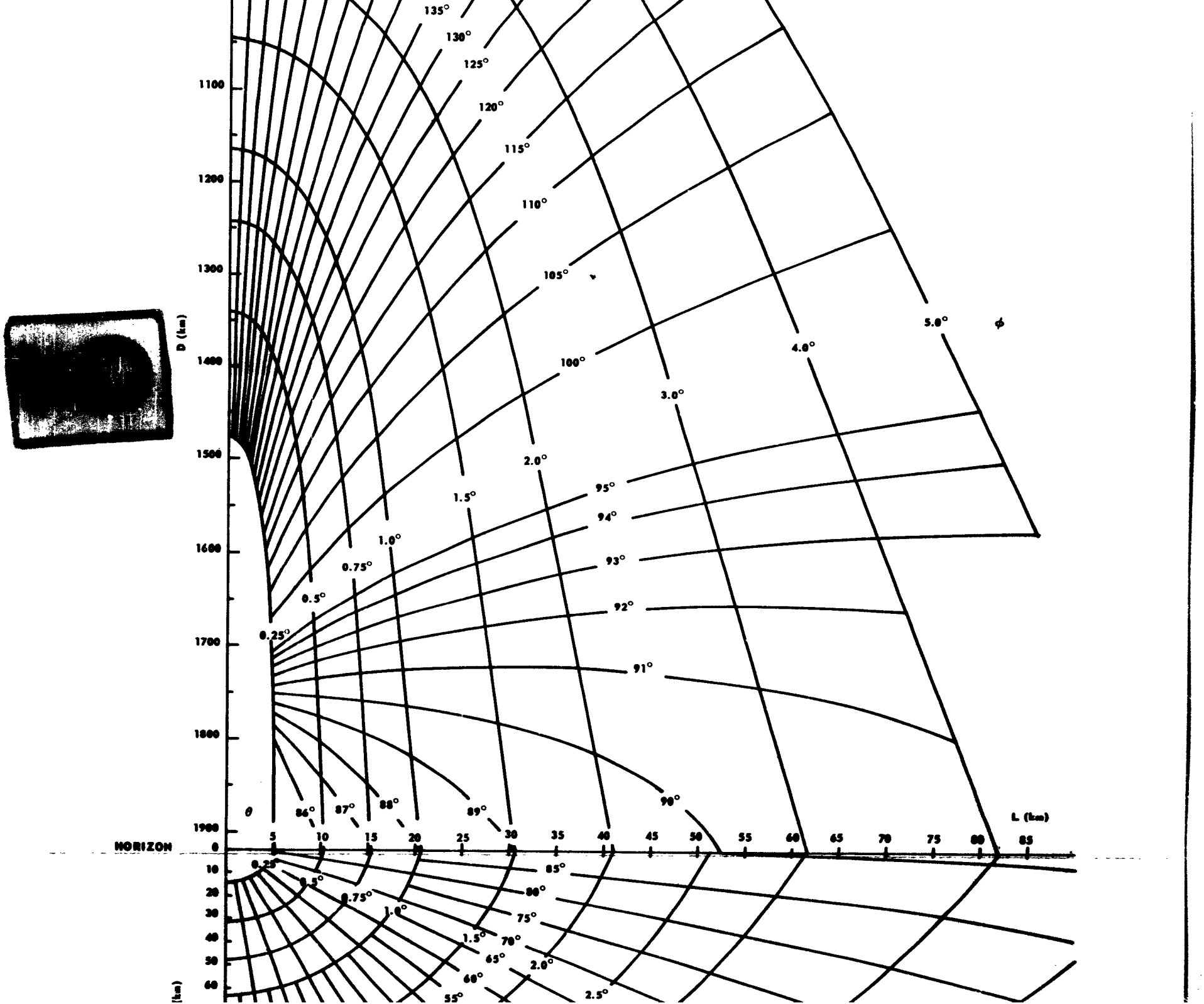
D (km)
1100
1200
1300
1400
1500
1600
1700
1800
1900
135°
130°
125°
120°
115°
110°
105°
100°
95°
94°
93°
92°
91°
90°
89°
88°
87°
86°
0.25°
0.5°
0.75°
1.0°
1.5°
2.0°
3.0°
4.0°
5.0°
ϕ
θ
HORIZON
0
5
10
15
20
25
30
35
40
45
50
55
60
65
70
75
80
85
L (km)
10
20
30
40
50
60
(km)
85°
80°
75°
70°
65°
60°
55°
2.5°

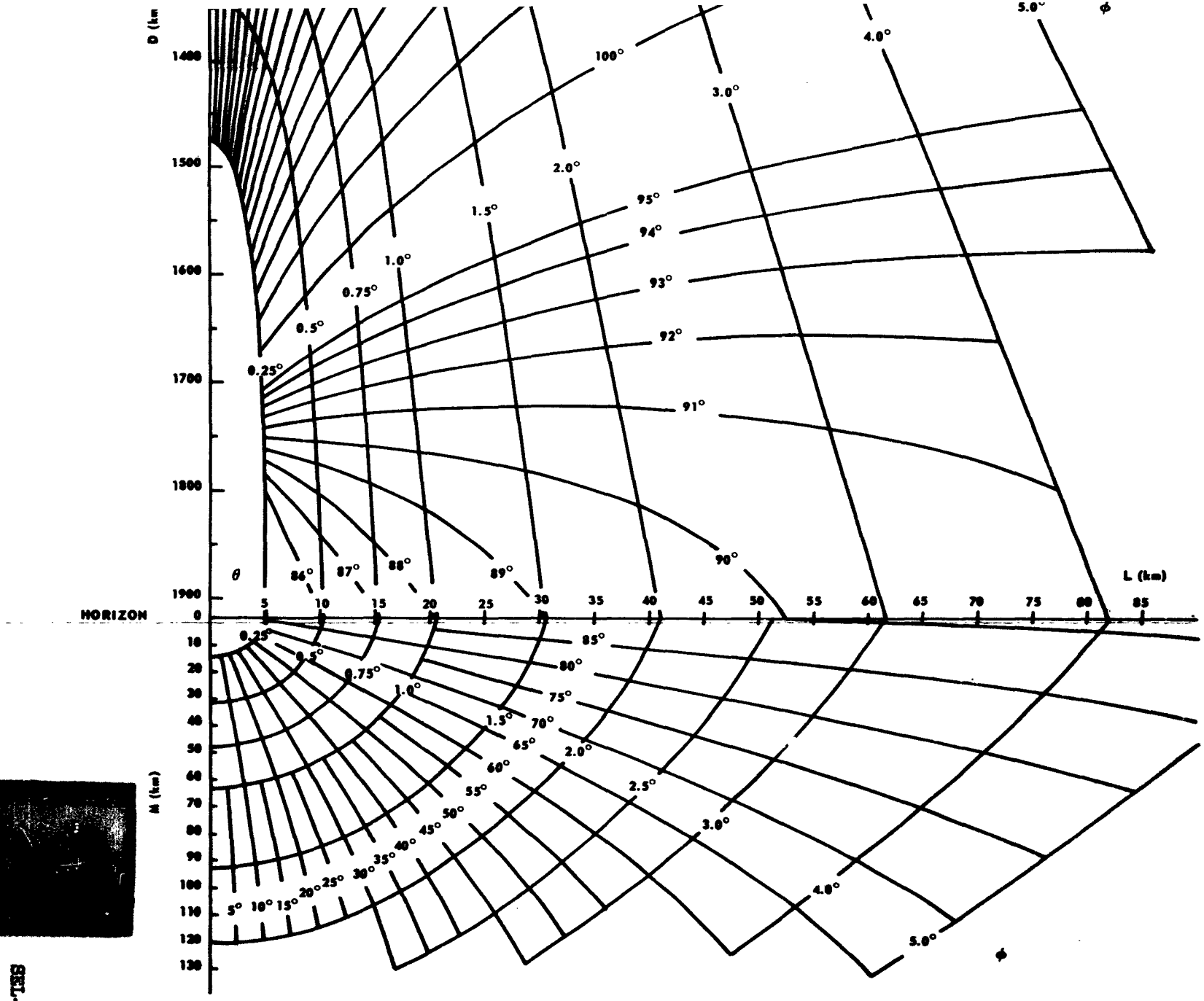

SEL-63-019

FIG. 17c. H = 350 km, D_T = 1500 km.

SEL-63-019

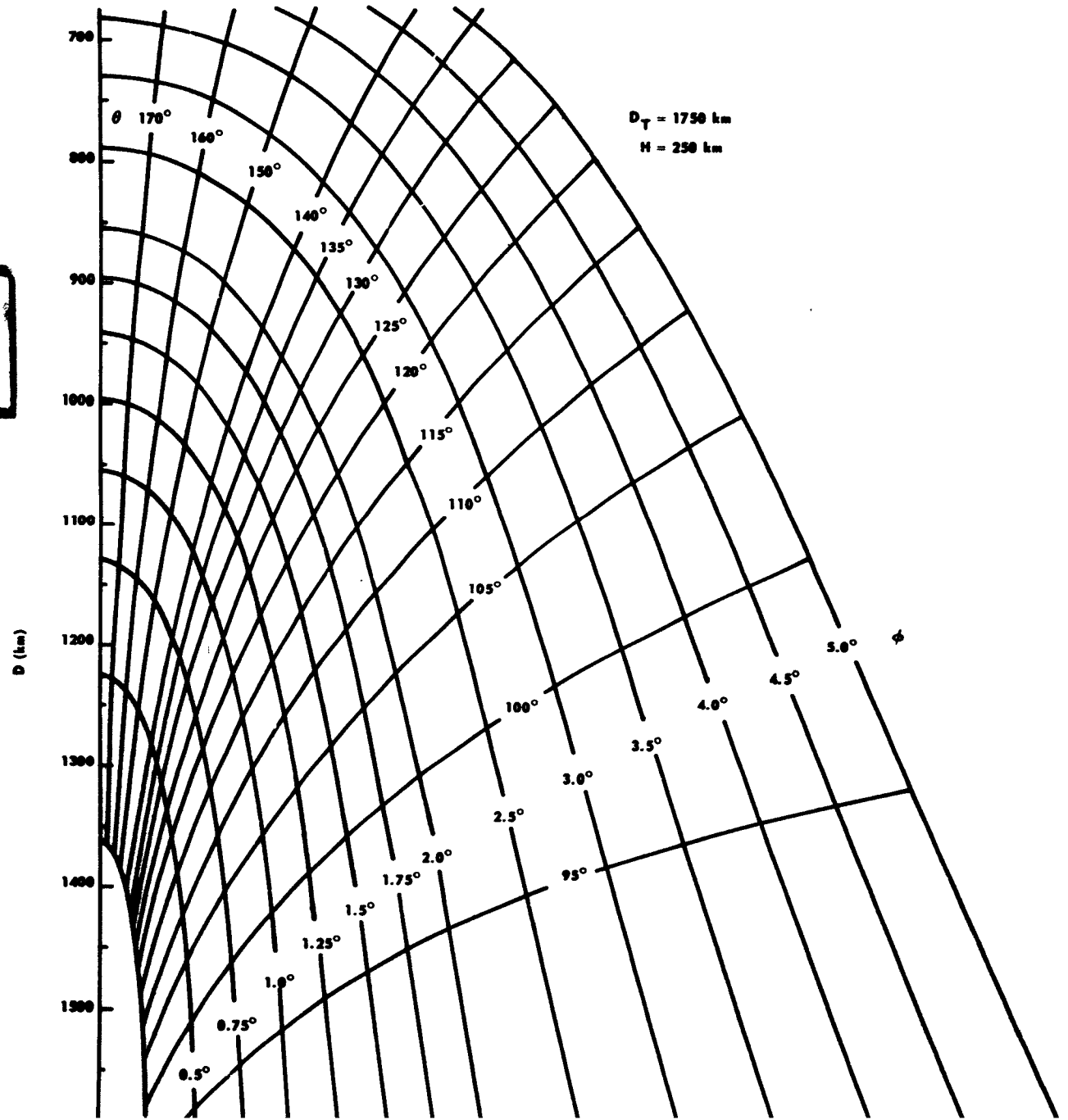
D_T = 1750 km
H = 250 km
θ
170°
160°
150°
140°
135°
130°
125°
120°
115°
110°
105°
100°
95°
φ
0.5°
0.75°
1.0°
1.25°
1.5°
1.75°
2.0°
2.5°
3.0°
3.5°
4.0°
4.5°
5.0°
D (km)
700
800
900
1000
1100
1200
1300
1400
1500

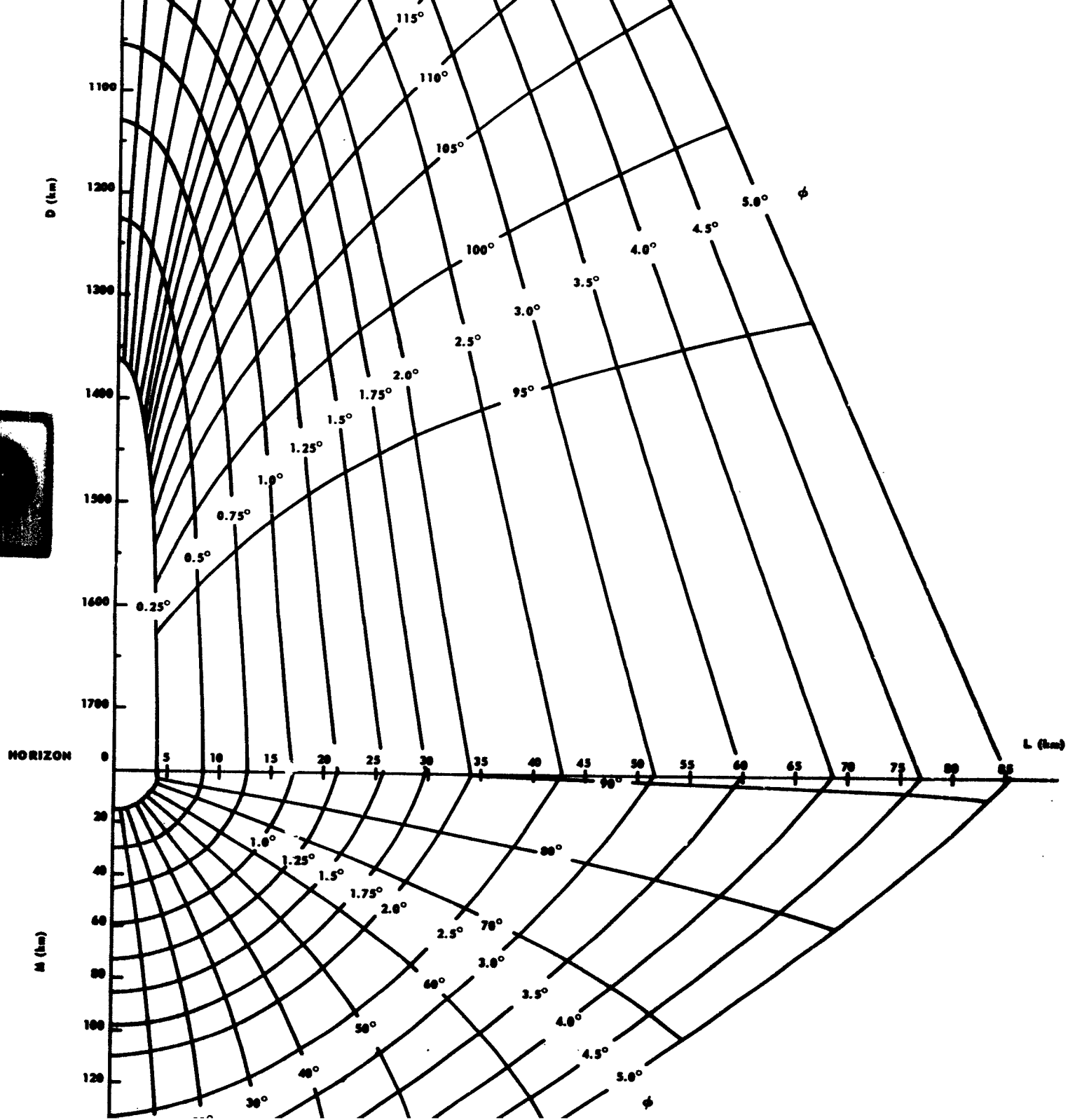
D (km)
1100
1200
1300
1400
1500
1600
1700
115°
110°
105°
100°
95°
90°
80°
70°
60°
50°
40°
30°
5.0°
4.5°
4.0°
3.5°
3.0°
2.5°
2.0°
1.75°
1.5°
1.25°
1.0°
0.75°
0.5°
0.25°
HORIZON
0
5
10
15
20
25
30
35
40
45
50
55
60
65
70
75
80
85
L (km)
M (km)
20
40
60
80
100
120
φ

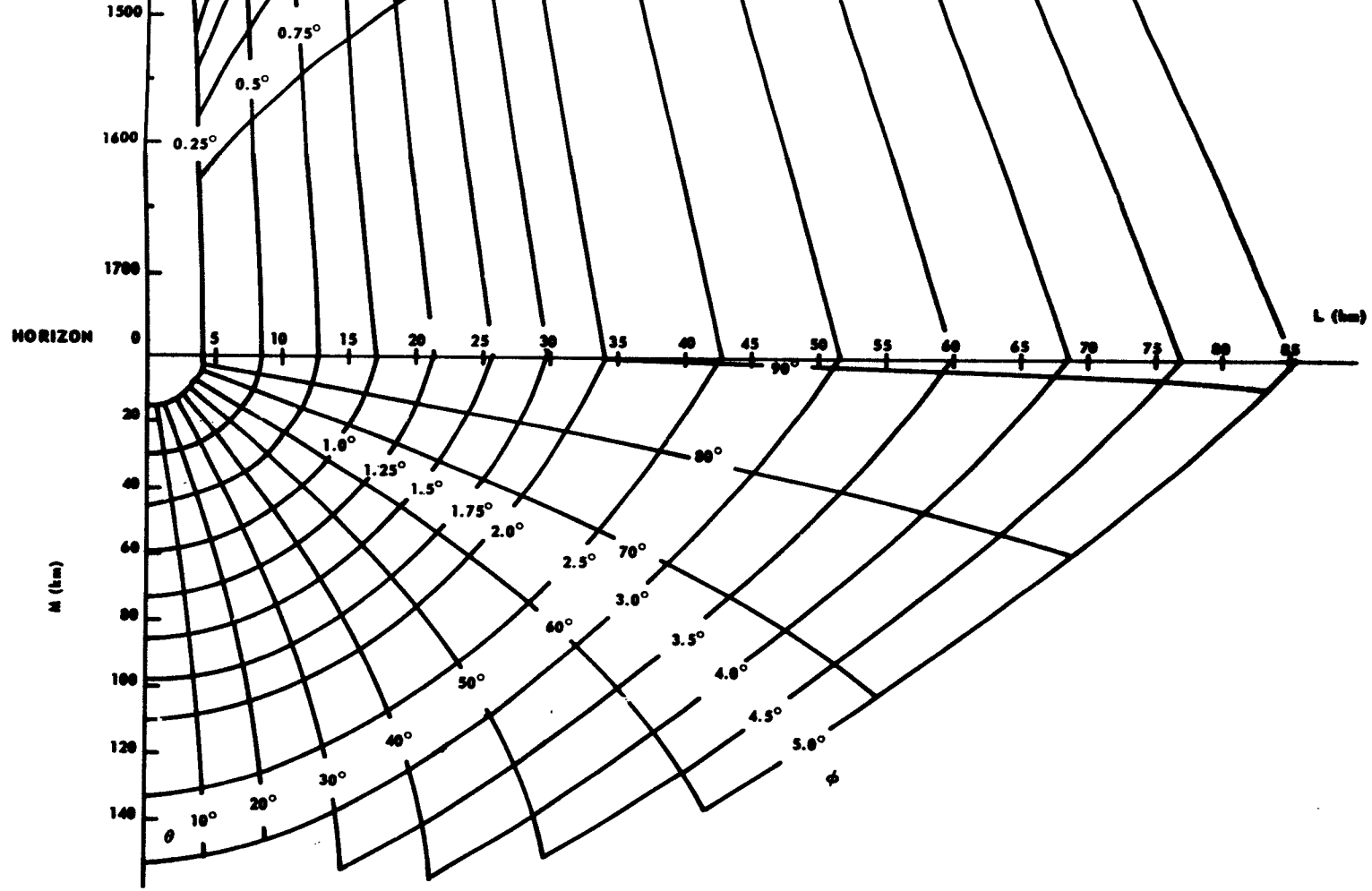

FIG. 17d. H = 250 km, D_T = 1750 km.

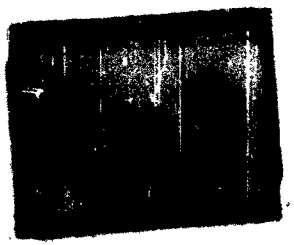

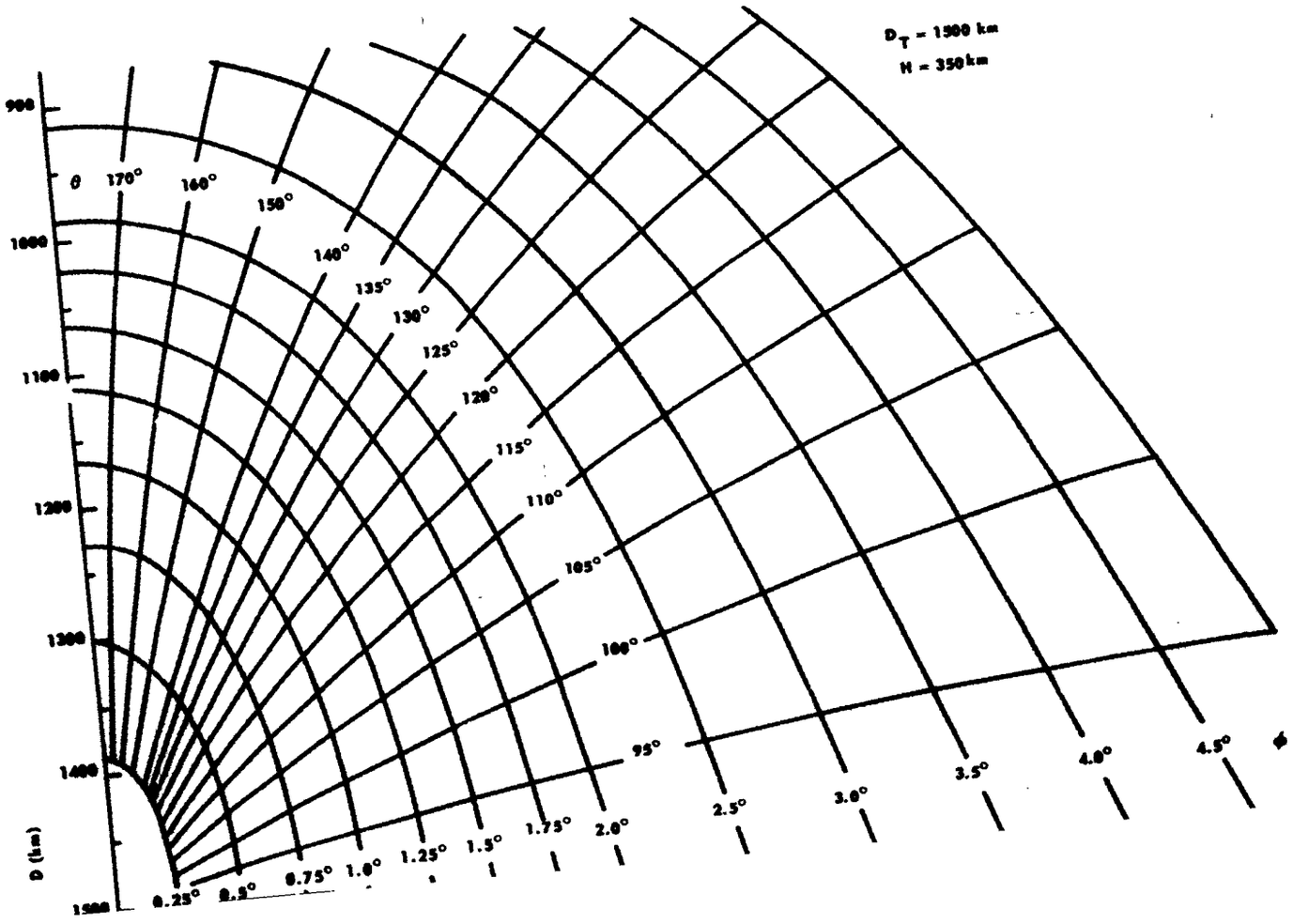
D_T = 1500 km
H = 350 km
θ
170°
160°
150°
140°
135°
130°
125°
120°
115°
110°
105°
100°
95°
900
1000
1100
1200
1300
1400
1500
D (km)
0.25°
0.5°
0.75°
1.0°
1.25°
1.5°
1.75°
2.0°
2.5°
3.0°
3.5°
4.0°
4.5°
φ

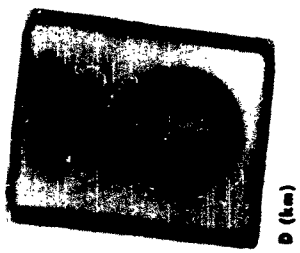

D_T = 1500 km

H = 350 km

θ 170° 160° 150° 140° 135° 130° 125° 120° 115° 110° 105° 100° 95° 90° 85° 80° 75° 70° 65° 60° 50° 40° 30° 20° 10°

1000 1100 1200 1300 1400 1500 1600 1700 1800 1900

D (km)

0.25° 0.5° 0.75° 1.0° 1.25° 1.5° 1.75° 2.0° 2.5° 3.0° 3.5° 4.0° 4.5° φ

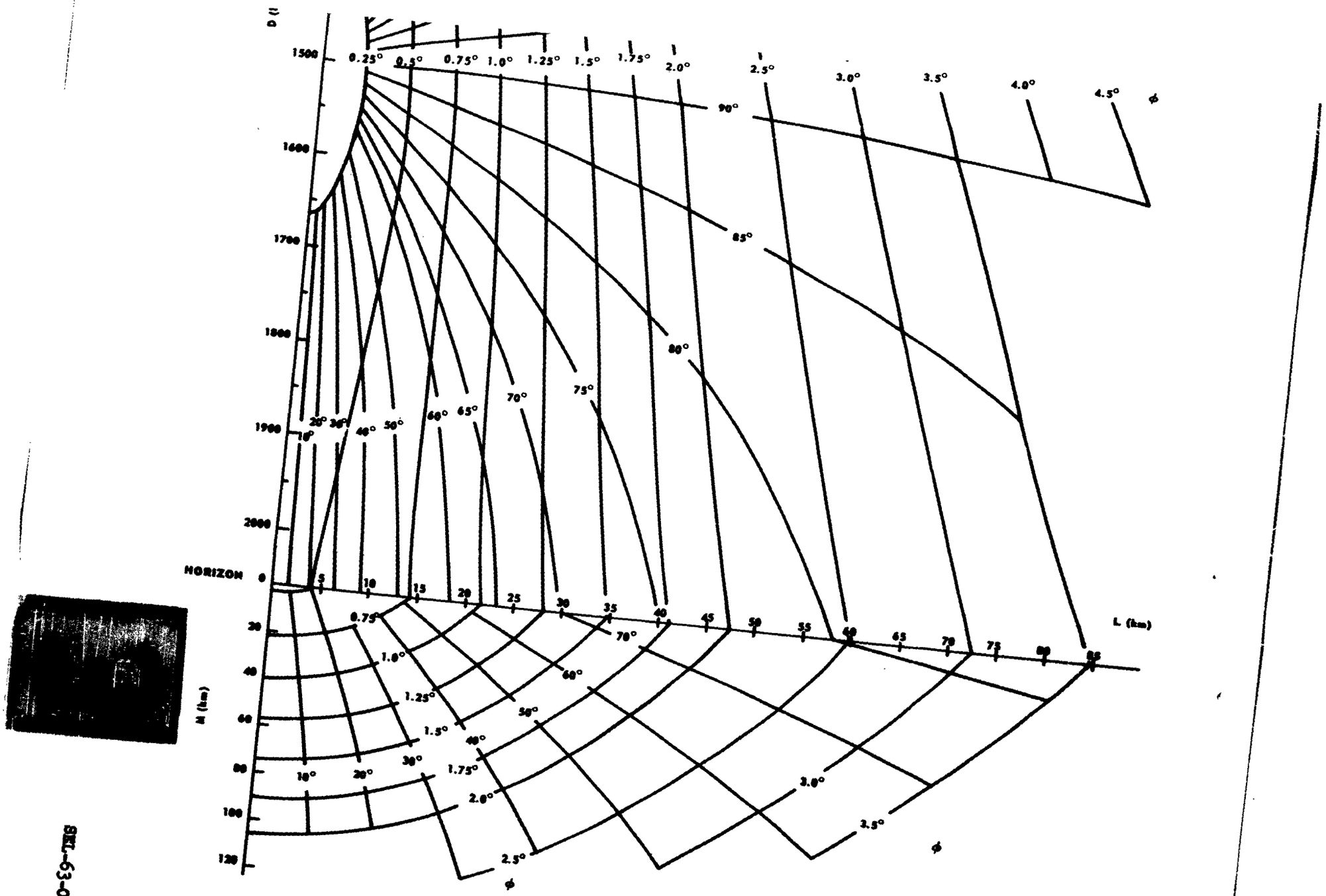

FIG. 17e. H = 300 km, D_T = 1750 km.

The three examples just cited should have a great significance in determining the role of effective ionospheric tilts in RTW propagation.

Case 1 is representative of the situation for a ray traversing the twilight zone from the light to the dark hemisphere. It is seen that conditions are appropriate for launching a tilt mode through the dark hemisphere. From Fig. 17b it is seen that values of θ from 0 deg to $\pm$82 deg (for $\emptyset$ = 2 deg) result in the ray missing the earth.

Case 2 is representative of the situation where propagation is along the twilight line, particularly in the dawn region, as seen in Fig. 14. The divisions shown in Fig. 14 are at 1000-km intervals. It is very significant that the 33.5-km deviation for a 3000-km path calculated above is negligible for most practical purposes. This leads to a conclusion that normal RTW propagation should take place in paths which are quite close to being great circles.

Case 3 is representative of the situation for a ray traversing the twilight zone from dark to light hemispheres. It is seen that the hop length is shortened substantially, and it is thus suggested that many dark-hemisphere tilt modes will be converted into "hop modes" upon reaching the light hemisphere.

In the above analysis it was presumed that a tilted mirror was a reasonable model of an ionosphere exhibiting a horizontal gradient of electron density. Since this may be a poor analog of an actual ionosphere, it is reasonable to ask what characteristics would be required of the real ionosphere in order for the mirror analogy to be valid. Basically, these requirements are that the horizontal gradient must exist over a distance at least as long as the ray path would normally exist in the ionosphere, and that the electron density variations should be "smooth." That these conditions are very likely met in the real ionosphere may be inferred from Fig. 14, where it is seen that, for example, in the area of maximum f_oF2 gradient (sunrise region) the gradient is relatively smooth and apparently exists over a distance exceeding 2000 km.

Peterson and Villard [Ref. 20] have produced machine-computed ray-path plots for hf propagation in a model ionosphere exhibiting horizontal gradients of electron density. One such plot, showing the launching of tilt modes (as referred to in the present report) is shown in

Fig. 18. For this example the assumptions were: (1) a Chapman ionization distribution, (2) magnetic field neglected, (3) h_{max} = 300 km, (4) ionospheric scale height = 100 km, (5) spherical earth and ionosphere, (6) a decrease in the maximum electron density with distance described by $N_o = 10^6 (1 - x/5000)$, and (7) f = 20 Mc. In this instance it is seen that rays having takeoff angles below 6 deg miss the earth's surface. The range of takeoff angles which correspond to rays that miss the earth would be significantly increased if h_{max} increased with x, a situation which often is the case in the real ionosphere.

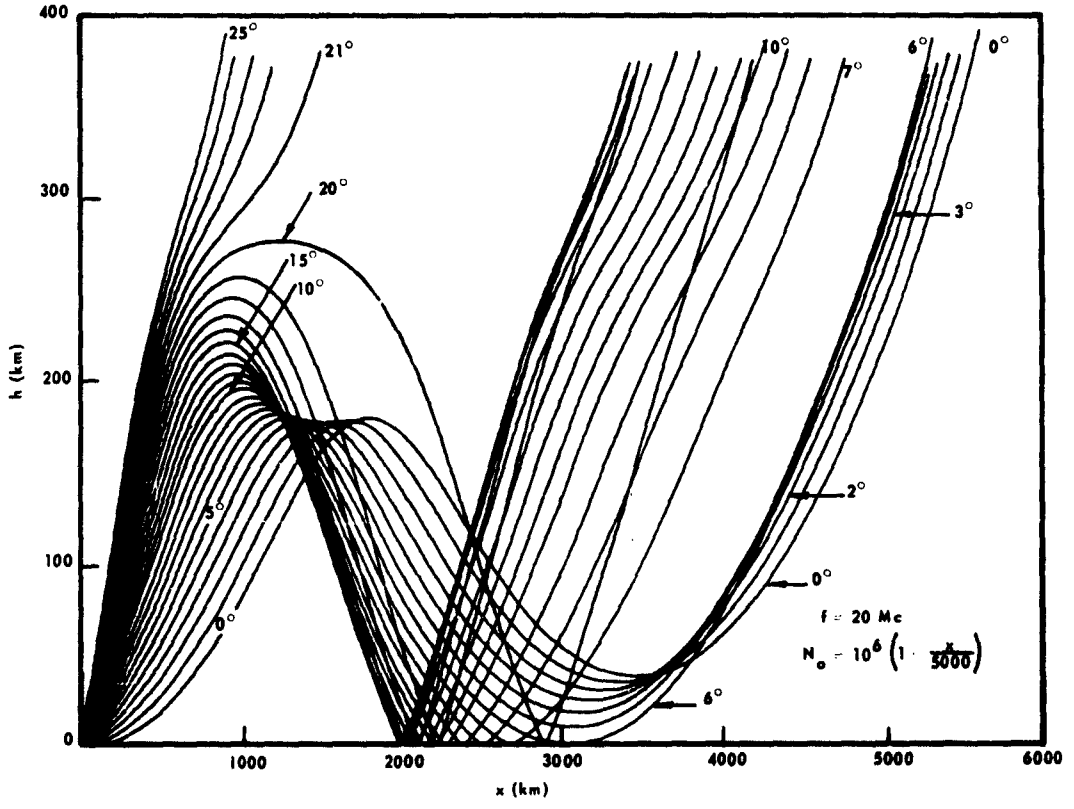

FIG. 18. RAY-PATH PLOTS IN A MODEL IONOSPHERE EXHIBITING A HORIZONTAL GRADIENT OF ELECTRON DENSITY.

E. THEORETICAL TIME DELAYS AND PULSE DISPERSIONS

As in the case of hf propagation over shorter distances, if earth-ionosphere-earth hops are encountered in RTW propagation, it would be expected that a multiplicity of modes, corresponding to various transmitting horizontal and vertical takeoff angles, should exist in normal RTW propagation. Further, this mode structure should be frequency dependent, with fewer possible modes as frequency increases, resulting in the least (and very small) pulse dispersion at the MUF.

Thus, despite the rather extensive earlier literature to the contrary [Refs. 6 and 8], it should be expected that time delays and pulse "dispersions" will be time, frequency, and azimuth dependent. The precise dependence should depend upon the interaction of a great many factors, but a few general statements may be made.

It has been shown by de Voogt [Ref. 10] that, assuming a simple but reasonable ionospheric electron-density profile and earth-ionosphere-earth hop modes, time delays should increase with increasing radio frequency for modes having fixed takeoff angles. Also, since modes having greater takeoff angles should be possible for lower frequencies, pulse dispersion (caused by mode superposition) should increase with decreasing frequency.

Since the time taken for a ray in free space to travel around the world at the earth's surface is on the order of 133 msec, it can at least be stated that the RTW time delay should exceed this figure for great-circle paths. The theoretical time delays determined by de Voogt fall in the 136-145 msec range.

Any precise statement concerning theoretical RTW-signal time delays and pulse dispersions would best be based upon ray tracings in an accurate ionospheric model. In the absence of sufficient information to construct such a model, the above statements must suffice.

III. EXPERIMENTAL ARRANGEMENTS AND OBJECTIVES

A. MANUAL EXPERIMENTS

In the period from April through October 1961, briefly in January 1962, and in June and July 1962, systematic studies of circulating signals were made at Stanford, California, using manually controlled, 50-kw, 1-msec pulse transmissions in the 12- to 28-Mc range [Ref. 21]. The transmitting antenna was normally a rotatable 11- to 60-Mc Collins log-periodic antenna, model 237A2, having a 64-deg 3-db horizontal beamwidth. Receiving was carried out using a similar rotatable log-periodic antenna (in the range above 20 Mc), plus various rhombic and Vee antennas having beamwidths of 10 to 15 deg. Receiving antennas were oriented 180 deg away from the transmitting-antenna azimuth when possible. After October 1961, two rotatable log-periodic antennas were often used simultaneously to obtain optimum-azimuth vs time-of-day information.

In this particular experimental work, the receiver was a Hammarlund SP 600 JX with a preamplifier and logarithmic I-F amplifier-detector. The detector output was displayed on an oscilloscope in the usual "A" display, together with time markers, and photographed for later analysis. Typical displays used are shown in Fig. 19.

These displays are 35-pulse film integrations of the A-scope display. The pulse repetition rate was approximately 4 pps, except during time-delay measurements when it was 5 pps, derived from the same crystal-controlled standard as were the timing marks. The displayed voltage is log-detector output. In Fig. 19a ground backscatter, as diminished by the transmitting-antenna front-to-back ratio, is seen after the transmitted pulse. At approximately 138-msec delay the first circulation of the pulse is seen. At about 276 msec the second circulation is displayed. Here the pulse repetition rate was 3 pps to enable the second circulating pulse to be observed. Figure 19b shows a typical range-measuring display, with 10-msec timing marks. The second circulating pulse is displayed at about 275 msec minimum delay; note that the second pulses arrived "around the time base," and the 200-msec pulse period must be added to the apparent delay. Figure 19c shows an expanded

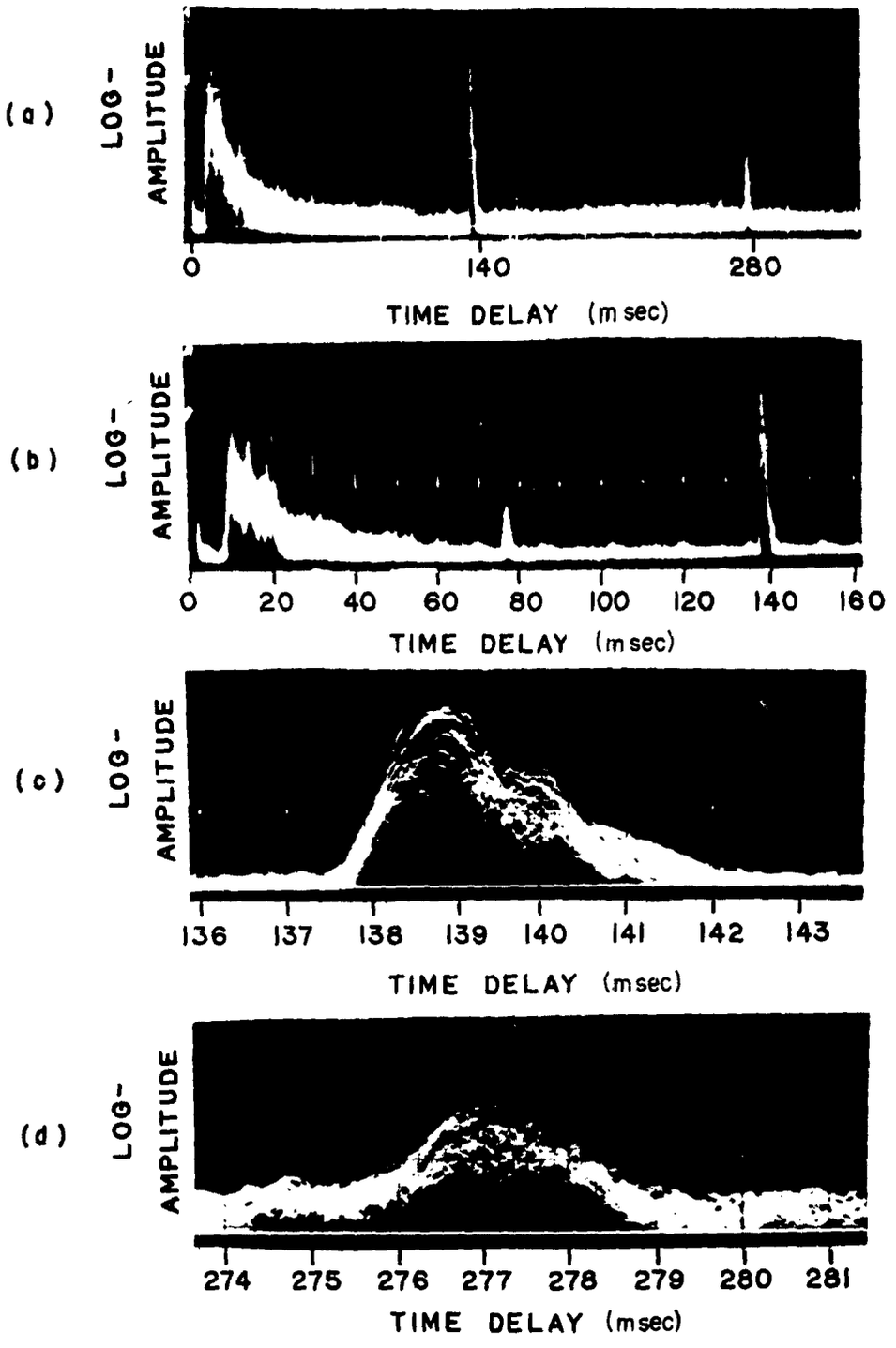

FIG. 19. TYPICAL A-SCOPE DISPLAYS USED DURING MANUAL RTW-PROPAGATION EXPERIMENTS.

scale integration for the first circulating pulse, with 1-msec time marks. Figure 19d is a similar integration, but for the second circulation. All measurements shown in Fig. 19 were made at 15.1 Mc, 1815-1820 PST, 10 October 1961. The width of the transmitted pulse was 1 msec. The apparent width of a 1-msec received rectangular pulse (which was greater due to the 3-kc receiver bandwidth) was 1.6 to 2.0 msec.

The principal objectives of the manual experiments included (1) determination of the frequency band (particularly the MUF), in which RTW propagation was possible, as a function of time of day and month; (2) time delays and pulse dispersions as functions of frequency and time, and (3) the effect of magnetic storms on the occurrence and propagating frequency band for circulating signals. Also, backscatter measurements were sometimes made during the circulating-signal measurements, using the Collins log-periodic antenna and 1-msec, 50-kw pulses, in order to obtain possible correlations of backscatter conditions with the RTW propagation conditions.

B. AUTOMATIC EXPERIMENTS

In addition to the manual experiments, automatic transmissions were made to determine the characteristics of RTW signals during the period 24 March - 21 May 1962. In these tests, a Granger Associates Model 902 step-frequency transmitter-receiver was used, transmitting on the Collins log-periodic antenna described above (normally oriented in the theoretical minimum-absorption azimuth) and receiving on a Hygain LP 13-30 log-periodic antenna, oppositely oriented, at a height of approximately 70 ft. Step-frequency transmissions were made at 15-min intervals, 24 hr per day, over the 10.8- to 32-Mc range using 1-msec pulses, 5 pps, and 10 pulses per channel (the frequency range being divided up into 65 frequencies). The peak power output was presumably 30 kw.

In these tests, an oscilloscope sweep of 8-msec duration was caused to begin approximately 135 msec after the initiation of the transmitted pulse, the oscilloscope beam being intensity modulated by the 500-kc receiver I-F output. The receiver gain characteristic was logarithmic, and the bandwidth was 6 kc until 10 April, after which it was 1 kc.

Examples of the RTW ionograms thus obtained may be seen in the following chapter on experimental results.

Also, during this later period, more than 200 manual runs were conducted in which a frequency sweep was made in each of the 12 possible transmitting azimuths (spaced 30° apart). In this way, it was possible to determine optimum-azimuth information and the suitability of automatically programming the antennas to the theoretical minimum-absorption azimuth.

The primary objectives of the automatic experiments were to determine the times of day in which RTW propagation could be achieved, with the available system sensitivity, and the frequency band(s) of propagation. It was also desired to determine the variations of these characteristics with geomagnetic field activity. In addition, the optimum azimuth determinations, described above, were of primary interest.

IV. EXPERIMENTAL RESULTS AND COMPARISON WITH PREDICTIONS

A. THE OBSERVED FREQUENCY OF OCCURRENCE OF RTW PROPAGATION

It is implied by Hess [Ref. 6] that the ability to transmit hf radio waves around the world is a function of time of day, season, geographical latitude, long-term ionospheric variations (presumably corresponding to the sunspot cycle), ionospheric "storms," radio frequency, and antenna patterns. It is clear that system sensitivity, chiefly determined by the transmitter power, antenna gain(s), and receiver sensitivity, will also be a major factor in determining the apparent ability to transmit hf signals around the world.

In the Stanford experimental work, it was found that RTW propagation was possible on essentially a daily basis, with the number of hours of propagation possible per day being dependent particularly upon season and geomagnetic activity, and also, as would be expected, upon radio frequency and the other factors mentioned above. The most favorable times of day for RTW propagation are without doubt the sunrise and sunset periods, but these are by no means the only periods in which this propagation is possible, as theory would suggest.

The automatic experiments, described earlier, provided a good picture of RTW-propagation conditions (for a given equipment sensitivity) in the equinox transition period. In the period 24 March - 21 May 1962 conditions typical of both winter and summer months were present in varying degrees. In Fig. 20 are shown the times when the equipment was presumably operational and the portions of these times when an RTW signal was observed on at least one frequency in the 10.8- to 32-Mc range.

Also shown in Fig. 20 is a summation of the 3-hr-range planetary magnetic indices, K_p, for each 24-hr period [Ref. 22]. It is seen that during periods of high geomagnetic field activity the ability to achieve RTW propagation was significantly reduced. Correlations of magnetic field activity with various characteristics of RTW signals will be presented in greater detail in a later section.

There are many interesting, and typical, features of RTW propagation that are illustrated in Fig. 20. Some of these features are as follows:

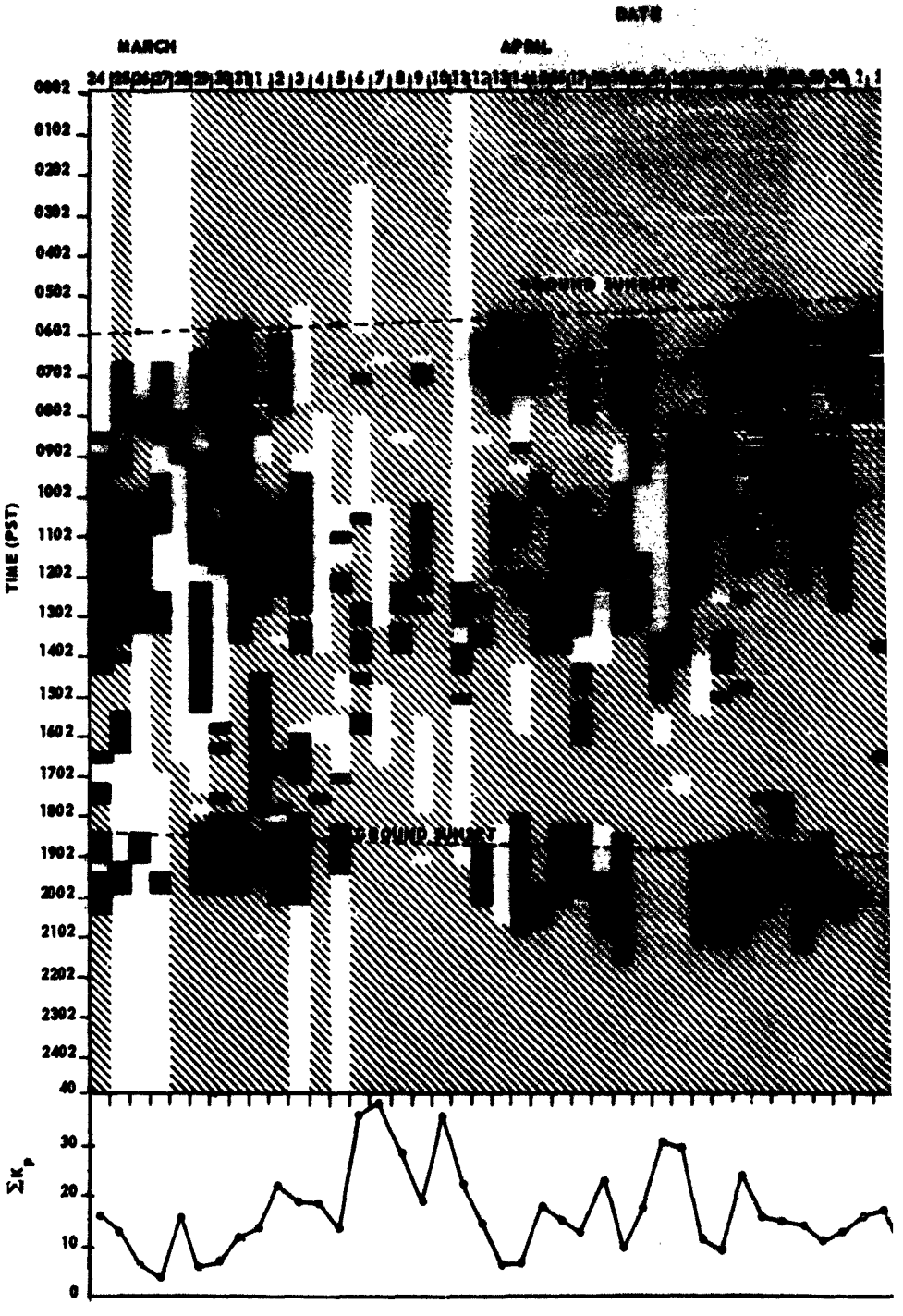

FIG. 20. TIMES DATA WERE AVAILABLE (SHADED) AND WHEN RTW PR
AT STANFORD, 24 MARCH - 21 MAY 1962. ΣK_p for each 24-hr perio

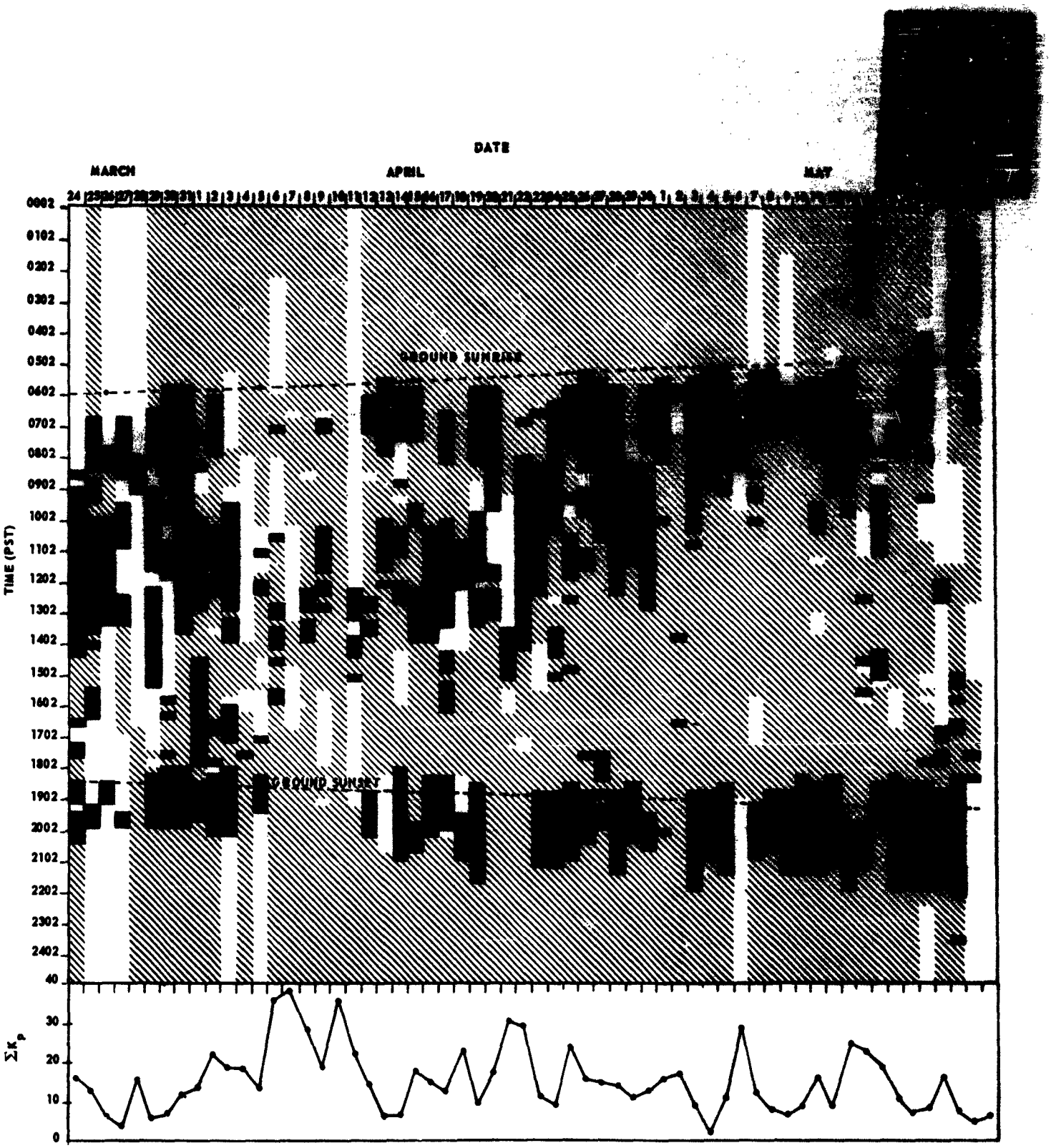

FIG. 20. TIMES DATA WERE AVAILABLE (SHADED) AND WHEN RTW PROPAGATION WAS OBSERVED (SOLID) AT STANFORD, 24 MARCH - 21 MAY 1962. ΣK_p for each 24-hr period is also shown.

1. Typical of winter days, and of some summer days, the morning onset of RTW propagation began very near to the time of ground sunrise (upper limb). In summer, RTW propagation was found to often begin considerably in advance of ground sunrise and it was occasionally possible throughout the entire night period (over a very limited frequency range, however). Evidence of the increasing probability of this condition is seen for 14, 20, and 21 May.

2. Evening propagation began close to the time of ground sunset, becoming somewhat earlier as summer was approached.

3. RTW propagation was possible over most of the daylight hours very early in the test. This feature was characteristic of winter, when it was found that such propagation could normally be obtained throughout the entire daylight period, but ceased abruptly after sunset.

4. The length of time in which RTW was possible following ground sunset increased greatly as time progressed from winter solstice toward summer solstice, reflecting the change in length of the twilight period.

5. The length of time in which RTW was possible following ground sunrise decreased markedly as time progressed from winter solstice toward summer solstice, apparently reflecting an increase of path absorption in the daylight hemisphere and a decrease of F2-layer critical frequencies in the antipodal region (which was approaching winter).

6. There appears to be a lesser correlation of magnetic activity with midday RTW-propagation conditions than with the twilight conditions. This finding should be expected since, as will be seen later, the midday propagation azimuths were such as to cause the ray paths to maintain the greatest possible distances from the auroral zones, while this was not the case for twilight propagation.

7. There was a marked minimum in RTW-signal activity in late afternoon, which corresponded to the predawn period in the antipodal region. This minimum was found to be more pronounced in summer than in winter.

Figure 21 shows the percent of records on which RTW signals were detected vs local time for two periods which corresponded to the two halves of the test period. Most of the features previously mentioned are clearly illustrated. These include, for example, the daytime propagation that was observed earlier in the test period, the predominant twilight time (morning and evening) propagation particularly later in the period, and the late afternoon minimum of RTW-signal activity.

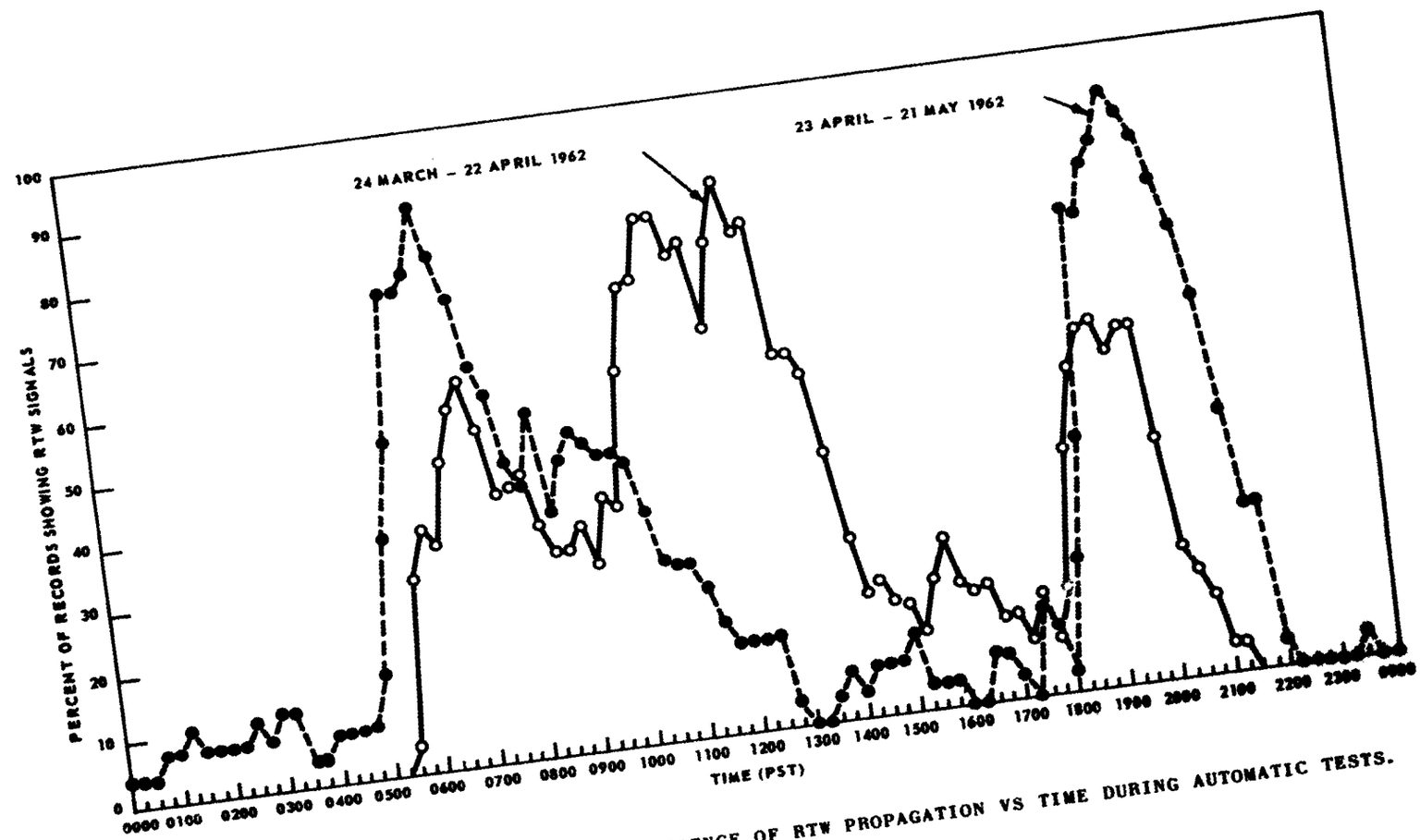

FIG. 21. PERCENT OF RECORDS SHOWING PRESENCE OF RTW PROPAGATION VS TIME DURING AUTOMATIC TESTS.

B. THE VARIATION OF THE OPTIMUM AZIMUTH WITH TIME AND FREQUENCY

1. Winter Measurements

A principal aim of the experimental work after October 1961 was the accurate determination, so far as was possible with the available equipment, of the optimum (minimum attenuation) azimuth for hf RTW propagation as a function of time of day and frequency. There is no reason why it should not be possible to have more than one such azimuth at a given time and frequency, and this situation was occasionally found to exist, as will be seen in the section on spring (1962) measurements.

The situations for winter and summer were found to be less complex than for the equinox periods, and will be considered first. In Fig. 22 are presented photographs of A-scope displays (log-detector output vs time delay) made on 31 December 1961 for varying antenna azimuths, at 15.1 Mc, at successive times of day. On these displays, which are 35-pulse film integrations, the RTW-signal presence is apparent, and it is seen that the optimum RTW azimuth varied from 270° to approximately 330° in 5 hr. More information concerning the methods employed to obtain these records, and concerning the other interesting features of RTW propagation which are notable from these photographs, has been given elsewhere [Ref. 15].

The results of 6 days of such measurements are shown in Fig. 23. The solid line is the theoretical minimum-absorption azimuth from Eq. (4) and Fig. 4. The dashed line is the predicted maximum f_oF2 azimuth from using the three-point method. The world map and the curves from which the 1400 PST point was determined were shown, respectively, in Figs. 7 and 8.

Considering the accuracy with which the antenna could be positioned (possibly no better than 10 deg) and to which the resulting records could be interpreted (5 deg), it is concluded, from this relatively small sample, that it is very likely possible to predict the optimum azimuth for RTW propagation during winter day with good accuracy, merely by considering absorption and average f_oF2 conditions. This is particularly likely since the period in which the measurements were made was relatively quiet magnetically. The result is made less general by the fact that only one frequency was used in the test, but, as will be seen shortly,

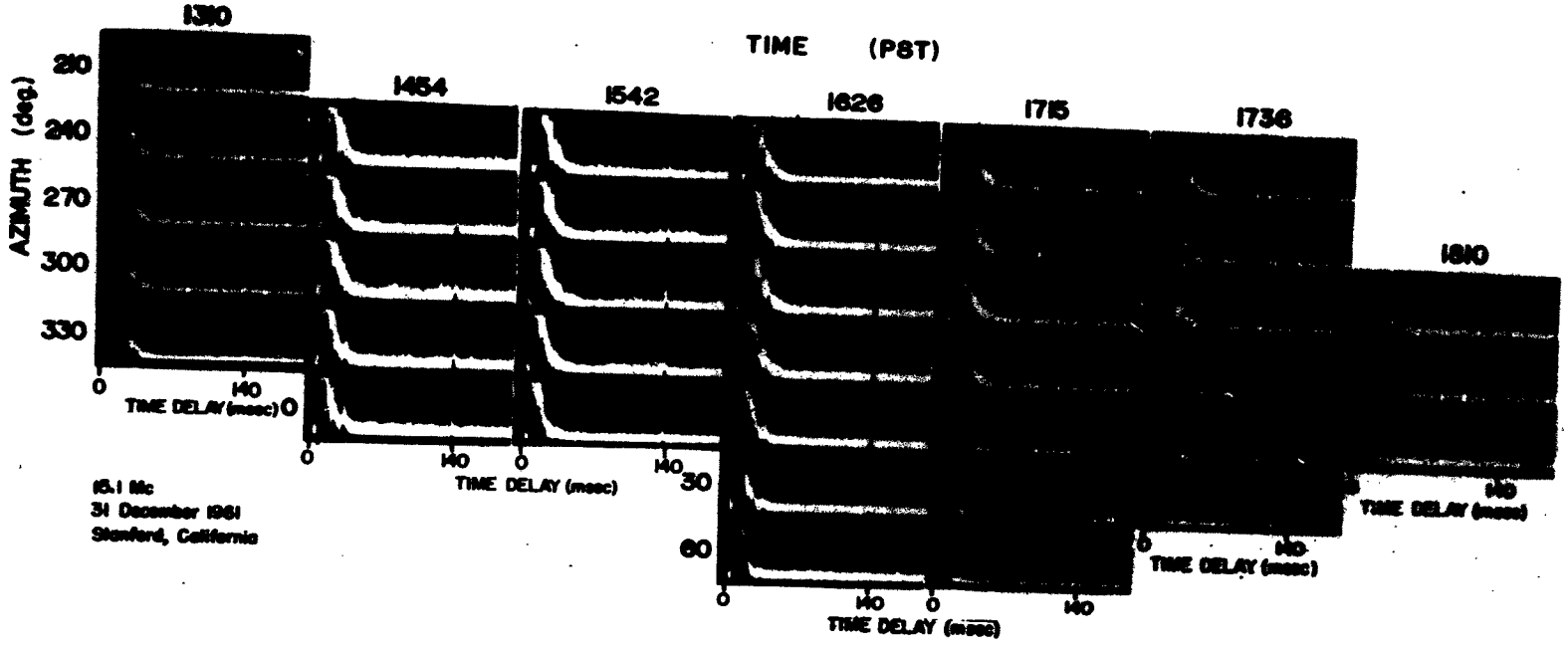

FIG. 22. A-SCOPE DISPLAYS SHOWING VARIATION OF RTW-SIGNAL PROPAGATION CHARACTERISTICS WITH TIME.

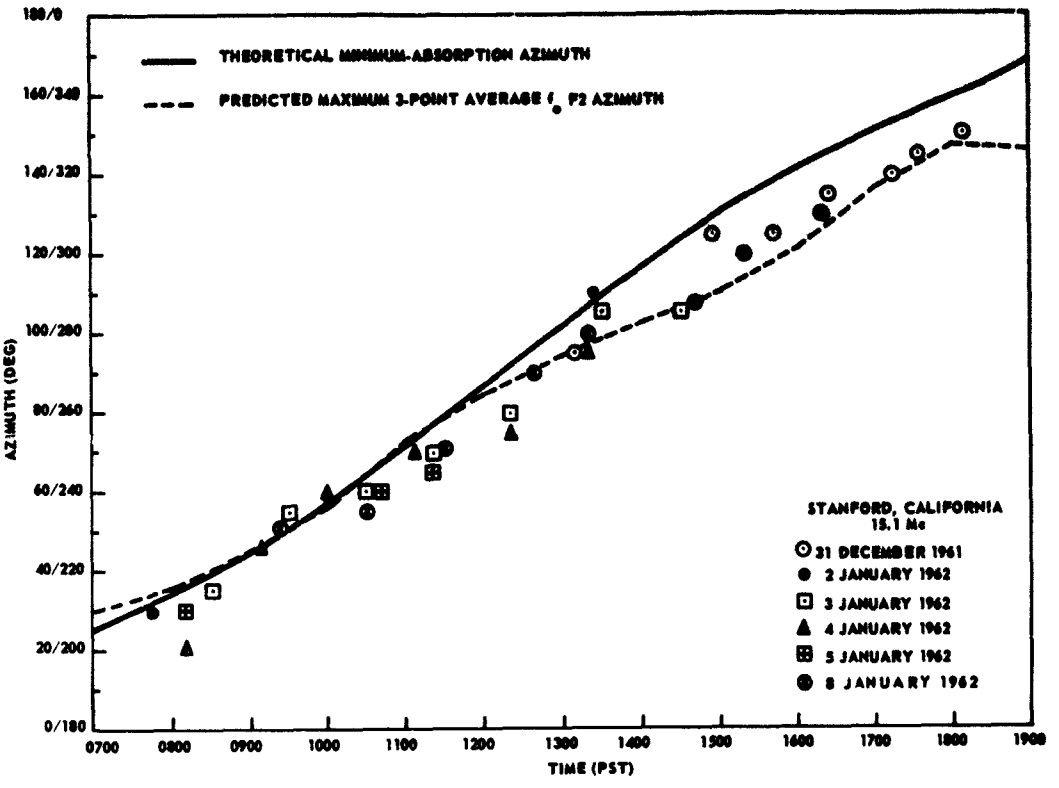

FIG. 23. PREDICTED CURVES AND EXPERIMENTAL POINTS FOR OPTIMUM RTW-PROPAGATION AZIMUTH VS TIME FOR WINTER DAY.

measurements made in summer night (on three frequencies) substantiate the findings for winter day. (This would be qualitatively expected, since the antipodal region was in summer night throughout the winter-day measurements.)

2. Summer Measurements

During the months of June and July 1962 a manual experiment similar to the one described above for winter day was conducted for summer night (using two log-periodic antennas and 1-msec, 50- to 100-kw pulses). In this case, frequencies of 12.5, 15.1 and 18.1 Mc were used sequentially, with the overall sequence being repeated at approximately 45-min intervals. Very little difference in optimum azimuths was found

between these frequencies (at a given time), but a marked time variation of the optimum azimuth, was noted as expected.

The experimental points determined for optimum azimuth vs local time (PST) are shown in Fig. 24. Also shown is the theoretical minimum-absorption azimuth (solid line) and points determined for the predicted

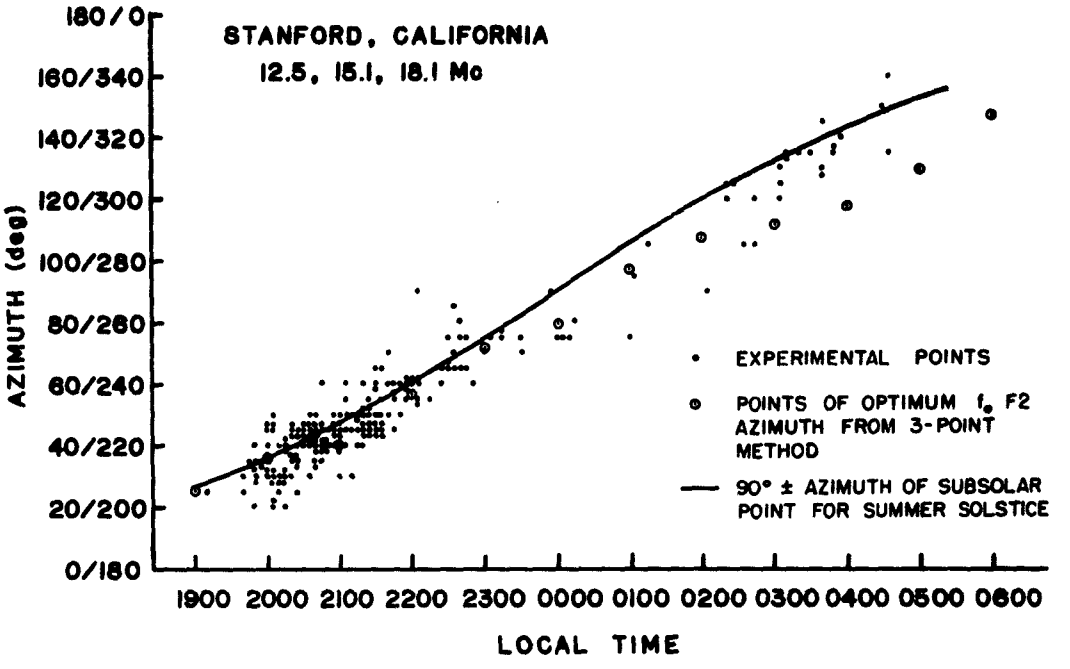

FIG. 24. PREDICTED CURVES AND EXPERIMENTAL POINTS FOR OPTIMUM RTW-PROPAGATION AZIMUTH VS TIME FOR SUMMER NIGHT. The experimental points are for the period 14 June - 25 July 1962.

maximum $f_o F2$ azimuth (three-point method). (The theoretical curves were shown for an entire day in Fig. 9.) It was not possible to conduct the experiment at times other than those shown, and hence the curves of Fig. 24 may be considered incomplete. However, the curves obtained in Spring 1962, which follow, should provide a good indication of what may generally be expected.

In spite of the very limited data presented in Fig. 23, the experimental results given in this figure are remarkably similar to the results shown in Fig. 24 (changing either time scale by 12 hr). The

theoretical maximum three-point average f_oF2 curves are also remarkably similar. The theoretical minimum-absorption curves are identical due to the method by which they were derived.

Note that data were usually not obtainable for a period of 3 hr or so, centered on 0100 LT, as evidenced by the sparseness of data points (Fig. 24). This time corresponds to winter midday at the antipodal region--a time of theoretical maximum path absorption for the period shown (cf Fig. 5), if the primary propagation modes are passing through the D region in the daylight hemisphere. This finding has been used to substantiate the theory that earth-ionosphere-earth hop modes are predominant in RTW propagation in the daylight hemisphere.

3. Spring Measurements

During Spring 1962 the Granger 902 step-frequency transmitter-receiver was often used to determine the optimum azimuth(s) for RTW propagation. In this instance it was possible to obtain optimum-azimuth vs frequency information, although single-frequency measurements were sometimes made in the interest of saving time. The results of one such measurement are shown in Fig. 25.

The upper record of Fig. 25 shows the presence of RTW propagation at 15.7 Mc, 0715 PST, 28 April 1962. It is seen that the optimum azimuth was approximately $165^\circ/345^\circ$. The lower record, begun immediately after the upper record was completed, shows the presence of RTW propagation at 18.2 Mc, but with the optimum azimuth $105^\circ/285^\circ$. The apparent slight disagreements between the azimuths 180° apart are most likely due to inaccurate receiving-antenna positioning, since the method used was simply to turn on the rotating motor by equal increments of time per desired 30° rotation. No evidence of nonreciprocity of the RTW propagation was found during any of the tests.

It is interesting to note in Fig. 25 that the apparent time delays increased by approximately 1 msec when the frequency and azimuth of RTW propagation changed. More will be said about this in Sec. E of this chapter.

Figure 26 shows earlier records made on 28 April 1962 on more widely separated fixed frequencies, and interlaced in time. Here it is seen that the optimum azimuths at the lower and higher (16.6 Mc)

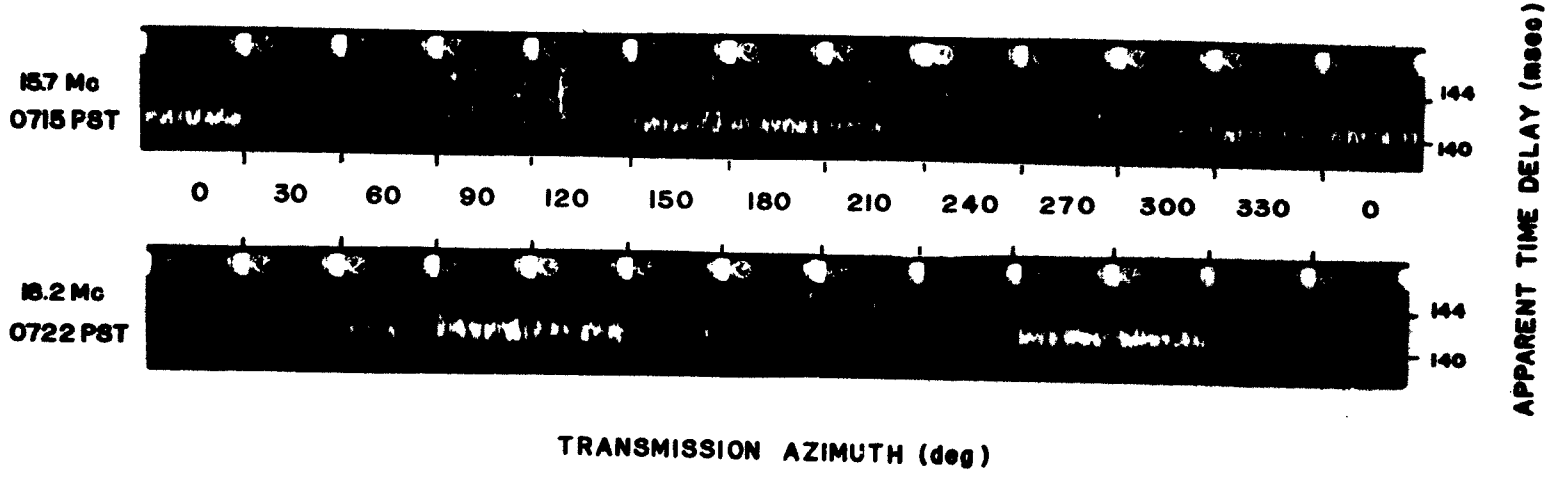

FIG. 25. INTENSITY-MODULATED DISPLAYS SHOWING RTW SIGNAL STRENGTH VS AZIMUTH AT TWO FREQUENCIES, 28 APRIL 1962, STANFORD.

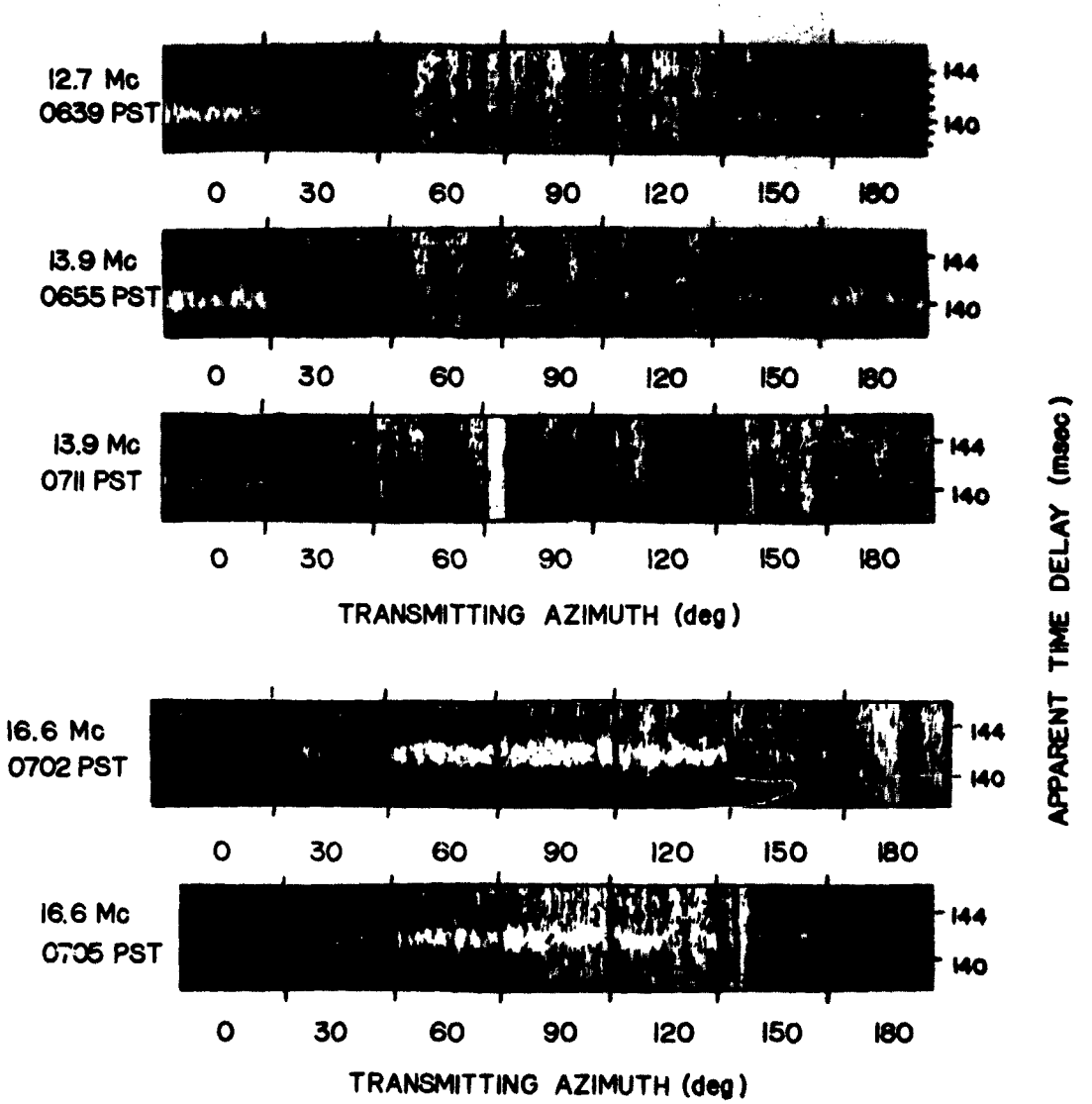

FIG. 26. INTENSITY-MODULATED DISPLAYS SHOWING RTW SIGNAL STRENGTH VS AZIMUTH AT THREE FREQUENCIES, 28 APRIL 1962, STANFORD.

frequencies were almost precisely orthogonal. This situation was very common at this particular time of day in April. In Fig. 27a are shown step-frequency measurements made at 0644 PST, 26 April 1962. Here it is seen that 165° was the approximate optimum azimuth for frequencies up to 15.1 Mc, but that the frequencies 15.9 to 17.0 Mc propagated around the world best at approximately 90° azimuth.

Figure 27b shows typically how the situation changed in the 2-hr period following a situation such as that shown in Fig. 27a, which was made 2 days earlier. The minimum propagating frequency (considering all azimuths) has increased markedly (to 15.1 Mc) and the maximum propagating frequency has increased even more, to 22.2 Mc in this instance. The generally north-south propagation has ceased, and the optimum azimuth has now become on the order of 120°.

Note in the records of Fig 27 that the minimum RTW time delays appear to decrease with increasing frequency for a given azimuth, directly contrary to theory. A possible explanation for this is that lower-angle (hence, shorter time delay) propagation is improved at higher frequencies due to the changing of antenna vertical patterns with changes in frequency. The intensity-modulated display could thus provide an erroneous indication of the variation of minimum time delay with frequency. More will be said of this in Sec. E of this chapter.

In Fig. 28 are summarized the azimuthal measurements made in April 1962 for hourly periods in which three or more measurements were available (some twilight periods had ten measurements per hour). The solid lines show the experimental data, obtained by averaging the measurements made in the hour centered on the time shown. It is seen that the multiple optimum azimuths occurred only in the immediately postdawn and presunset periods.

It is evident in Fig. 28 that, while the correlation between the experimental optimum azimuths and the theoretical minimum-absorption azimuths was excellent at twilight times (particularly for lower frequencies, as illustrated in Fig. 27a), there was no such correspondence during the daylight period. However, the correspondence with the maximum average f_oF2 azimuth (obtained by the three-point method) was good.

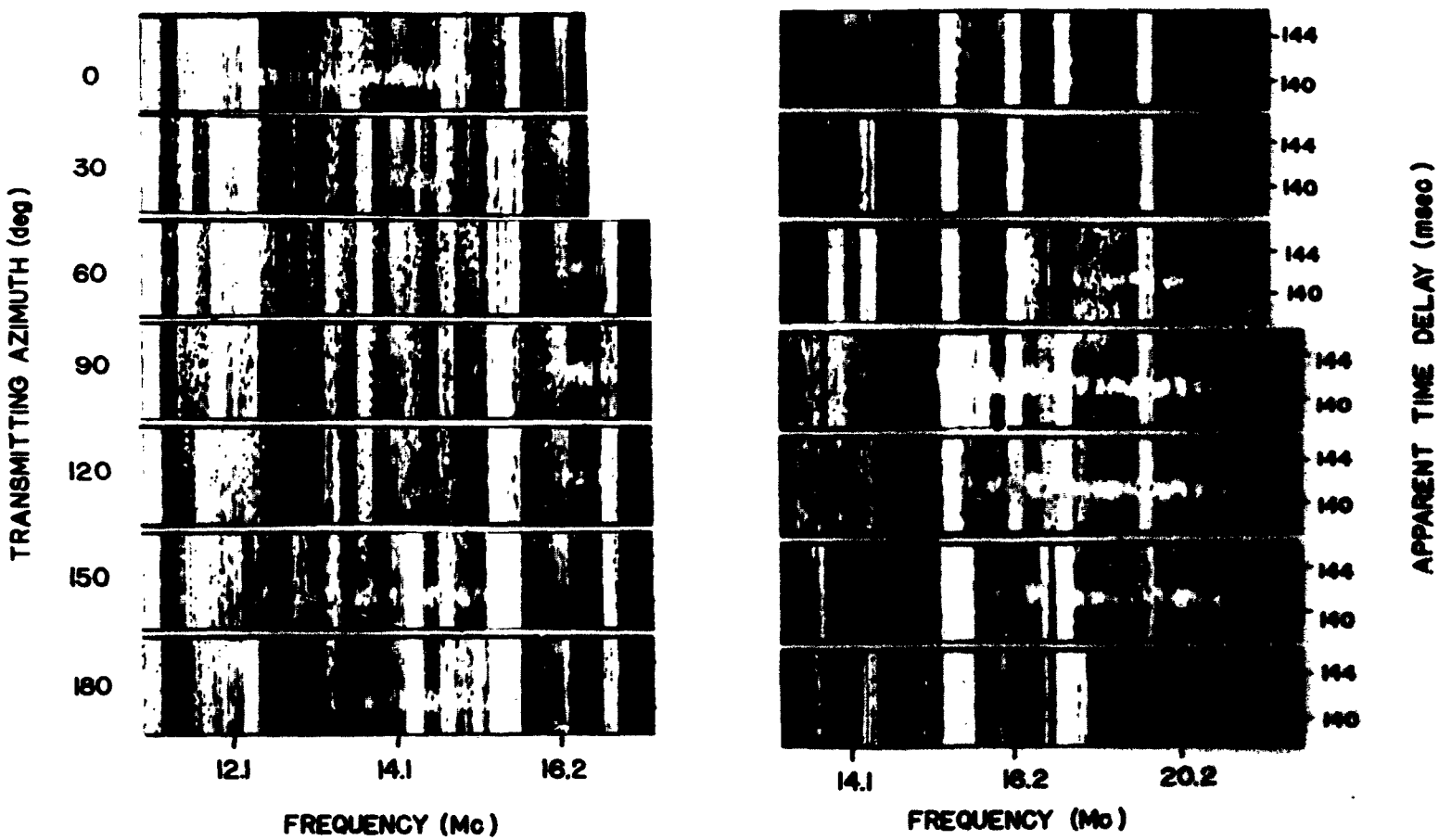

a. 26 April 1962, 0644 PST

b. 28 April 1962 0855 PST.

FIG. 27. STEP-FREQUENCY RECORDS SHOWING RTW SIGNAL STRENGTH VS FREQUENCY AND AZIMUTH AT STANFORD.

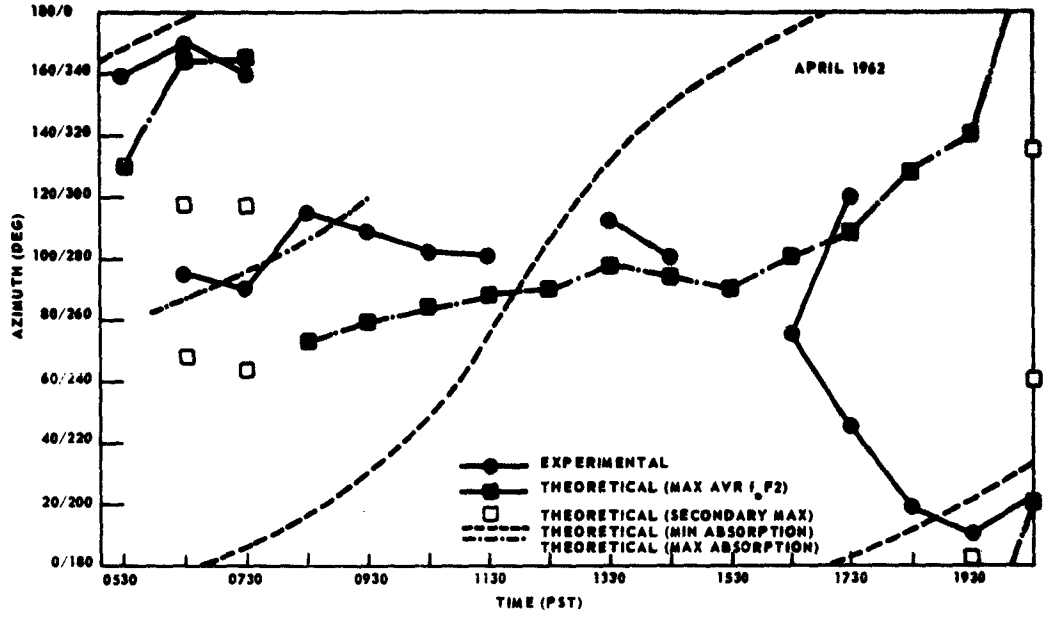

FIG. 28. THEORETICAL AND EXPERIMENTAL CURVES OF RTW-SIGNAL OPTIMUM AZIMUTH VS TIME. (April 1962, Stanford)

Figure 29 shows the optimum azimuths measured in May, with the April measurements also shown for comparative purposes. The two sets of data points, although differing in detail, are seen to be qualitatively similar except for the actual number of obtained points. The diagram of Fig. 20 shows why it was not possible to obtain as complete information for May as for April.

Figure 30 shows the three-point average f_oF2 vs azimuth obtained for 0730 PST in April, RASSN 50. It is significant that, except for the region immediately surrounding the minimum at 30°, the variation in the average f_oF2 is negligible. The minimum in propagation capability at approximately 30° azimuth at this time was noted experimentally, as can be seen in Figs. 25 and 28.

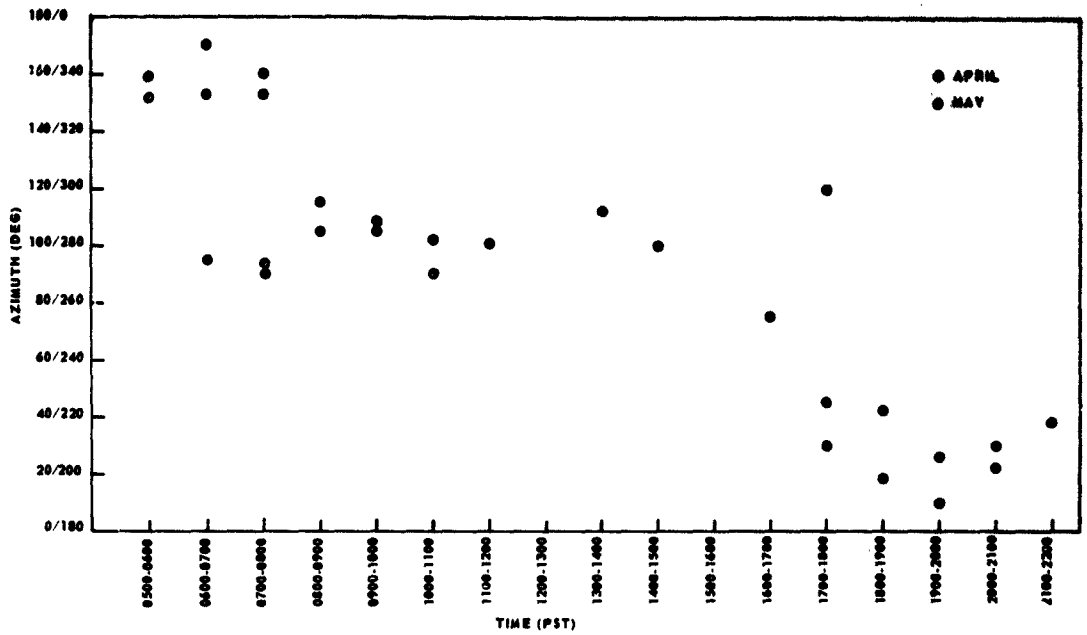

FIG. 29. EXPERIMENTAL AVERAGE RTW-SIGNAL OPTIMUM AZIMUTHS VS TIME. (2 April 21 May 1962, Stanford)

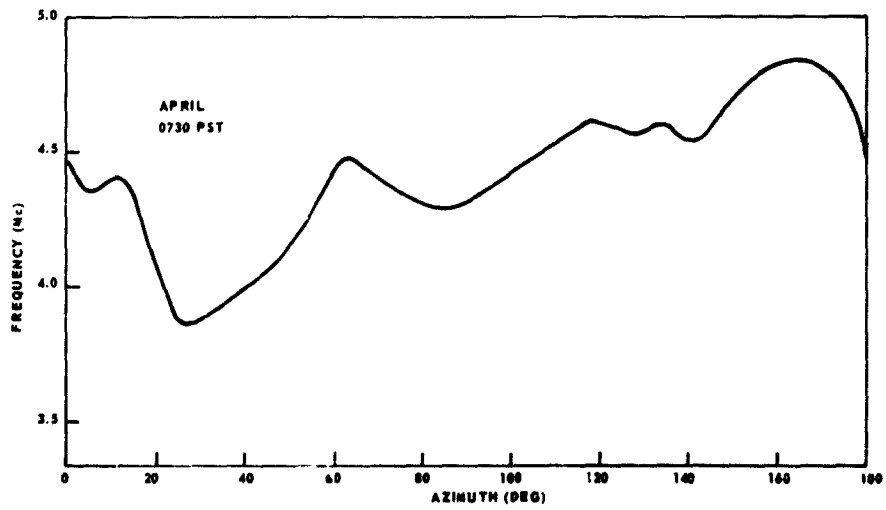

FIG. 30. PREDICTED THREE-POINT AVERAGE f_0F2 VS AZIMUTH AT STANFORD, APRIL, RASSN 50, 0730 PST.

4. An Explanation for Multiple Optimum Azimuths and "Echo of the Second Kind"

The explanation for the postdawn multiple optimum azimuths appears to be the following. The lower frequencies propagate best, as expected, in the minimum-absorption azimuth, as shown by Figs. 27a and 28, which is also the maximum average f_oF2 azimuth (Fig. 30). However, frequencies too high to propagate in this azimuth, due to insufficient critical frequencies, can be propagated in a generally east-west direction, through the subsolar point region, due to the higher critical frequencies in the sunlit hemisphere and the appropriate tilting conditions at the edges of the sunlit hemisphere. Note that the measured experimental azimuths in the 0630 - 0930 PST period lie very close to the azimuth of the subsolar point (theoretical maximum-absorption azimuth).

As mentioned earlier, ionospheric tilts on the path through the subsolar point should theoretically (on the basis of the simplest assumptions) be oriented longitudinally at the twilight line, enabling tilt modes to be launched through the dark hemisphere. The world map of f_oF2 for 0800 PST, RASSN 50, together with the great-circle path through the subsolar point, are shown in Fig. 31. The existence of the presumably required ionospheric tilts is strongly suggested by the predominantly longitudinal gradients of f_oF2. The dashed portions of the great-circle path indicate the approximate regions where tilt modes would be required if a frequency of 22 Mc is to be propagated, as was shown in Fig. 27b.

Also shown in Fig. 31 is the "twilight zone" great-circle path in which the lower frequencies were experimentally observed to be propagating (Fig. 28). Note that, although the minimum f_oF2 is essentially the same on this path as it is on the subsolar point path, the length of path in the low critical frequency regions is significantly greater on the twilight zone path, and hence the number of opportunities for ray penetration of the ionosphere is increased.

The absorption on such RTW paths through the subsolar point region would be expected to be quite high at lower frequencies if the D layer were being repeatedly traversed by the dominant ray paths (see Fig. 6). Figure 27a suggests that the lower frequency attentuation is

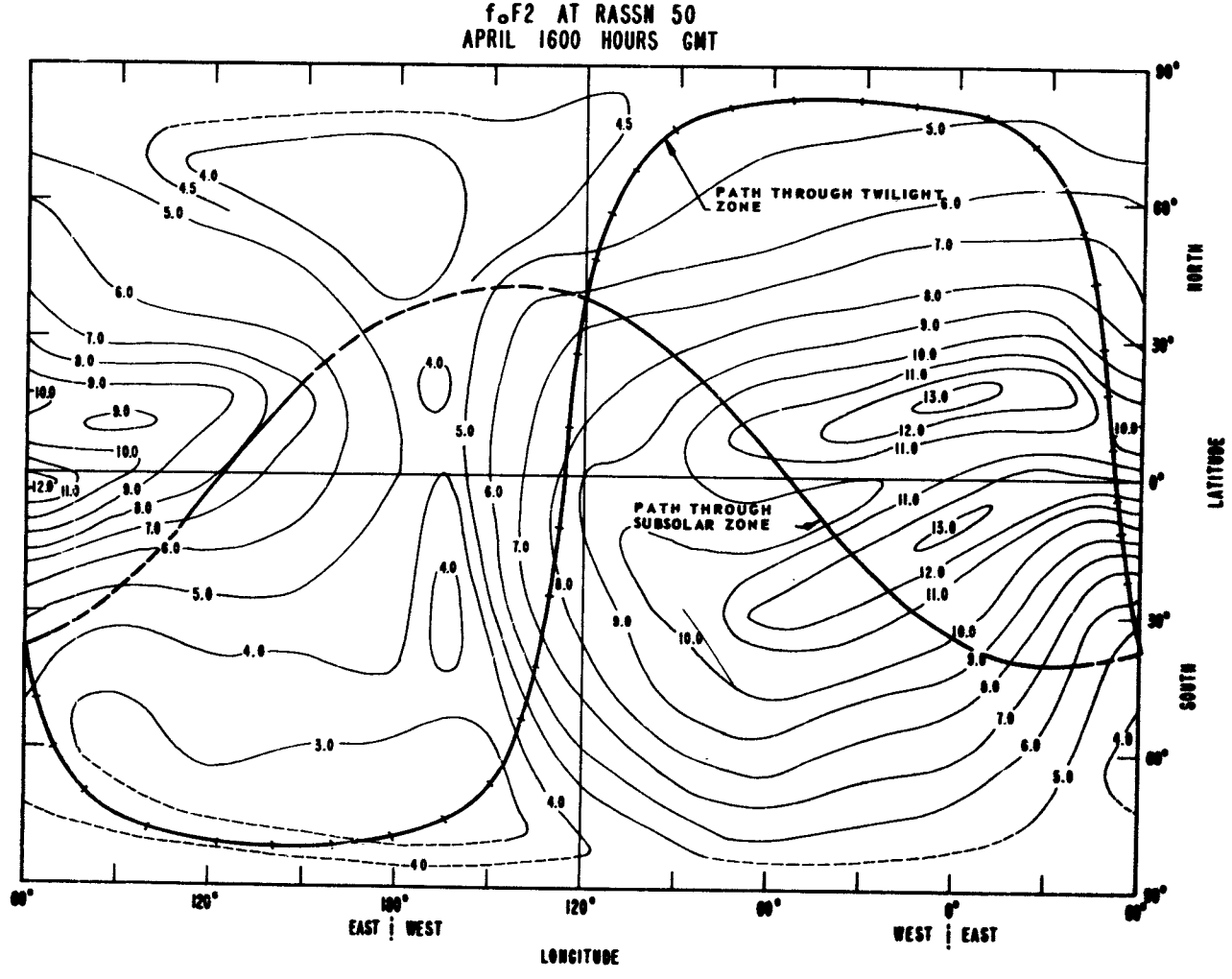

FIG. 31. WORLD MAP OF f_oF2 WITH TWILIGHT-ZONE AND SUBSOLAR-POINT GREAT CIRCLES THROUGH STANFORD. (RASSN 50, April, 1600 GMT)

indeed quite high compared with the propagation taking place in the theoretical minimum-absorption azimuth. This is indicated by the extremely sharp minimum frequency cutoff.

The observed RTW propagation through the subsolar point region is clearly a cause of "echo of the second kind" reported by Bailey [Ref. 13]. He has designated the usual twilight zone echo observed on distant hf radiotelegraph transmissions (due to RTW propagation) as "echo of the first kind;" and the echo occurring on circuits having short path lengths greater than 8,000 to 10,000 km--when the short path is most intensely illuminated--as "echo of the second kind." Bailey also stated that this echo (second kind) is more severe at times of high sunspot numbers and at those times when the subsolar point is between the transmitting stations and on the short path between stations. Applying the theory noted above, the characteristics noted by Bailey may be accounted for as follows:

1. At times of higher sunspot numbers, higher frequencies may be, and are, used due to the higher F2-layer critical frequencies available. Since absorption increases much less than the critical frequencies at times of higher sunspot numbers, attenuation on usual communications paths through the subsolar point would be greatly reduced.

2. "Echo of the second kind," as explained here, could only be experienced at stations in the sunlit hemisphere, since the tilt modes in the dark hemisphere would not reach the earth. The subsolar point would be required to lie on (or reasonably near) the great circle through the stations in order for the ionospheric tilts at the edges of the sunlit hemisphere to be utilized optimally. (It appears very doubtful, however, that the subsolar point would necessarily have to lie between the stations for the effect to be observed.)

5. Autumn Measurements

During 7 days in October 1961, a 20- to 60-Mc rotatable log-periodic antenna (receiving) was used in conjunction with the Collins LPA (transmitting) for optimum-azimuth measurements. A very small number of measurements were made at randomly chosen frequencies, the results of which are shown in Fig. 32. The general correspondence with the theoretical minimum-absorption azimuth (characteristic of winter) is evident, but deviations during daytime toward east-west are also present, as was

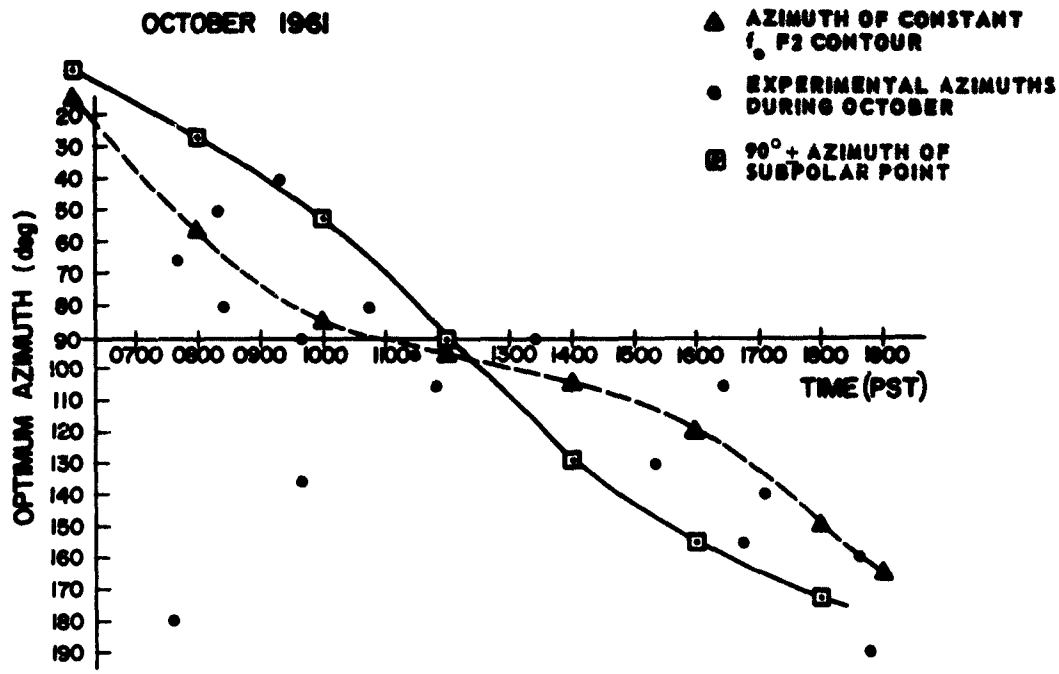

FIG. 32. OPTIMUM RTW-SIGNAL AZIMUTHS OBSERVED IN OCTOBER 1961, WITH CURVES OF THEORETICAL MINIMUM ABSORPTION AZIMUTH AND AZIMUTH OF CONSTANT f_0F2 CONTOURS AT STANFORD.

the case in the spring measurements. Although evidence is present in Fig. 32 which suggests multiple optimum azimuths, this phenomenon was not recognized at the time, probably due to the use of the manually tuned transmitter.

In addition to the theoretical minimum-absorption azimuth, the azimuth of the constant f_0F2 contours at Stanford (from the world map) is also shown in Fig. 32. This curve, besides having an interesting correlation with the data points (this is not generally true for all months) very graphically illustrates the well-known fact that the F2-layer density does not change in direct proportion to the sun's zenith angle (or, to put it another way, that constant f_0F2 contours are not circles centered on the subsolar point).

C. THE PROPAGATING FREQUENCY RANGE

1. Experimental Results

The principal objective during the experimental study of round-the-world propagation was to obtain, as completely as possible, information on the propagating frequency range and the variation of this range with time. It was believed that these data could provide more insight into the propagation mechanism for RTW signals than could any other information obtainable with comparable effort (such as time delays, pulse dispersions, optimum azimuths at fixed frequencies, signal strengths, and so on).

During the manual experiments (May - September 1961, described earlier) time permitted only the determination of the maximum RTW frequency as a function of time. Also, since the minimum transmitting frequency available was 12 Mc, it was not possible to measure the minimum propagating frequency when it was less than 12 Mc, as was often the case. In this period, the rather rough daily curves of MUF vs time were averaged every 20 min for 5 to 10 quiet days of each month. Figure 33a shows the average maximum frequencies propagated as a function of time of day for 10 magnetically quiet days in May for the lower curves, and for 7 quiet days in June for the upper curves. Similar curves for July and August are presented in Fig. 33b.

The curves of Fig 33 begin and end at onset and termination, respectively, of RTW propagation in azimuths roughly approximating the appropriate ground sunrise or sunset twilight-line azimuth for the month being considered. Since antenna azimuths generally were not optimized during the measurements, the curve shapes will be influenced somewhat by antenna patterns (caused by the change in optimum azimuth). Since the received signal strengths were high and the transmitting beamwidth was very broad (64°, 3-db beamwidth), this effect may be considered slight except possibly for the periods well after sunset and sunrise. At these times signal strengths decreased markedly (as would be expected due to path absorption).

There were times in these summer months when RTW propagation was apparently possible throughout the night period. These occurrences

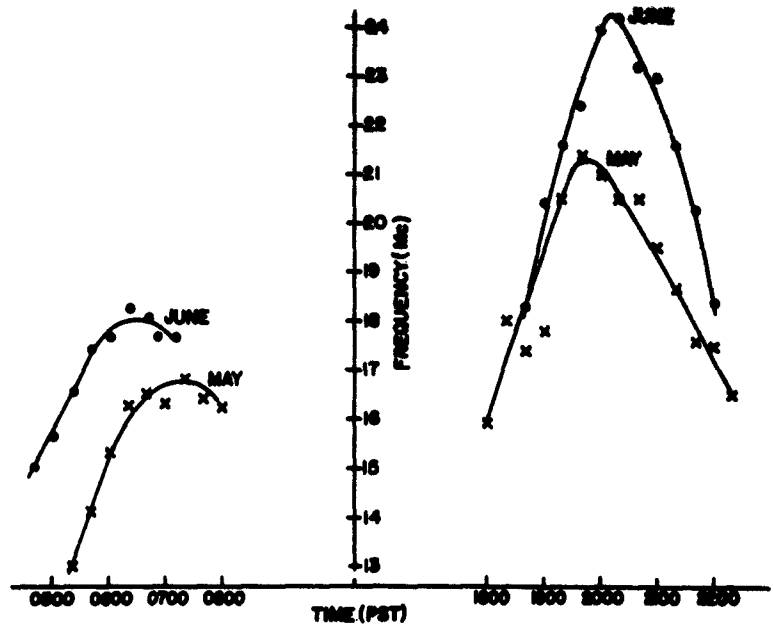

a. May and June

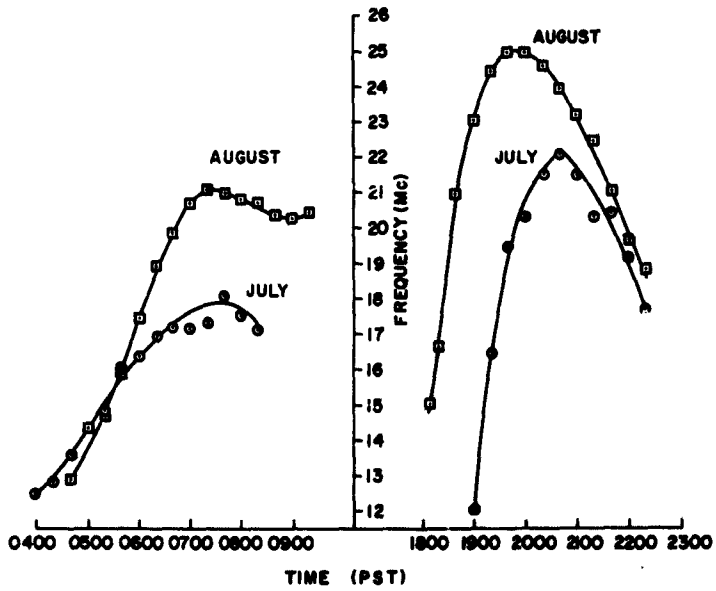

b. July and August

FIG. 33. AVERAGE MAXIMUM FREQUENCIES PROPAGATED AROUND THE WORLD VS TIME FOR QUIET DAYS IN 1961 AT STANFORD.

were not monitored sufficiently to determine the average propagating frequency range. The MUF at these times was normally in the 12- to 15-Mc range.

Since there were many more significant magnetic disturbances in July 1961 than in the surrounding months, and since August was unusually calm, it would appear that the normal positions for the July curves, Fig. 33b, should be somewhat higher (making them higher than June, Fig. 33a). Similarly, the August curves, for the same sunspot number, would normally be expected to be slightly lower. These conclusions arise from correlations that have been made between RTW signal MUF and magnetic indices, which will be given in the following section.

The automatic, sweep-frequency measurements in Spring 1962 provided more complete information concerning the RTW-propagation frequency range, and particularly gave the first LUF information obtained in the present study. Figure 20 showed the times when propagation was obtained during these tests. In Figs. 34a and b are shown the average frequencies propagating as a function of time for 24 March - 22 April and 23 April - 21 May, respectively (times not having four or more data points are omitted). As shown, magnetically quiet days were averaged for the twilight times while all days were used in the averages during most of the daytime. The reasons for this procedure were (1) high magnetic activity caused less effect on daytime propagation, as seen in Fig. 20, and (2) much less difference was noticeable in frequencies obtained, on disturbed days, during midday than during twilight periods. This would be expected, since, as seen in Fig. 28, the propagating azimuths in daytime were nearly east-west, avoiding the auroral zones (where the greatest effects of magnetic storms are normally noticed) by wide margins.

The usual criterion for selecting days for the averages of Fig. 34 was $\Sigma K_p < 12$ (arbitrary) but some days (or parts of days) with greater ΣK_p were included in the averages if RTW propagation appeared "normal" (from Fig. 20 and from the frequencies obtained). Days considered "quiet" in the first period were 26 through 31 March and 1, 13, 14 and 19 April with the exception of 28 March (PM) and 1 April (AM), which were omitted. Quiet days selected for the second period were 24 through

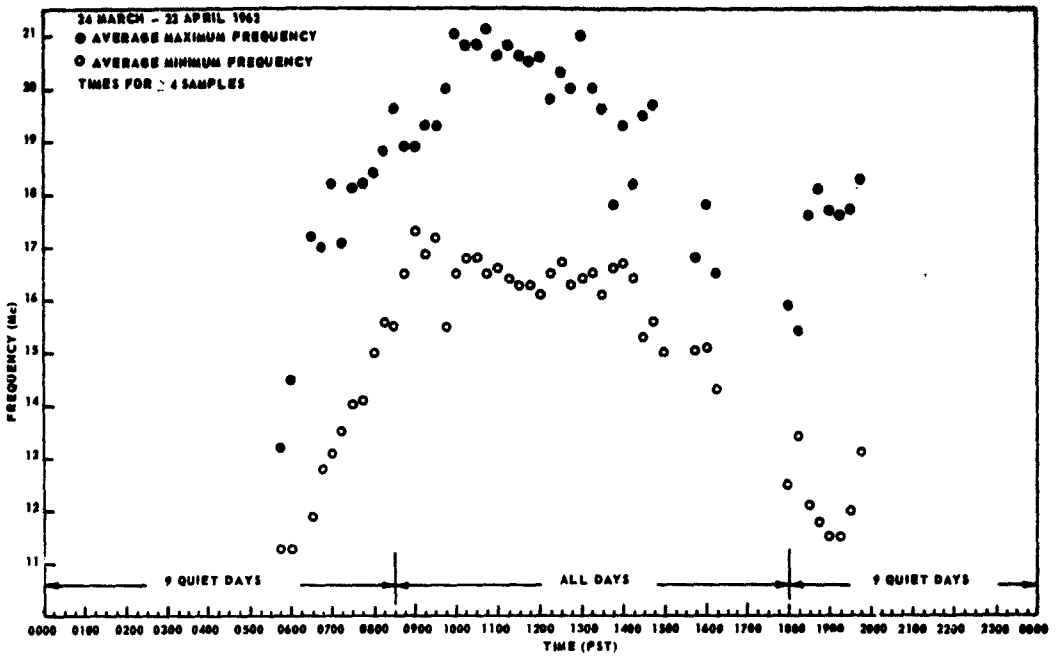

a. 24 March - 22 April 1962.

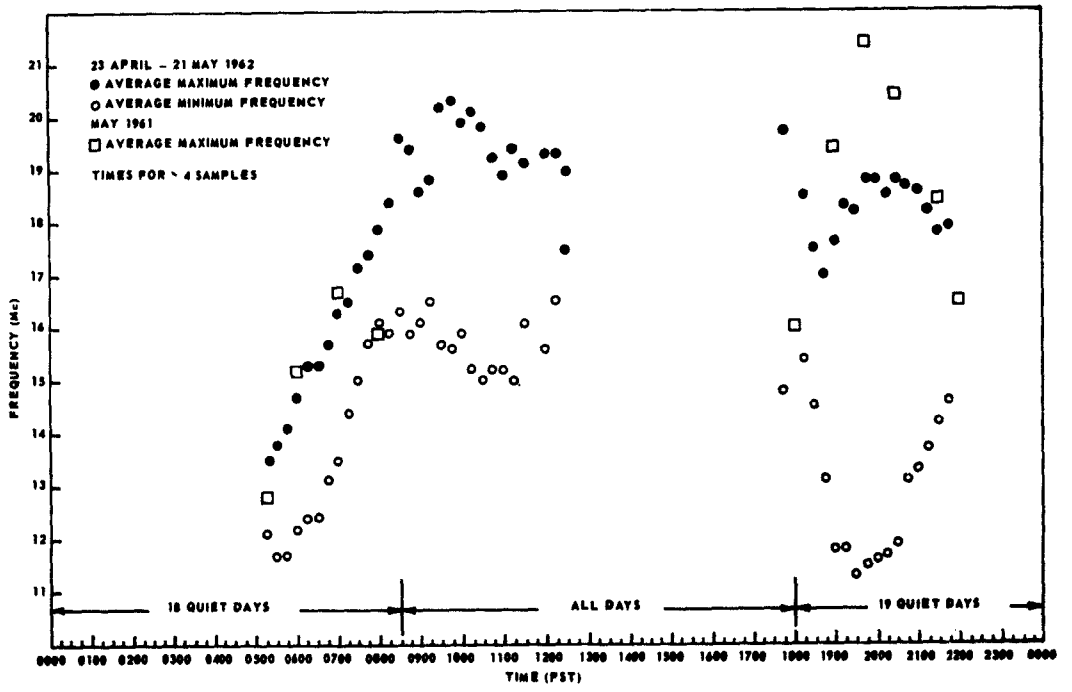

b. 23 April - 21 May 1962

FIG. 34. AVERAGE MAXIMUM AND MINIMUM FREQUENCIES PROPAGATED AROUND THE WORLD VS TIME, AT STANFORD.

28 April, 29 (PM), 30 (AM), 1 May (AM), 3, 4, 5, 8, 9, 10 (PM) May, 11, 12, 16 (PM), 17, 18, 20, 21. ΣK_p and the days of occurrence of RTW propagation in these periods are shown in Fig. 20.

Some significant features of Fig. 34a are:

1. The MUF and LUF increased steeply, and nearly linearly, after dawn. The MUF rise reflects the rise in f_0F2 in the vicinity of the transmitter, while the LUF rise is attributed to the increased absorption, also in the vicinity of the transmitter on the optimum RTW path.

2. The LUF reaches a minimum at sunset (when the transmission point is on the twilight line), again reflecting the fact that the twilight-line path is the minimum-absorption RTW path.

3. There was a peak in MUF in the postsunset period. This peak was very pronounced in the summer curves of Fig. 33.

4. The MUF was maximum in the vicinity of noon.

5. The LUF had a maximum in the vicinity of 0900 PST. This may not be real, since the antennas were programmed to rotate, at 2-hour intervals, to the theoretical minimum-absorption azimuth. As was seen for April 1962 in Fig. 28, this azimuth was in very great error until nearly noon, being orthogonal to the actual RTW-signal optimum azimuth at 0900 PST. In the 1200-1400 PST period the antennas were properly oriented. If the 0900 peak is real, as Fig. 34b would suggest, it could be caused by a change in mode structure, in which a greater part of the path was in tilt modes at midday, resulting in decreased absorption. Increased focusing at midday could also cause the effect.

6. RTW propagation was very spotty in the 1500-1800 PST period, due in part to the improper antenna bearings, and in part, apparently, to the fact that the MUF and LUF (for the system sensitivity available) overlapped on many days. It is significant that this period corresponded with the "predawn" period in the antipodal region.

The data plotted in Fig. 34b for the 23 April - 21 May period are similar in many ways to that plotted in Fig. 34a for the earlier period, but with significant exceptions. Some of these exceptions follow:

1. The afternoon minimum of RTW-signal activity is more pronounced than in the preceding period. Note the apparent joining of the MUF and LUF in the vicinity of 1245 PST. This is attributed in part to the fact that absorption for this period should be higher than in the previously considered period. Also, the antipodal

region was approaching winter, with attendant lower predawn minimum f_oF2's.

2. There is a steep rise in LUF following 1115 PST and a pronounced dip immediately preceding this rise. During this period, the transmitting and receiving antennas were set east-west for the hours between 0800 and 1800 PST. Considering the antenna beamwidths, it is seen in Fig. 29 that the antenna directions were proper; hence the phenomenon must be considered real. Also from consideration of Fig. 29, it is concluded that the phenomenon is caused by the great change in optimum azimuth in this morning period, accompanied by a change in mode structure. (Since propagation in midmorning was through the subsolar-point region, it would appear likely that tilt modes were more prevalent on this path than on the earlier morning path when the LUF was the same but the optimum azimuth was the theoretical minimum-absorption azimuth.)

3. The sunset propagation period became better defined and larger than for the earlier month. The typical summer MUF peak, seen in Fig. 33, is evident.

4. The sunset period exhibited a well-defined LUF minimum occurring shortly after ground sunset.

5. The LUF increased significantly after the sunset minimum. This is interpreted as being caused by absorption in the daylight hemisphere, requiring D-layer penetrations of the predominant RTW mode in that hemisphere. A trace of this phenomenon is seen in Fig. 34a also.

6. Data points from one year earlier (Fig. 33) are shown. The higher-frequency evening peak is presumed due to the decreased sunspot number in 1962. The cause of the coincidence in morning curves is not explained by this fact, however. The difference is possibly due to variations in magnetic activity and/or to the fact that much less data were available for construction of the manually obtained May 1961 curves.

7. The May 1961 curve turns downward in the postdawn period. This is almost certainly due to the fact that the antennas used were fixed in directions well away from that which was appropriate at the time of this down-turn. As previously mentioned, the antennas were correctly positioned in May 1962.

2. LUF and Path Loss Predictions

If the LUF and path loss are to be determined for RTW propagation in a nonempirical manner, it is necessary to have detailed information concerning the propagation medium and the global geometry of the propagation mode(s). As seen in Fig. 6, for example, the

assumptions made concerning the geometry of the propagation mode can have first-order effect on the path loss due to absorption.

To whatever extent the ionosphere represents a sphere concentric with the earth, focusing of the ray paths may be expected to affect the apparent path loss. Although this focusing is not expected to be great, it may nonetheless be significant, particularly in the cases where RTW propagation takes place through the subsolar-point region, when effective ionospheric tilts are almost totally longitudinal. Lacking information on the extent of focusing, calculations of effective path loss must be based almost totally on empirical information.

During the experimental tests which have been described earlier, no systematic measurements of RTW signal strength were attempted. During the automatic tests this would not have been readily possible due to the use of an intensity-modulated display (see Fig. 25). During the manual tests this would have been possible, but time did not permit making the measurements. Further, since receiving antennas were fixed and the optimum azimuth was at that time unknown, the results of such measurements would have had doubtful value. Also, the takeoff angle(s) and azimuth(s) of the propagating mode(s) would have had to be known, along with the antenna patterns, if such measurements were to be very useful. This information was not known.

During the manual tests, pulse signal strengths, after the first circulation of the earth, averaged on the order of 30 μv across 50 ohms from the receiving antenna (the equipment parameters were given earlier). During the study, variations from no signal to signals of over 100 μv were encountered, depending on time of day, frequency, and particularly, magnetic conditions.

Second circulations of the pulses were always found to be 15 db to 20 db or more down from the first circuit. Hess [Ref. 12] and Isted [Ref. 8] have given figures of 5 to 10 db. It is possible that the shorter pulse length of the experimental work described here is the cause of at least part of the difference, since the received pulses were found to be significantly dispersed compared with the 1-msec pulse transmitted. Hence, the use of longer pulses would result in greater "overlapping" of the received pulses corresponding to the different

paths involved. It is assumed that the total path-length differential for the second circuit is twice that for the first circuit; hence an apparently stronger received signal on the second circulation would be obtained for greater pulse lengths than used in the present work.

If the second circulating signal is considered to be primarily a repetition of the mode structure of the first circulation, which is reasonable to assume--particularly if the ray paths are close to being great circles, it may be concluded that the difference in field strength between the first and second circulations should be a first-order measure of path loss due to absorption. If this is so, then Isted's findings at 37 Mc are not surprising in light of Fig. 6. It is not clear from Hess' reports how often, or at what frequencies, differential signal strengths of as low as 5 db were obtained. However, in one test description [Ref. 9], it appears that differential signal strengths averaged approximately 9.5 db at the "best" times, at 20 Mc. Comparing Fig. 6, and in consideration of the foregoing, there does not appear to be any reason to rule out earth-ionosphere-earth hop modes in RTW propagation (with associated D-layer absorption) on the basis of reported observations of the differential signal strength between first and second circulating signals.

If it is assumed that RTW propagation in the sunlit hemisphere is predominantly the usual hop mode, then it is possible to make predictions concerning the relative path losses as functions of frequency and time, at least to whatever extent absorption will be the cause of such changes in path loss. It is clear that the variation of the azimuth of propagation, as well as the precise variation of mode structure, can affect absorption losses. Some calculations follow which show the qualitative association of signal strength and LUF with theoretical absorption variations.

It is qualitatively noticeable in Fig. 22, from the change in signal-to-noise ratio, that the RTW signal strength gradually increased as the afternoon progressed. The change in signal strength from 1310 PST to 1715 PST was on the order of 15 db. A quantitative estimate of the theoretical signal-strength change due to absorption changes will now be derived.

From curve 1 of Fig. 6, it is determined that the absorption for the path through the subsolar point, at 15 Mc, may be on the order of 39 to 48 db, depending on the assumption of mode structure. Using these numbers for α_{ss} in Fig. 5, the absorption at 1310 LT is predicted to be between 18 and 22 db. From Fig. 6, the minimum absorption (at sunset) should be between 6 db and 16 db, depending on the propagation mode assumed. Hence, within the small number of choices of mode assumption possible in Fig. 6, it is possible to predict changes, due to absorption, in signal strength of from 2 db to 16 db.

The fact that the measured change in field strength was roughly 15 db could mean that the propagation mode was experiencing 22 db of absorption at 1310 PST and, say, 7 db of absorption at 1715 PST. This conclusion has obvious connotations regarding the propagation modes. Other elements, such as a change in the focusing factor, could play a significant part in the change in signal strength. In any case, more than 1 day's data, together with a greater understanding of the focusing possibilities and the propagational mode variations, should be available before any firm statement is made concerning prediction of absorption effects on signal strength. Even so, it is interesting that use of curves 1 and 4 in Fig. 6 predicts the change in signal strength in Fig. 22 so closely.

Next, consider the prediction of the LUF variation in Fig. 34a. If it is assumed that the variation is due to absorption changes only, the curves of Fig. 6 are applicable for α_{ss} and α_{min}. Further, to the extent that propagation is in the minimum-absorption azimuth, Eq. (5) will aid in determining the theoretical variation of absorption with time. Figure 28 shows that the optimum azimuth was not close to the theoretical minimum-absorption azimuth after about 0800 PST, and this must be taken into account. However, as noted previously, the antenna directions were in the theoretical minimum-absorption azimuths throughout the day; therefore the LUF variation may reflect propagation in this azimuth, at least until 0900 PST, at which time the rise in the LUF ceased.

If the only variable in path loss is assumed to be absorption, and if system sensitivity is not a function of frequency, then the LUF curve of Fig. 34a will represent a constant-absorption curve. Curves 3 and 4 of Fig. 6 give estimates of theoretical limits of absorption when it is minimum.

Choosing curve 3 of Fig. 6 arbitrarily, it is predicted that the absorption at 11.3 Mc (the measured minimum morning LUF) will be 28 db. It is then of interest to construct an LUF vs time curve in which absorption is a constant, 28 db. Using Eq. (5), however, it is not obvious how this should be done, since Eq. (5) gives absorption the value zero at sunrise, not 28 db. It would just as clearly be incorrect to add 28 db to all values of α obtained by Eq. (5) in conjunction with, say, curve 1 of Fig. 6. A reasonable compromise appears to be the modification of the result of Eq. (5) as follows.

A partial plot of the factor α/α_{ss}, from Eq. (5), is given in Fig. 35 for 7 April (the middle day of the experimental period represented in Fig. 34a). The morning minimum occurs at approximately 0550 PST. As seen in Fig. 34a, this is precisely the time of the experimental minimum

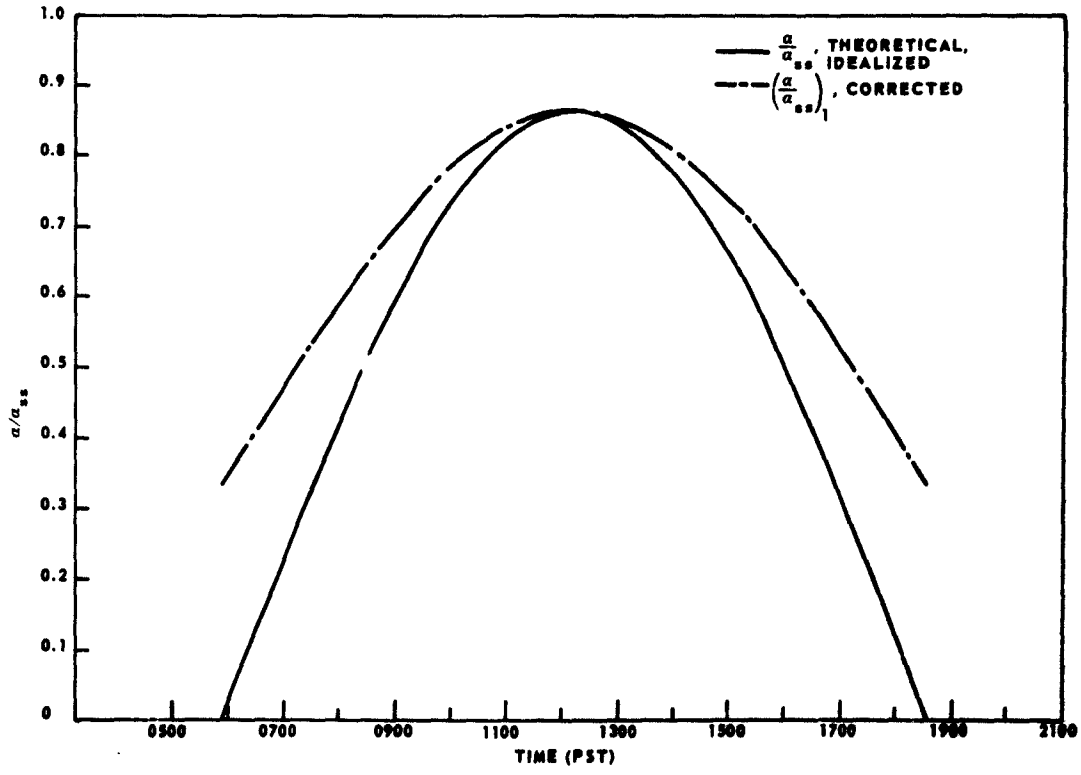

FIG. 35. IDEALIZED AND CORRECTED CURVES OF α/α_{ss} VS TIME FOR 7 APRIL AT 37°25' N LATITUDE.

LUF. The theoretical α/α_{ss} curve of Fig. 35 must now be modified to take into account the fact that the absorption is not zero at 0550 PST, but presumably 28 db for 11.3 Mc. It is a curious feature of the curves of Fig. 6 that the ordinate values of curve 1 are almost precisely three times those of curve 3, although they were independently obtained from semi-empirical world maps and nomograms [Ref. 14]. Hence the twilight-line absorption may be accounted for by placing a point at α/α_{ss} = 0.333 at 0550 PST, in Fig. 35. It is now necessary to construct some reasonable curve between this point and the noon point α/α_{ss} = 0.863. This has been done by adding a linearly decreasing portion of the twilight-line value to the theoretical curve. Specifically, a new curve, $(\alpha/\alpha_{ss})_1$, is constructed so that

$$\left(\frac{\alpha}{\alpha_{ss}}\right)_1 = \frac{\alpha}{\alpha_{ss}} + \frac{0.863 - \frac{\dot{\alpha}}{\alpha_{ss}}}{3(0.863)} \qquad (6)$$

at all times. This method appears to be as reasonable as any other, the resultant curve being shown in Fig. 35.

With the curve for $(\alpha/\alpha_{ss})_1$, it is possible to construct a theoretical LUF curve for the period represented by Fig. 34a. This is done by use of curve 1 of Fig. 6 and assuming a constant absorption of 28 db. This curve is plotted in Fig. 36 along with the experimental points from Fig. 34a.

It is seen in Fig. 36 that the predicted LUF vs time curve does not account for the midday decrease in LUF. As stated previously, agreement should not be expected due to the fact that the experimental optimum azimuth was not the theoretical minimum-absorption azimuth, for which the predicted curve applies, in midmorning. However, in the immediate vicinity of noon, the predicted curve is expected to be applicable, since the measured azimuth was approximately the minimum-absorption azimuth. A variation of the mode structure at midday is a possible explanation for the LUF decrease observed. In midmorning, when RTW propagation was optimum through the subsolar point region, $\alpha/\alpha_{ss} = 1$ and the curves of Fig. 6 could presumably be used directly to find the LUF for a specified absorption. From Fig. 6, the LUF for 28-db absorption for a path through the subsolar point region is between 18 and 19.5 Mc,

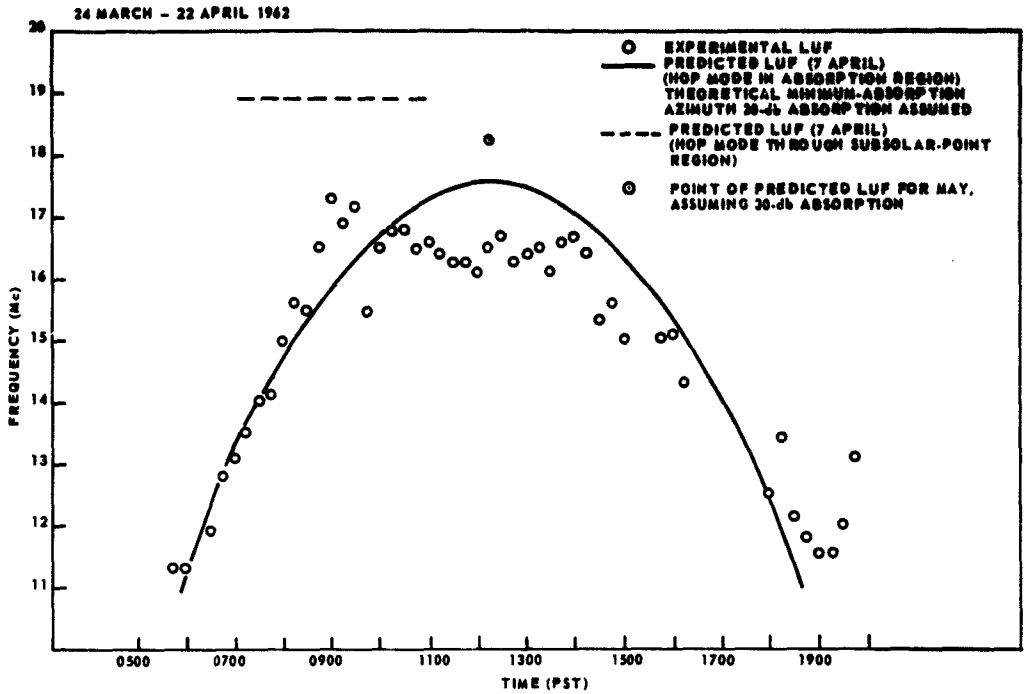

FIG. 36. CURVES OF EXPERIMENTAL AND PREDICTED LUF FOR RTW PROPAGATION VS TIME. (24 March - 22 April 1962, Stanford; constant absorption of 30 db assumed)

depending on assumption of mode. The lower figure is in better agreement with the experimental results, as seen in Fig. 36.

It is interesting to consider some of the implications of assuming that the foregoing premises (concerning the effects of absorption on RTW-signal path loss) are basically correct. For instance, it might be desired to know what increase in system sensitivity would have been required to decrease the midday LUF from approximately 16.6 Mc to 15 Mc, in the situation shown in Fig. 34a. From curve 2 of Fig. 6, α_{ss} = 40 db for 15 Mc. From Fig. 35 it is seen that $\alpha = 0.863\ \alpha_{ss}$, or 34.5 db. Since the assumed maximum allowable absorption was 28 db (in Fig. 36), a 6.5-db improvement in system sensitivity would apparently be required. (This could have been achieved in the experiment by increasing power from 30 kw to 135 kw, for instance.)

The above calculation of the change in path absorption with a change in frequency showed $d\alpha/df$ to be a comparatively large negative number. It should be expected, therefore, that if the many assumptions (given in this section) regarding absorption are reasonably correct, the LUF should be well defined (not showing great variations day-to-day except possibly for days of magnetic disturbances) due to the comparative stability of the D layer day-to-day. In Fig. 37 are shown the daily LUF data points for the period 24 March - 22 April 1962, for 1215 PST. The average of these values is the 1215 PST point of Fig. 34a.

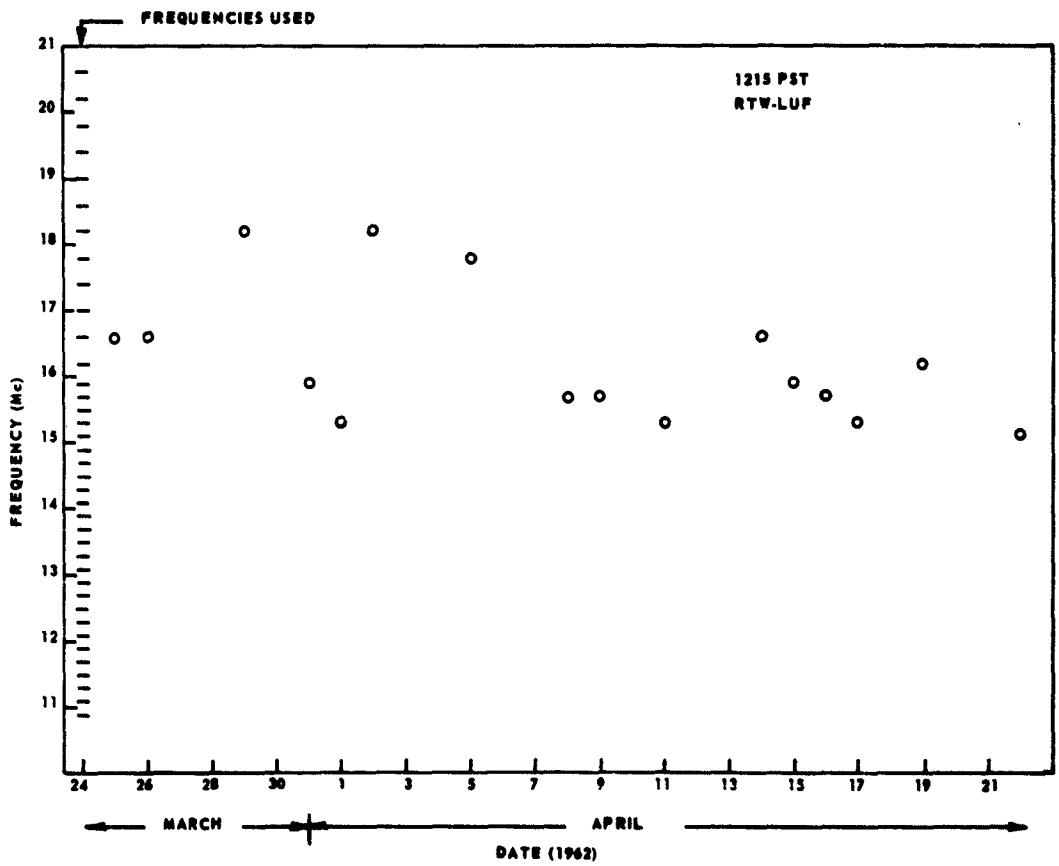

FIG. 37. DAILY EXPERIMENTAL RTW-SIGNAL LUF MEASURED IN THE PERIOD 24 MARCH - 22 APRIL 1962 AT STANFORD, 1215 PST.

Due to the intense interference which almost always appeared on most, and very often on all, of the five operating frequencies in the 16- to 18-Mc range, the three data points above 17 Mc (Fig. 37) have doubtful validity. Even if valid, it is seen that more than half of the LUF's were in the 15- to 16-Mc range, indicating the comparative stability of the LUF lower bound, and lending support to the above assumptions regarding the role of D-layer absorption in RTW propagation.

Another method which may be used to assess absorption effects on RTW propagation, in addition to LUF measurements and signal-strength measurements at a fixed frequency vs time, is the measurement of signal strengths vs frequency at a fixed time. Results of such an experiment have been reported for one day (25 January 1961, midmorning) by Hoogasian [Ref. 23]. The test, using pulse transmitters, employed six frequencies in the 13.9- to 27.8-Mc range, a log-periodic transmitting antenna, a sloping Vee receiving antenna, and similar, roughly calibrated receivers. The result showed an essentially linear signal-strength increase of 16 db as frequency increased from 14 Mc to 19 Mc (and a subsequent decrease in strength to the MUF around 26 Mc--presumably caused by a decrease in the number of propagating modes superimposed both in azimuth and in elevation).

A rough prediction for the presumed absorption change over this frequency range will now be made with the aid of Figs. 5 and 6. For 25 January, Fig. 5 shows α/α_{ss} would be on the order of 0.45 (at 0930 LT) for the theoretical minimum-absorption path (interpolating between curves). From curve 1, Fig. 6, for 14 Mc α_{ss} is 57 db, and α is thus on the order of 27 db. Similarly, α_{ss} for 19 Mc is 30 db, and α is thus approximately 13 db. Hence, the predicted change in signal strength due to absorption is 14 db.

The foregoing comparison of the observed dependencies of signal strengths on time and frequency and the LUF on time leave little doubt that D-layer absorption is important in determining the relative path loss in RTW propagation, although it is not a primary cause of absolute path loss. With suitable assumptions, the average effects of absorption on the strength of RTW signals appear to be quantitatively predictable. Further, the findings of this section strongly support the premise that

earth-ionosphere-earth hop modes are the dominant propagating mechanism for RTW propagation in the daylight hemisphere.

3. MUF Prediction

In order to accurately predict the variation of the RTW-signal MUF with time, it is necessary to have information regarding the propagation modes. If this information is not available, one may assume a propagation mode, and then calculate an MUF prediction. If the prediction corresponds with experimental data, it is reasonable to assume that the mode assumption was basically correct, providing such an assumption does not result in conflicts with other data. If the prediction does not correspond with experimental data, the manner in which the two quantities differ may provide a clue to the actual propagation modes.

The latter situation was found to be the case in RTW-signal MUF prediction. For example, Fig. 11 showed the June MUF predictions for twilight times. The assumptions made in obtaining the curves were great-circle propagation, 4000-km hop modes between F2 layer and ground, and RASSN 50. The position of individual reflections from the F2 layer was not specified. The 4000-km MUF for the ionosphere was calculated every 1000 km along each 40,000-km path, and the RTW-signal MUF was then selected as the highest 4000-km MUF in the 4000-km interval having lowest mean MUF. Figure 10 illustrated the method used.

Using the optimum experimental azimuths (which corresponded with the theoretical minimum absorption azimuths, as seen in Fig. 24), theoretical MUF vs time curves were constructed for June, as shown in Fig. 38. The curve for RASSN 85 applies for June 1961. The upper curves are the experimental curves from Fig. 33a. The theoretical and experimental curves are roughly similar in shape, and it appears that the curves obtained from the world maps are able to predict with a fair degree of accuracy the times of onset and termination of enhanced RTW-propagation conditions for that month, as well as the time when the highest frequency was propagating. Comparison of the curves for May in Figs. 11 and 33a shows that the same general correspondence exists for May (about 1.5 Mc should be added to the May curves of Fig. 11 to correct for the higher RASSN).

There is a great discrepancy between predicted and experimental maximum frequencies obtained in the evening hours for May, June, and July.

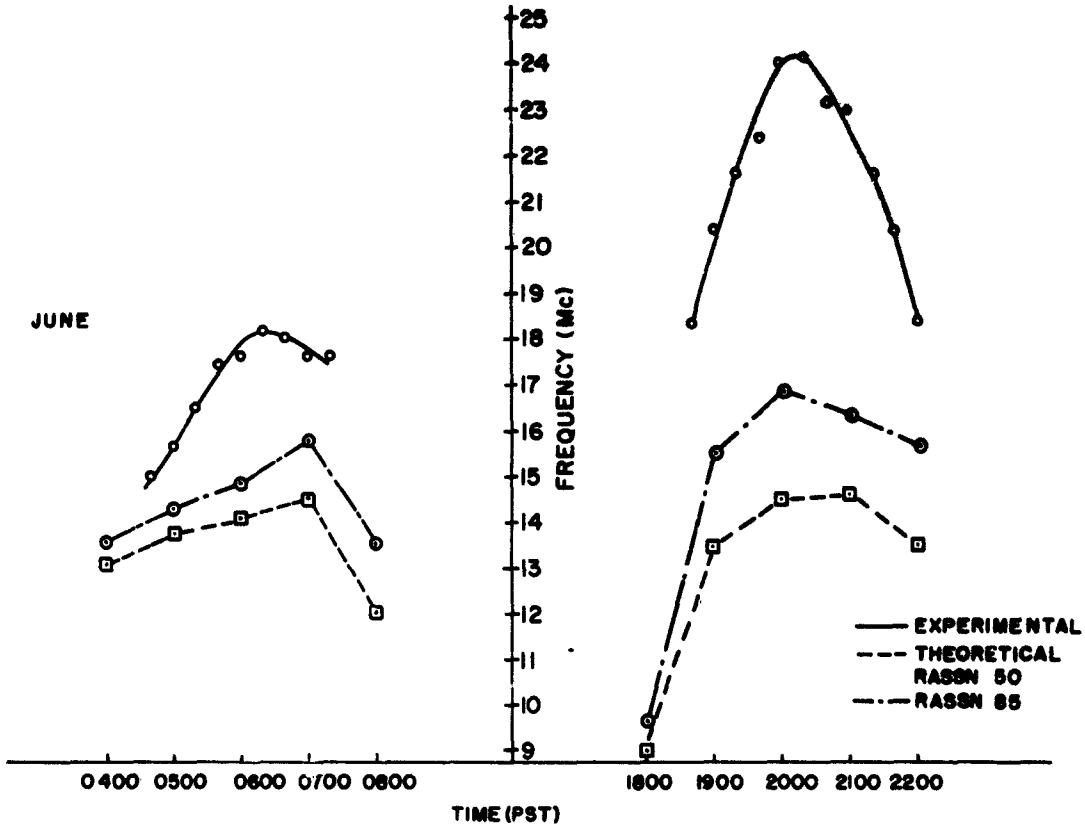

FIG. 38. EXPERIMENTAL AND PREDICTED CURVES OF RTW-SIGNAL AVERAGE MUF VS TIME, JUNE 1961, STANFORD.

In fact, the maximum frequencies predicted by the world maps, used in the way indicated above, were essentially equal for morning and evening.

In Fig. 14 was shown the world map of f_oF2 for 2000 PST, June, RASSN 50, together with the twilight-line great circle and the twilight-zone great circle through Stanford. It is seen in Fig. 14 that the minimum f_oF2 on the path through Stanford is predicted to occur to the northeast, and at relatively close range. The difference between the average experimental MUF (24 Mc) and predicted MUF (17Mc) for this path is quite significant, and has been explained on the basis of tilt modes through the low f_oF2 region [Ref. 21]. Substantiating evidence is presented in later sections.

In order to predict the MUF when ionospheric tilts are present (possibly permitting more shallow angles of incidence of the ray paths on the ionosphere), great detail must be known concerning the degree of effective tilt and the effective reflection height. The highest frequency that may be reflected from the ionosphere, f, is given by

$$f = kf_o \sec \phi$$

where k is a complicated function dependent on the ion distribution and distance, f_o is the critical frequency of the layer, and ϕ is the angle of incidence of the ray on the lower boundary of the ionosphere [Ref. 14].

For a virtual height of 350 km, and for a 4000-km path, k may be on the order of 3.75 [Ref. 14]. Based on a flat ionosphere where $f = f_o \sec \phi$, this would indicate an effective angle of incidence of $74^\circ 32'$. If, for example, this flat ionosphere is tilted longitudinally at 3 deg, making the angle of incidence $77^\circ 32'$, sec ϕ increases to 4.63, and the MUF would increase on the order of 24 percent. This type of situation, and particularly two such reflections occurring consecutively, can account for the observed MUF increases over predicted values based on assumed hop modes.

In Fig. 39 are shown the experimentally measured MUF's vs time for 24 March - 22 April 1962, together with a number of predicted curves from world maps. The predicted curves are for the 4000-km MUF at Stanford in the two directions (180° apart) associated with the experimental optimum azimuths (shown in Fig. 28). In the early-morning period two optimum great-circle paths existed, and hence four predicted curves are shown at this time.

It should not be expected that the RTW-signal MUF should always be determined at the point of transmission, but it is clear that the ionospheric conditions in the vicinity of the transmission point will place definite constraints on the MUF. In the early-morning period, in Fig. 39, it is seen that the experimental MUF was very markedly higher than the predicted twilight-zone 4000-km MUF to the northwest of Stanford, but considerably lower than the 4000-km MUF in the opposite direction.

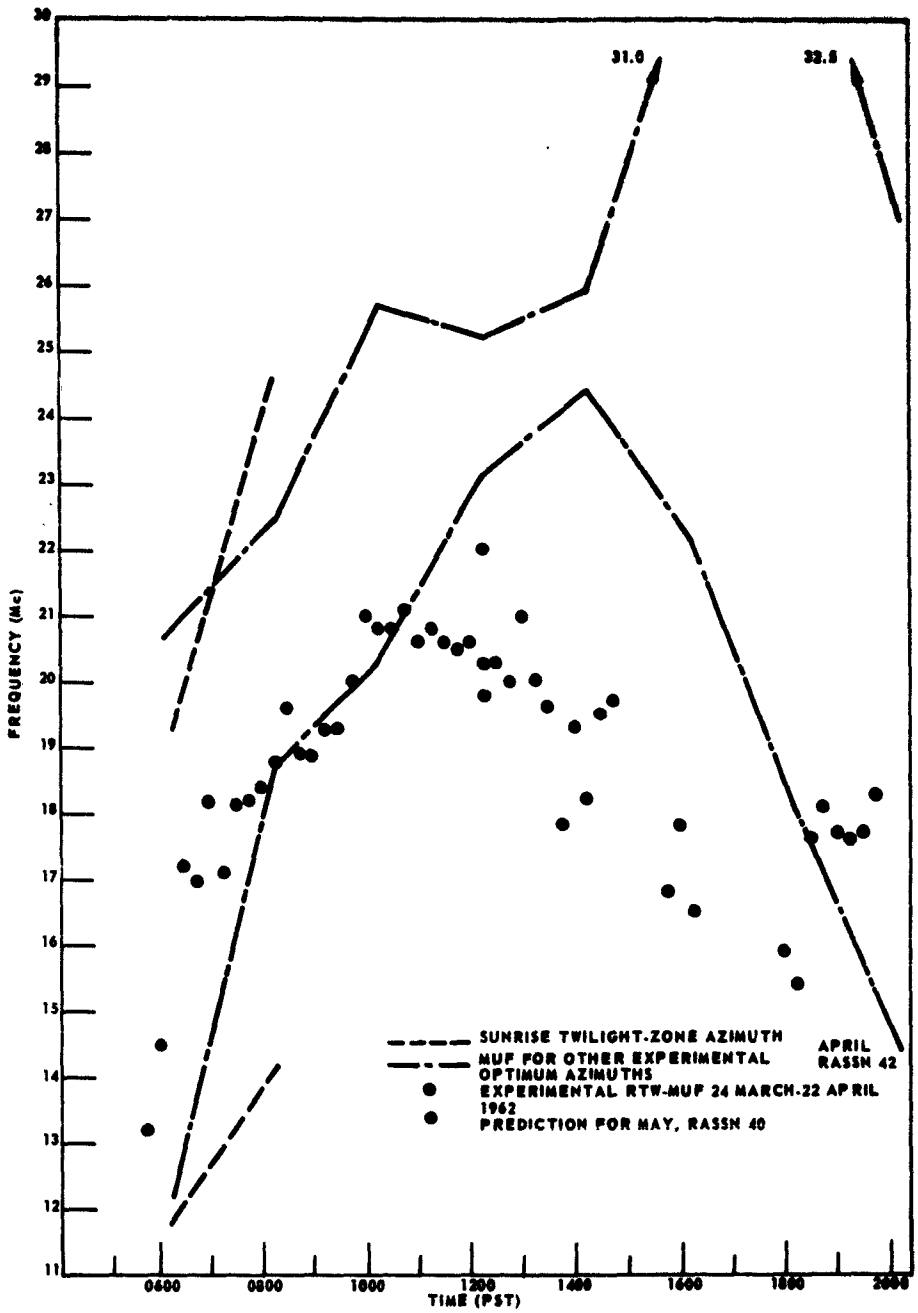

FIG. 39. PREDICTED 4000-km MUF IN TWO DIRECTIONS CORRESPONDING WITH EXPERIMENTAL OPTIMUM-AZIMUTH GREAT CIRCLE VS TIME TOGETHER WITH AVERAGE EXPERIMENTAL MUF'S AT STANFORD.

Hence, MUF enhancement due to the appropriately oriented dawn-region ionospheric tilt is indicated. It is remotely possible that the experimental MUF points could correspond to propagation conditions through the subsolar-point region (which would have been off the sides of the transmitting and receiving antennas), but such propagation was never noted during the variable azimuth tests when the antennas were in the twilight-zone directions (see Fig. 27a).

From 0800 to 1100 PST it is seen, in Fig. 39, that the experimental RTW-signal MUF was closely approximated by the predictions for local 4000-km MUF. After 1100 PST, predictions greatly exceeded the experimental MUF until the time of the usual sunset MUF increase. It is important to notice that the 4000-km MUF in one of the two directions corresponding to a great-circle path through Stanford always exceeded the experimental MUF significantly. This indicates that the usual hop mode could propagate in one of the two directions. This fact is consistent with the finding of Isted [Ref. 8] that RTW propagation was not possible at 37 Mc when there was no ground backscatter in the vicinity of the transmitter.

The predicted f_oF2 world map for 0800 PST was shown in Fig. 31, together with the twilight-zone and the subsolar-point great circles. Figure 40 shows the greatly changed situation at 1200 PST, together with the observed optimum great-circle path through Stanford (and the twilight line). Several important features are evident.

1. For propagation of 20.5 Mc (the observed MUF at 1200 PST), the usual hop modes must be ruled out over a continuous distance of approximately 16,000 km (where the f_oF2 would be less than 6 Mc).

2. At the points where hop modes at 20.5 Mc would not appear possible, the longitudinal gradient of f_oF2 is very marked (as high as 1.5 Mc/1000 km) and of apparent proper direction to aid the launching of tilt modes through the dark hemisphere.

3. There are no apparent f_oF2 gradients which suggest the possibility of having a tilt mode in any appreciable portion of the daylight hemisphere (a fact having a significant effect on absorption predictions).

4. The MUF for RTW propagation in the great circle shown should be a function of geographical position of the transmitter. For a transmitter at the point antipodal to Stanford, for instance, the

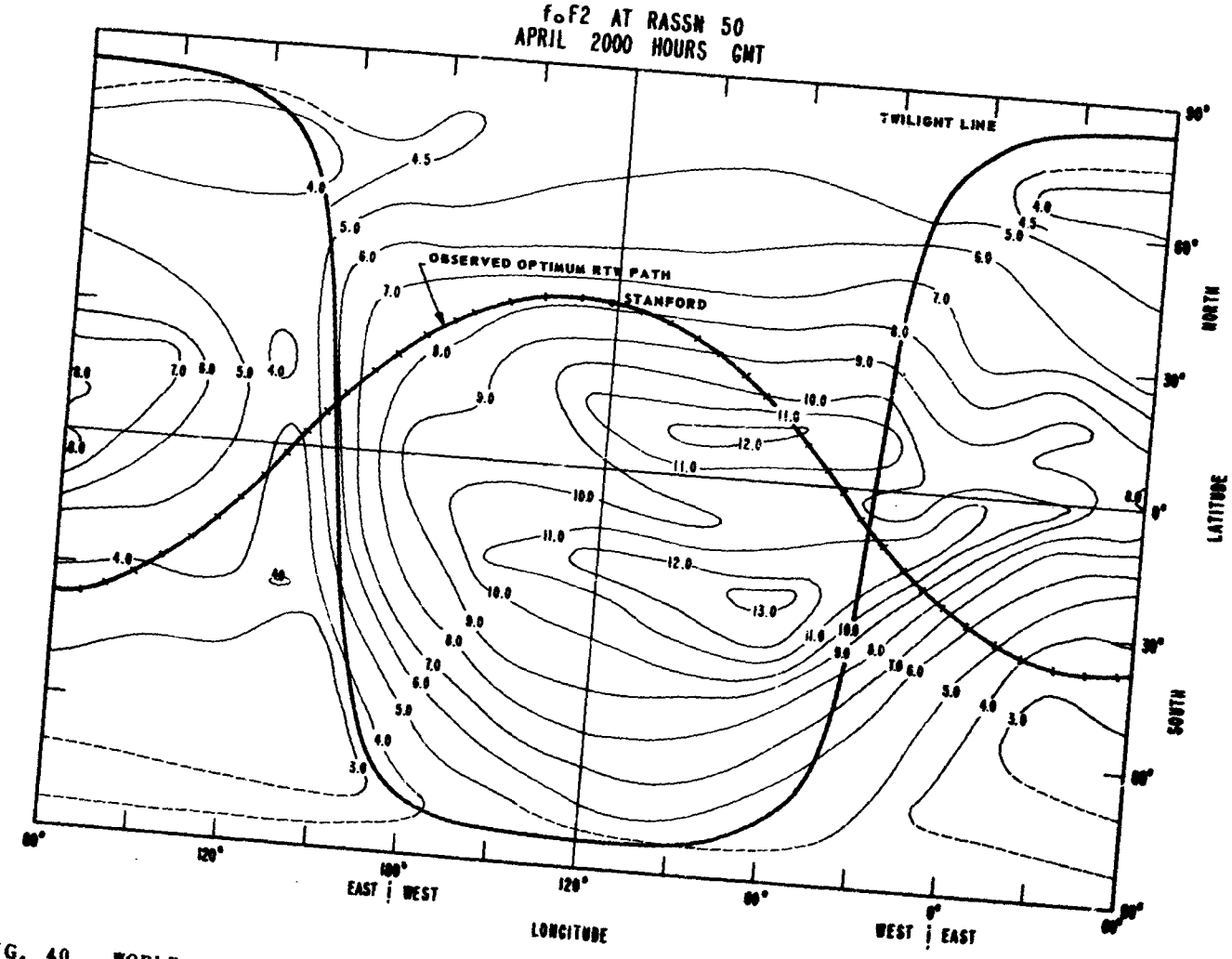

FIG. 40. WORLD MAP OF f_oF2 SHOWING TWILIGHT LINE AND OBSERVED OPTIMUM RTW PATH THROUGH STANFORD. (RASSN 50, April, 2000 GMT)

average MUF very likely would not exceed 13 to 15 Mc, and, similarly, the 20.5-Mc signals from Stanford should not reach the earth in this region. Stations located at most points along the great circle in the sunlit hemisphere, however, should have been able to hear the 20.5-Mc RTW signals from Stanford.

The predicted points for noon in May are added to Fig. 39. In this case the predicted minimum 4000-km MUF is 20.2 Mc, compared with the measured RTW-signal average MUF of 19.3 Mc (Fig. 34b).

Predictions of MUF vs time should best be based upon ray tracings in an accurate ionospheric model which particularly takes into account ionospheric tilts. General features, such as the morning rise and the evening fall of MUF caused by the varying of ionospheric conditions in the vicinity of the transmitter, may readily be predicted qualitatively, as seen in Figs. 38 and 39, and in comparing Fig. 11 with Figs. 33a and b.

D. THE EFFECTS OF GEOMAGNETIC STORMS

It has long been realized that RTW propagation, as well as hf propagation on shorter paths, is very markedly affected by geomagnetic storms [Refs. 6, 14]. However, it appears that the detailed correlations of the characteristics of RTW propagation with magnetic activity have not been appreciably explored. In the present experimental work, it was desired to determine in a more quantitative manner the dependence of RTW-propagation conditions on magnetic activity.

In general, the effect of magnetic storms was to decrease the propagating frequency range (mainly by decreasing the MUF), the signal strengths, and the duration of RTW propagation per day. In the more severe storms, some days were noted when RTW propagation was not obtainable at all. Examples of the latter situation were 7 and 10 April 1962, as seen in Fig. 20. It is seen that ΣK_p was very high for both of these days.

It is clear from Fig. 20 that there was a good correlation of the appearance of RTW propagation with changes in the magnetic index ΣK_p. In the earlier part of the experimental period represented, it is seen that the twilight-time RTW propagation was more seriously curtailed during periods of high magnetic activity than was the midday propagation,

although this too was significantly reduced. This fact should be expected since twilight RTW propagation took place on paths nearer the magnetic poles, where the effects of magnetic storms are greatest.

Figure 41 gives an indication of the detailed correlation between the evening duration of RTW propagation and magnetic activity. The solid line shows the number of evening runs (at 15-min intervals) in which RTW propagation was present for the days between 14 April and 16 May 1962. The dashed curve shows ΣK_p for a 12-hr period preceding and including the evening twilight period (1000 - 2200 PST). A significant correlation between the curves is evident, as is an occasional tendency for the changes in RTW activity to lag the changes in magnetic activity by 24 hr.

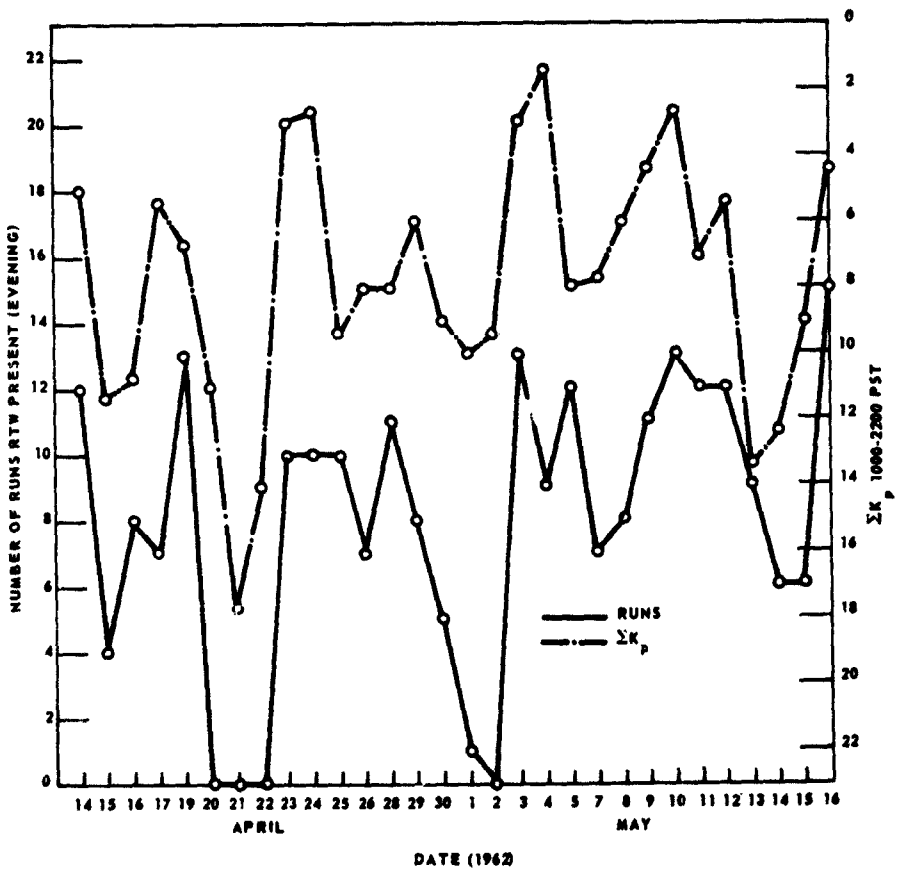

FIG. 41. CORRELATION OF EVENING DURATION OF RTW PROPAGATION WITH PRECEDING 12-HR ΣK_p DURING PERIOD 14 APRIL - 16 MAY 1962 AT STANFORD.

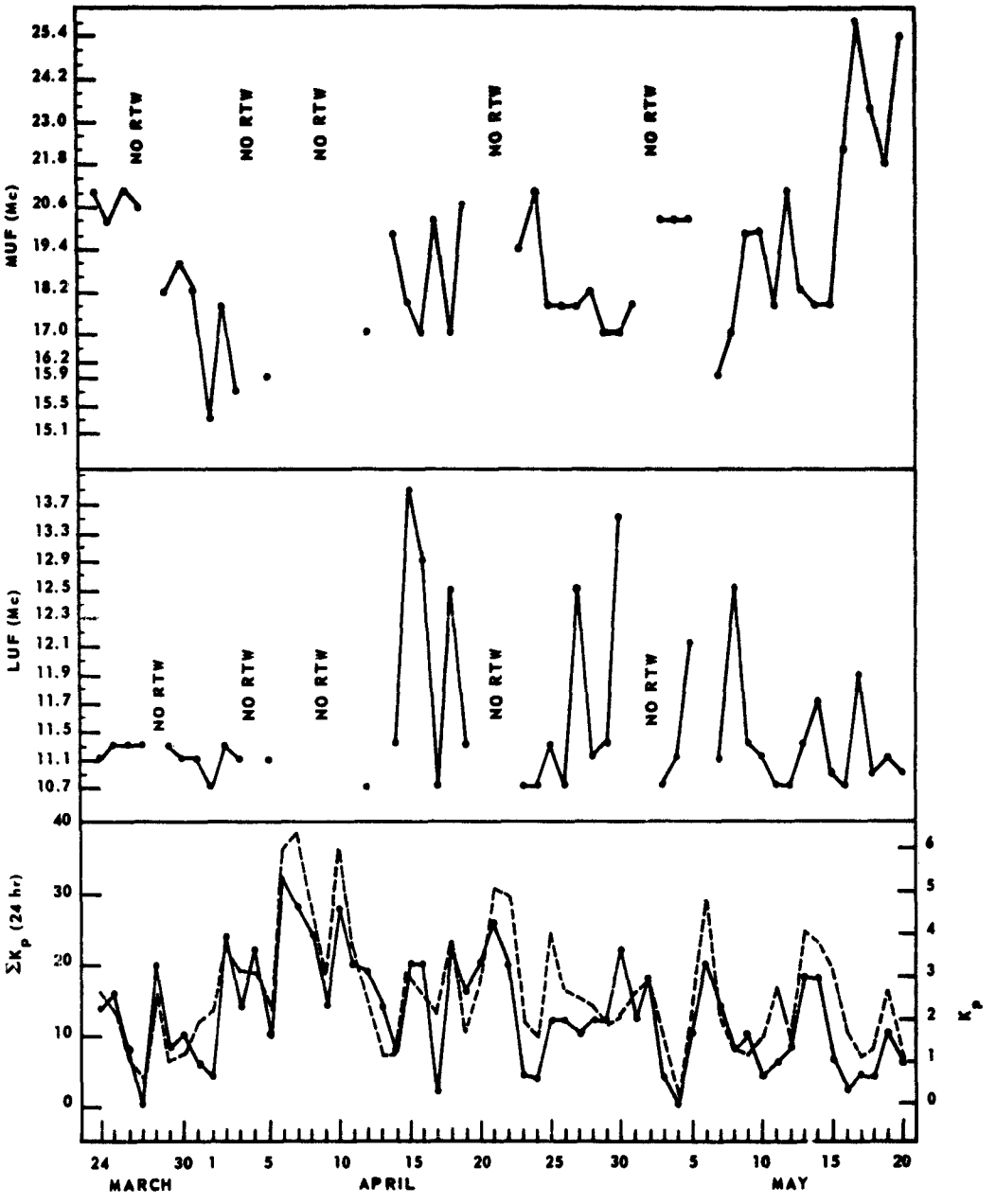

FIG. 42. CORRELATION OF EVENING LUF AND MUF WITH MAGNETIC ACTIVITY, 24 MARCH - 20 MAY 1962 AT STANFORD.

Figure 42 shows the evening MUF, LUF, K_p (evening) and ΣK_p (for the date) vs date in the period 24 March - 20 May 1962. The overall extent of the correlation of MUF and LUF changes with magnetic-activity changes is not obvious from this figure, but there are some periods in which the correlation was excellent. One such period was 14 - 19 April. In this period, it is seen that increased K_p was accompanied by a decrease in MUF and an increase in LUF, and conversely. At other times such a correlation is not so generally pronounced, although the tendency for this type of correlation is still present.

Figure 43 illustrates more clearly the correlation of evening MUF with K_p in the 24 March - 20 May 1962 period. The tendency for MUF to decrease with increased K_p, and conversely, is evident. Figure 44 is a similar plot, but for LUF. The tendency for LUF to increase with

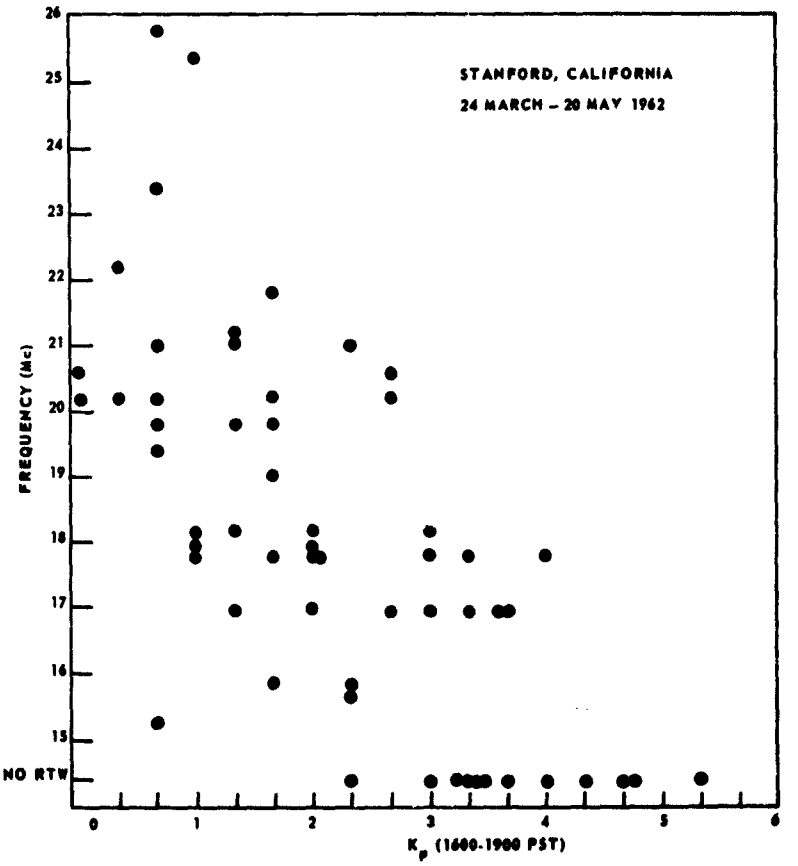

FIG. 43. CORRELATION OF EVENING RTW PROPAGATION MUF WITH K_p.

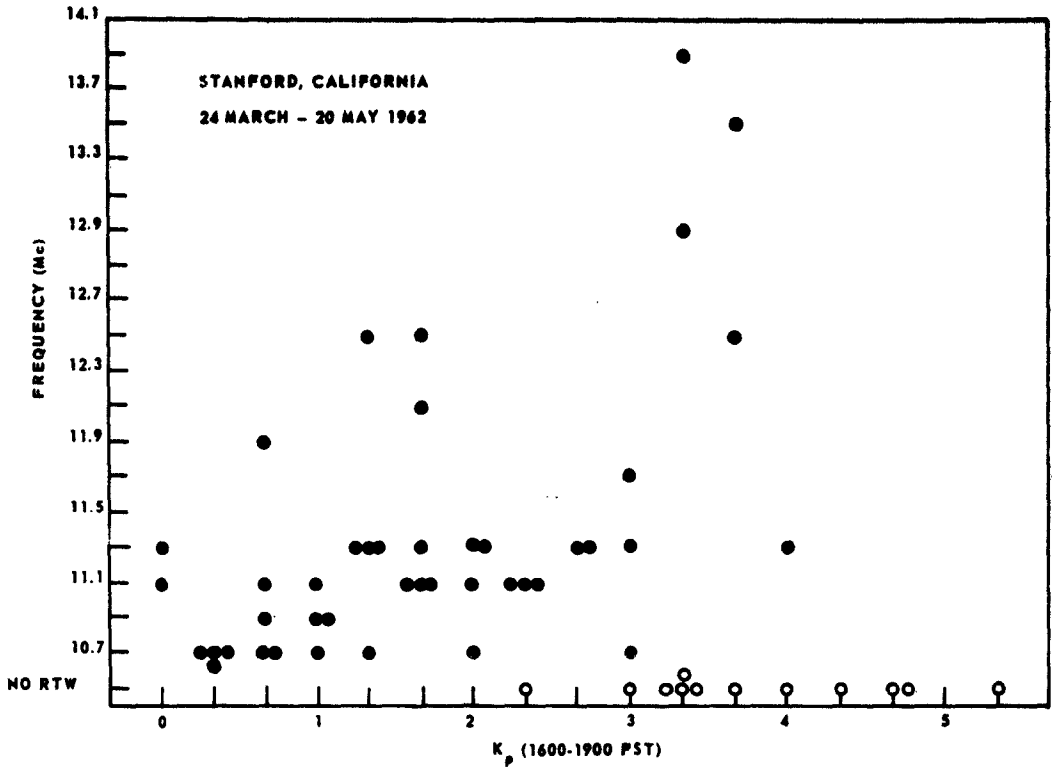

FIG. 44. CORRELATION OF EVENING RTW PROPAGATION LUF WITH K_p.

increasing K_p, and conversely, is present, but the correlation is not so pronounced as was the MUF correlation. The bunching of the LUF points in the 10.7- to 11.3-Mc range is quite possibly due to the fact that transmissions were not made below 10.7 Mc, and that interference was often very great on the four transmitting frequencies in this range. Hence, for example, a data point at 11.1 Mc may be merely an indication that the 10.7- and 10.9-Mc frequencies were not useful due to interference. Nonetheless, there is clearly a positive correlation between LUF and K_p. This should be expected, since lower ionospheric ionization and hence absorption, are often noted to increase during periods of disturbance of the earth's magnetic field [Ref. 14].

Figure 45 is similar to Fig. 43 but shows MUF vs K_p for mornings and evenings in July and August 1961. The August correlation is particularly striking; it is significant that it was a relatively quiet month magnetically, while July was comparatively disturbed. It has been noted that

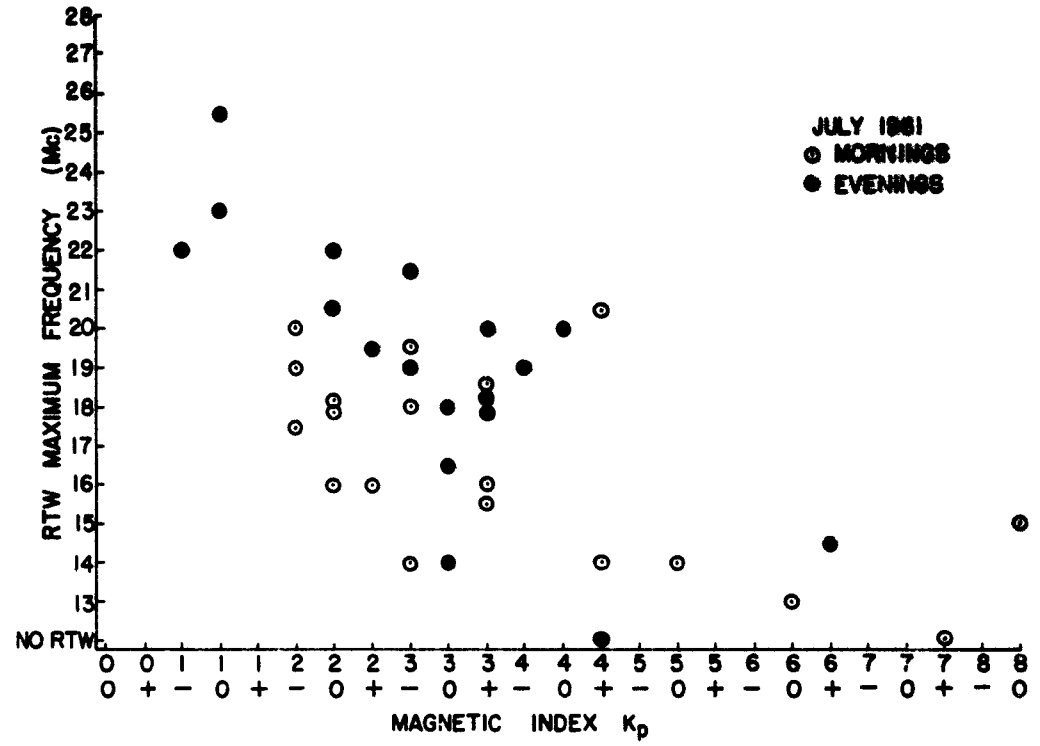

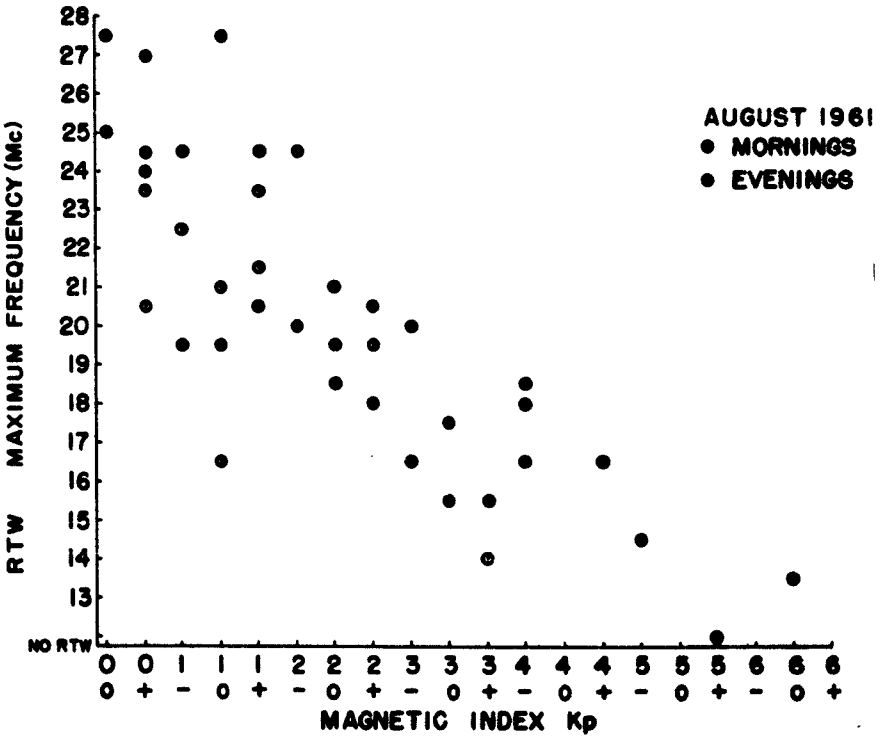

FIG. 45. CORRELATION OF MORNING AND EVENING RTW-PROPAGATION MUF WITH K_p FOR JULY AND AUGUST 1961, AT STANFORD.

RTW conditions remain generally depressed during prolonged disturbed periods, despite occasional undisturbed periods of short duration.

Figure 46 shows the morning and evening MUF's manually measured in the period May - September 1961, as well as the occurrence of RTW propagation. In this period there were no days in which both the morning and evening were monitored that RTW propagation could not at some time be obtained. The periods in which RTW propagation was not obtained always corresponded to periods of severe disturbance of the earth's magnetic field.

In general, the behavior of RTW occurrence, MUF, and LUF corresponds with that which has been noted on shorter paths. It is interesting to speculate upon the cause of the complete absence of RTW propagation on some highly disturbed days. It might at first be thought that the MUF and LUF merely overlap, figuratively, due to a general decrease in f_oF2 and increase in D-layer absorption. Examination of Figs. 43 and 44, however, shows this to be highly improbable, since there is a 1-Mc range between the highest LUF ever measured and the lowest MUF ever measured (in the 24 March - 20 May 1962 period). It appears more likely that the disappearance of RTW propagation is due to a destruction of normal mode structure during intense ionospheric storms, due to either changes in the height (and electron gradients) of the F2 layer or changes in smoothness of the layer. The presence of more intense lower layers (particularly sporadic E) could also cause the noted effects. One implication of this theory is that increased system sensitivity might not have made a significant difference in the ability to obtain RTW propagation in these periods.

The fact that marked changes in layer height often accompany ionospheric storms has long been suspected [Ref. 14] and has been shown in detail by Matsushita [Ref. 24]. Satellite measurements have also indicated great changes in ionospheric horizontal gradients during magnetic storms [Ref. 25]. These factors could readily account for the general behavior of the observed changes in RTW-propagation conditions during magnetic storms.

Since the correlation of RTW-signal activity with geomagnetic-field activity is good, and since the propagation mechanism does not appear

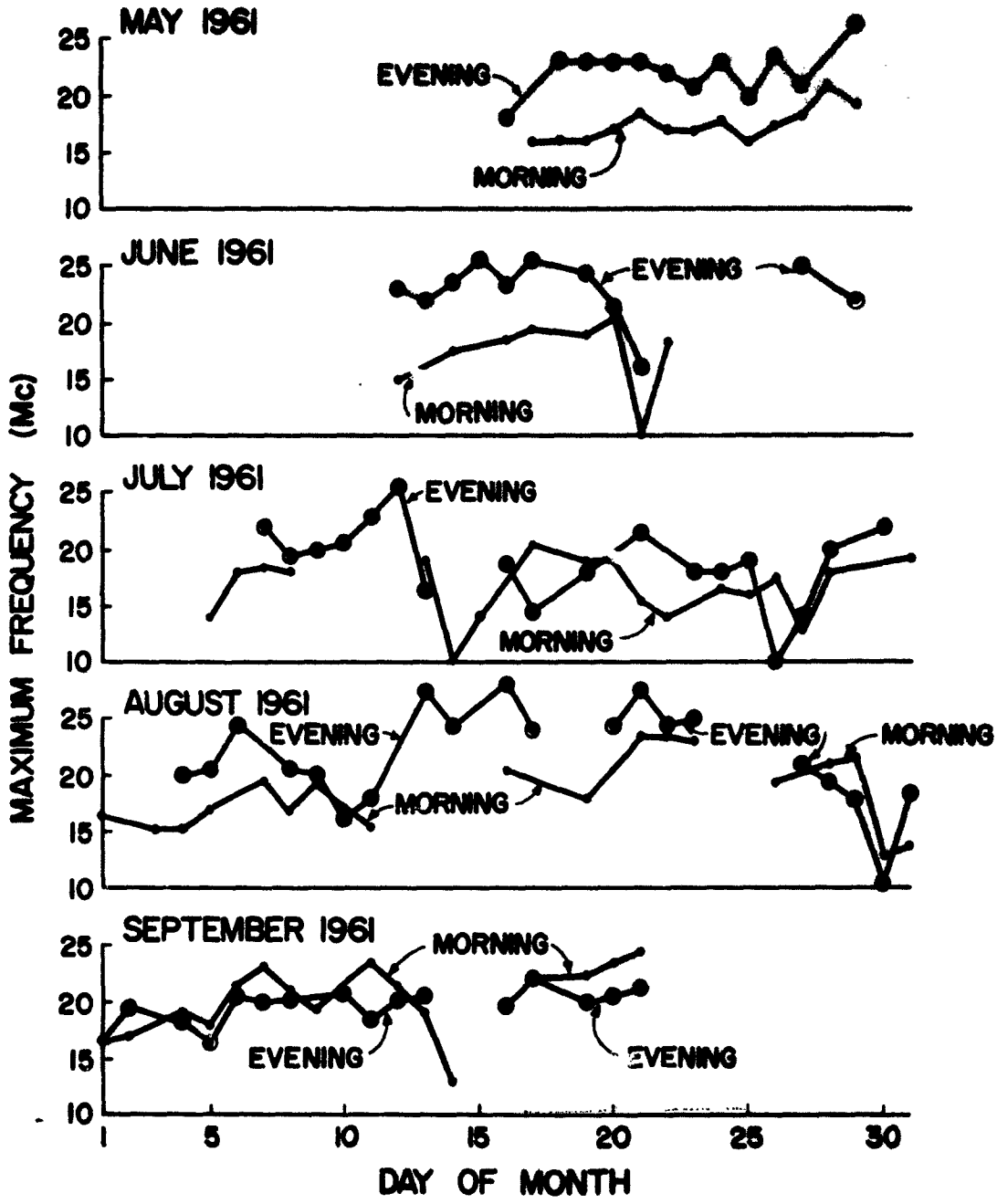

FIG. 46. MAXIMUM OBSERVED FREQUENCIES PROPAGATING AROUND THE WORLD VS DATE IN THE PERIOD MAY - SEPTEMBER 1961.

to differ substantially from that known for shorter paths (particularly in the sunlit hemisphere), the use of RTW signals for assessing general hf propagation conditions over a given (long) great-circle path appears possible in many cases. Such a use has been suggested by Kosikov [Ref. 26].

E. TIME DELAYS AND PULSE DISPERSION

It was desired to test the hypotheses of many earlier investigators that an RTW pulse was essentially undispersed and that the time delay was independent of frequency [Refs. 6, 8]. As stated earlier, this would not be expected for normal propagation. In the present work, as in that of others [Refs. 9, 10, 11, and 12], this feature of RTW propagation was not found. Figure 47 shows a typical time delay vs frequency determination, made in the 12- to 21-Mc range on 22 August 1961. Figure 48 illustrates graphically the information shown in Fig. 47. It is seen that both time delay and pulse dispersion were functions of frequency, in a manner much as would be qualitatively expected for the usual ionosphere-ground hop modes. Such an RTW frequency dependence has been predicted by de Voogt [Ref. 10] for the normal hop mode.

The effect of the receiver bandwidth (3 kc) was to broaden the received pulse approximately 0.6 to 1.0 msec, and to cause the apparent minimum time delay to be approximately 0.15 msec longer than the actual delay. The curves of Fig. 48 show apparent delay and should be corrected if actual delays are desired. Measurements will then be accurate to $\pm$0.1 msec for minimum delay time, and $\pm$0.2 msec for received-pulse width.

In general, it was found in the experimental work that minimum time delay and pulse dispersion varied rather widely with time as well as frequency. This would also be expected for the usual hop modes. The plots of Fig. 49 show apparent minimum-time-delay measurements as a function of frequency for July through September 1961. The dependence of minimum time delay on frequency is seen to vary in roughly the same way as in Fig. 48. The parallel lines drawn on Fig. 49 have a separation of 1 msec and a slope of 0.1 msec/Mc for all 3 months. August appears to have from 0.1 to 0.3 msec shorter minimum time delays, on the average, than July or September (which were essentially equal).

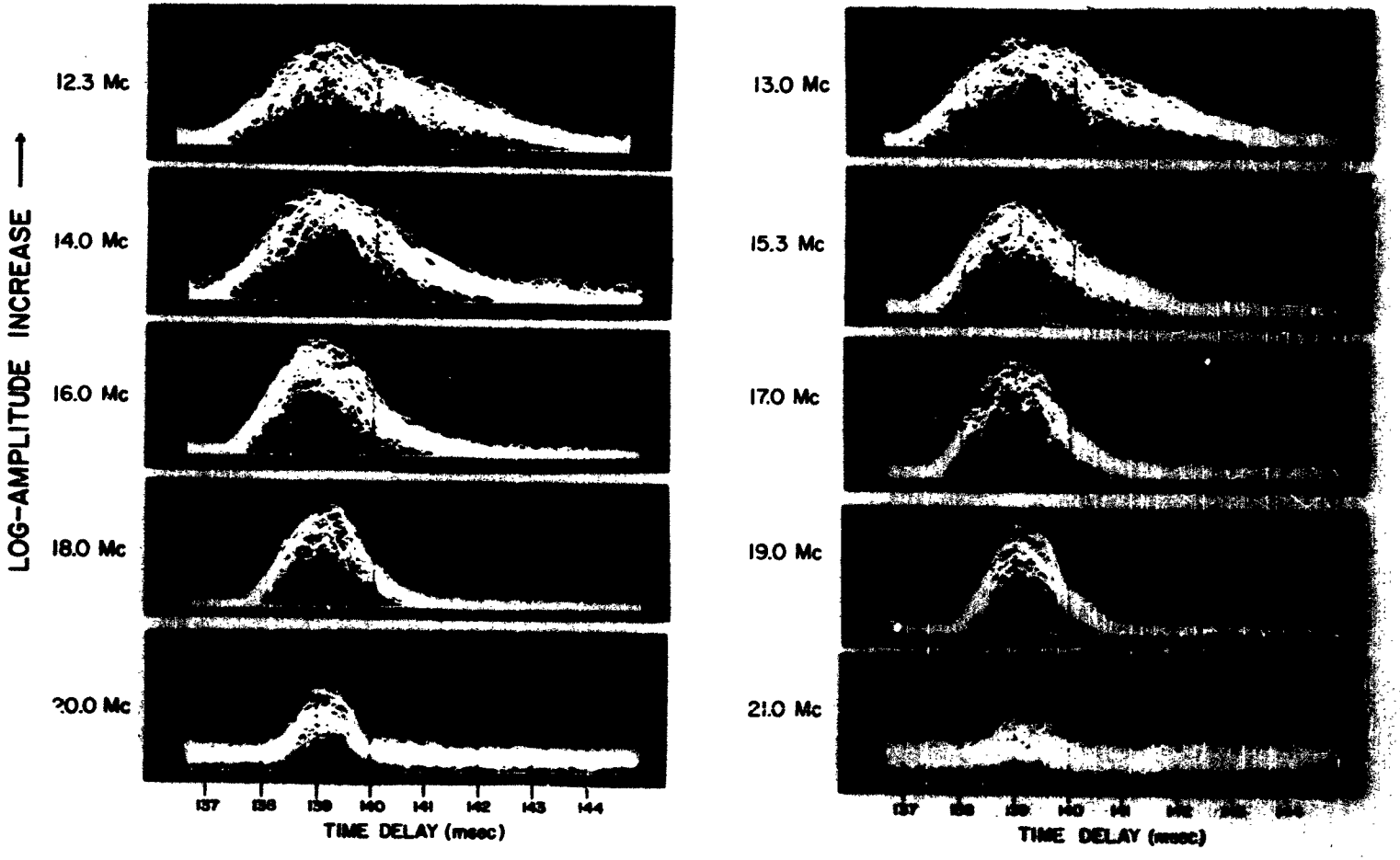

FIG. 47. RECEIVED, DETECTED RTW PULSES, LOG-AMPLITUDE VS TIME DELAY, FOR 1-msec TRANSMITTED PULSES (1950 PST to 2007 PST, 22 August 1961, at Stanford). Records show film integrations of 80 received pulses for varying frequency.

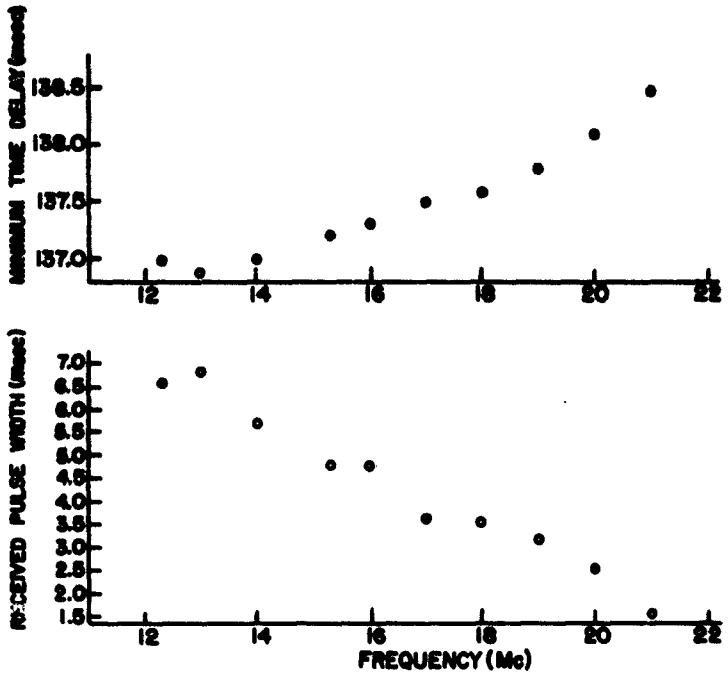

FIG. 48. MINIMUM TIME DELAY AND RECEIVED-PULSE WIDTH OF RTW SIGNALS VS FREQUENCY (22 August 1961, 1950 PST to 2007 PST at Stanford). Transmitted pulse length was 1 msec.

The theoretical time delays determined by de Voogt [Ref. 10] varied between 137.6 msec and 145.5 msec at 20 Mc for takeoff angles varying between 3° and $14^{\circ}48'$ (with varying assumptions of N(h) profile). It is significant that the presently reported experimental values correspond to the lowest angle of takeoff values determined by de Voogt. The theoretical values for 3° and $4^{\circ}20'$ for 20 Mc are shown in Fig. 49 along with the experimental points. In addition, dashed lines are shown which could connect the theoretical 20-Mc points with the 10-Mc points. The agreement is not as good at lower frequencies as at 20 Mc, which may be due to the fact that antenna radiation at such low angles would be significantly less at the lower frequencies. The general range of propagation wave angles implied here is in good agreement with those inferred by Hoogasian [Ref. 23], which were less than 10 deg.

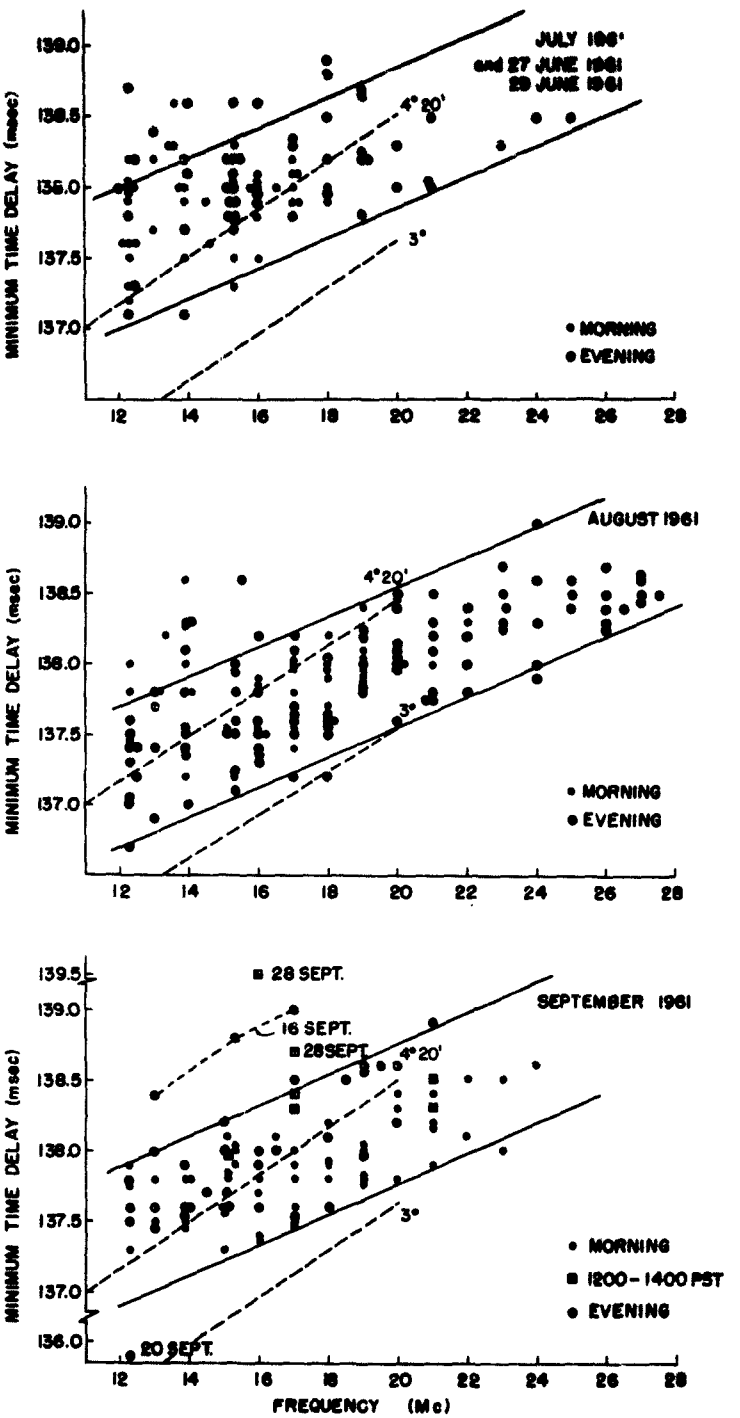

FIG. 49. APPARENT MINIMUM-TIME-DELAY MEASUREMENTS VS FREQUENCY FOR RTW TRANSMISSION, JULY - SEPTEMBER 1961. Also shown are theoretical time delays determined by de Voogt.

The plots of Fig. 50 are for the same months as those in Fig. 49, but they show apparent received-pulse width as a function of frequency. It is seen that, in general, received pulses having negligible dispersions were obtained only near the circulating-signal MUF, as would be expected for the usual hop modes.

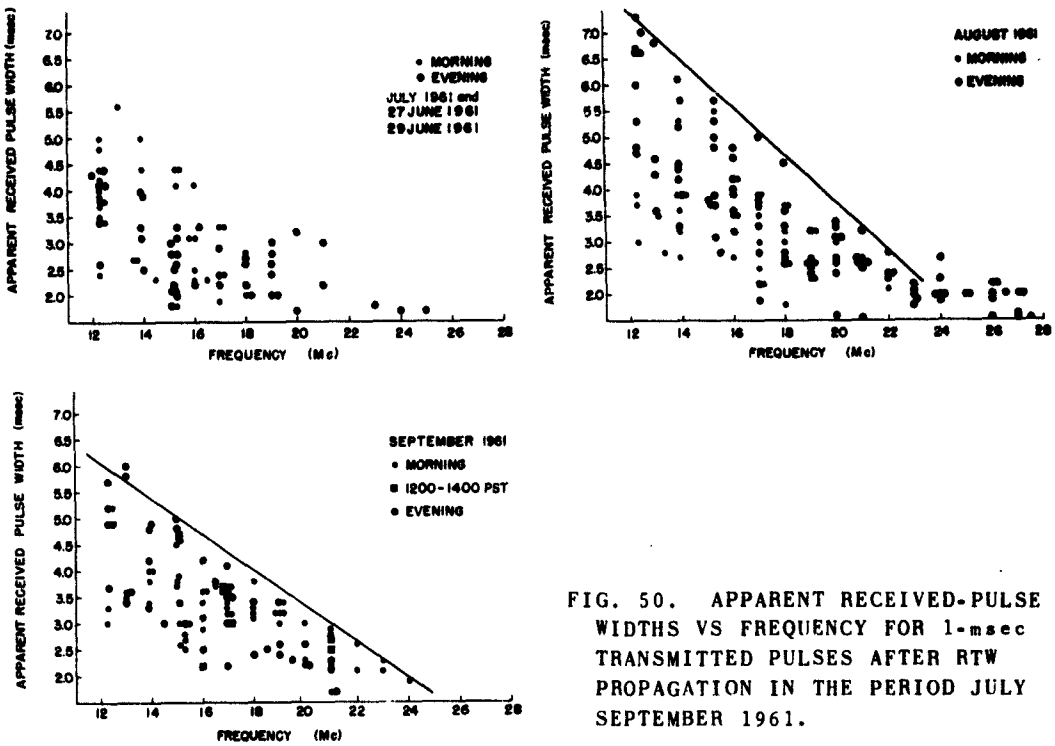

FIG. 50. APPARENT RECEIVED-PULSE WIDTHS VS FREQUENCY FOR 1-msec TRANSMITTED PULSES AFTER RTW PROPAGATION IN THE PERIOD JULY SEPTEMBER 1961.

Figure 51 gives time delays to the maximum amplitude of the return pulse. This quantity is much more consistent with varying frequency than minimum time delay or received-pulse width, indicating a dominant mode with time delay nearly independent of frequency. This could be partially due to the dependence of transmitting and receiving antenna elevation patterns on frequency. This finding could account for earlier reports of frequency-independent RTW time delays.

The rise time of the receiver when a rectangular 1-msec pulse was applied was approximately 0.55 msec. Hence, if the initial received component always corresponded to the dominant (maximum amplitude) ray

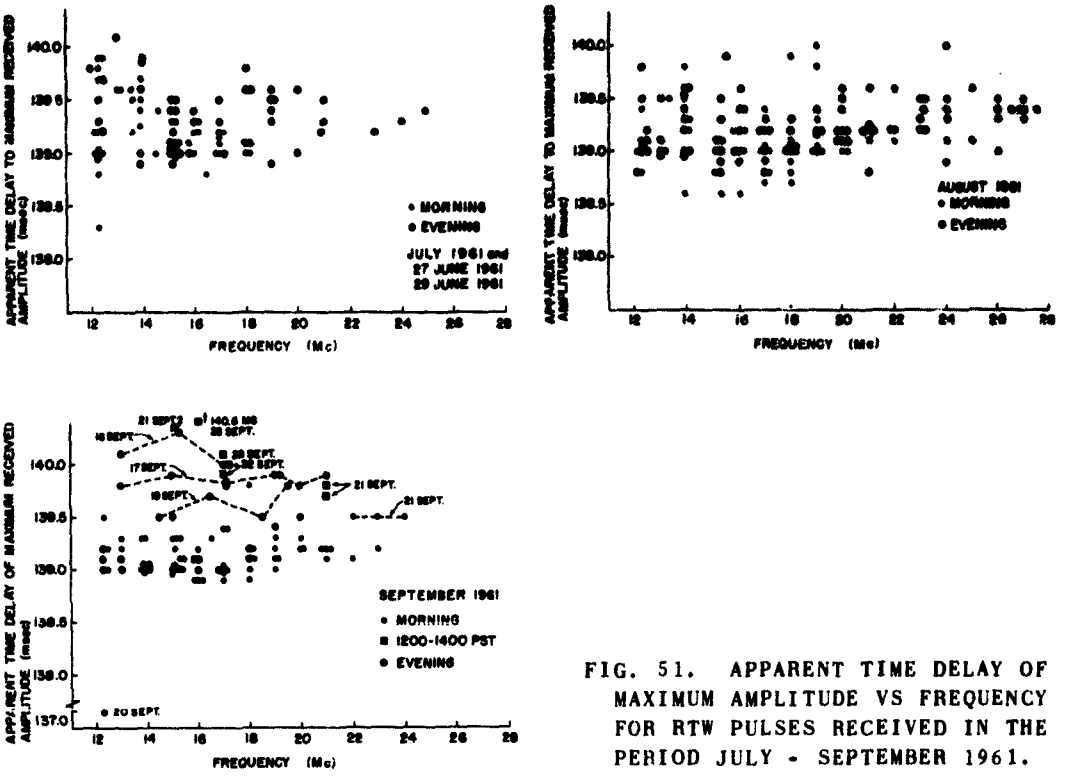

FIG. 51. APPARENT TIME DELAY OF MAXIMUM AMPLITUDE VS FREQUENCY FOR RTW PULSES RECEIVED IN THE PERIOD JULY - SEPTEMBER 1961.

path, the points of Fig. 51 would all lie approximately 0.55 msec above those of Fig. 49. Clearly, this is not the case. However, it is seen that most of the pulse broadening occurs after the peak amplitude is reached. This would be expected at the lower frequencies since higher and higher order modes contribute to the total received signal.

It is apparent from the foregoing that the RTW minimum time delays are definitely time and frequency dependent, in a manner not qualitatively different from that observed on shorter paths. Further, the evidence of the presence of a multiplicity of propagating modes is convincing. This evidence was also found by Hoogasian [Ref. 23]. Hence the presence of the normal earth-ionosphere-earth hop modes in RTW propagation cannot be ruled out on the basis of the experimental time delay and pulse dispersion data.

F. BACKSCATTER AND VERTICAL-INCIDENCE MEASUREMENTS AND THEIR IMPLICATIONS

The existence of appropriately oriented ionospheric tilts [Ref. 18], which would enable more grazing angles of incidence on the layer and thus permit reflections at frequencies higher than those predicted, has been supported by ionospheric backscatter measurements made concurrently with the circulating-signal measurements. For example, it was occasionally found in June 1961 that RTW propagation could be obtained while transmitting to the northeast when there was no ground backscatter apparent in that direction. A sample record is shown in Fig. 52. The records were made at 25.0 Mc at 2020 PST, 15 June 1961. The slight backscatter seen at 30 deg is attributed to other lobes of the log-periodic backscatter antenna. Note the RTW pulse arriving from the back of the antenna in Figs. 61b and 61c, indicated by arrows.

Vertical-incidence ionogram data,* available for the path at the same time as these records were taken, indicate an F2-layer 4000-km MUF for the first hop of less than 22 Mc, assuming an effective reflection height along the path that is parallel to the earth's surface (i.e., no tilt). However, comparison of Stanford, Winnipeg, and Churchill, Canada, ionograms (some points of which are shown in Fig. 53) indicated that an effective ionospheric tilt was present which could have enabled reflection of frequencies up to 27 Mc. The ray path, after reflection, would miss the earth by more than 100 km.

There has appeared at times isolated ground backscatter at very long range, up to 10,000 km beyond the next closest backscatter. Some examples are shown in Fig. 54. These backscatter measurements, made in the direction of optimum RTW transmission 17 and 19 September 1961, show a strong return at a radar range of 17,700 km. The next nearest return of consequence is at the 6000-km range. This phenomenon existed on the 2 days over a wide frequency range and lasted for over an hour. Note on the lower photograph that the RTW signal is also present, here being attenuated by the front-to-back ratio of the log-periodic antenna used in the radar measurements. Such occurrences, suggesting long regions of "tilt moding," were not uncommon during the investigation.

*From Winnipeg, Manitoba, Canada, approximately 2400 km northeast of Stanford.

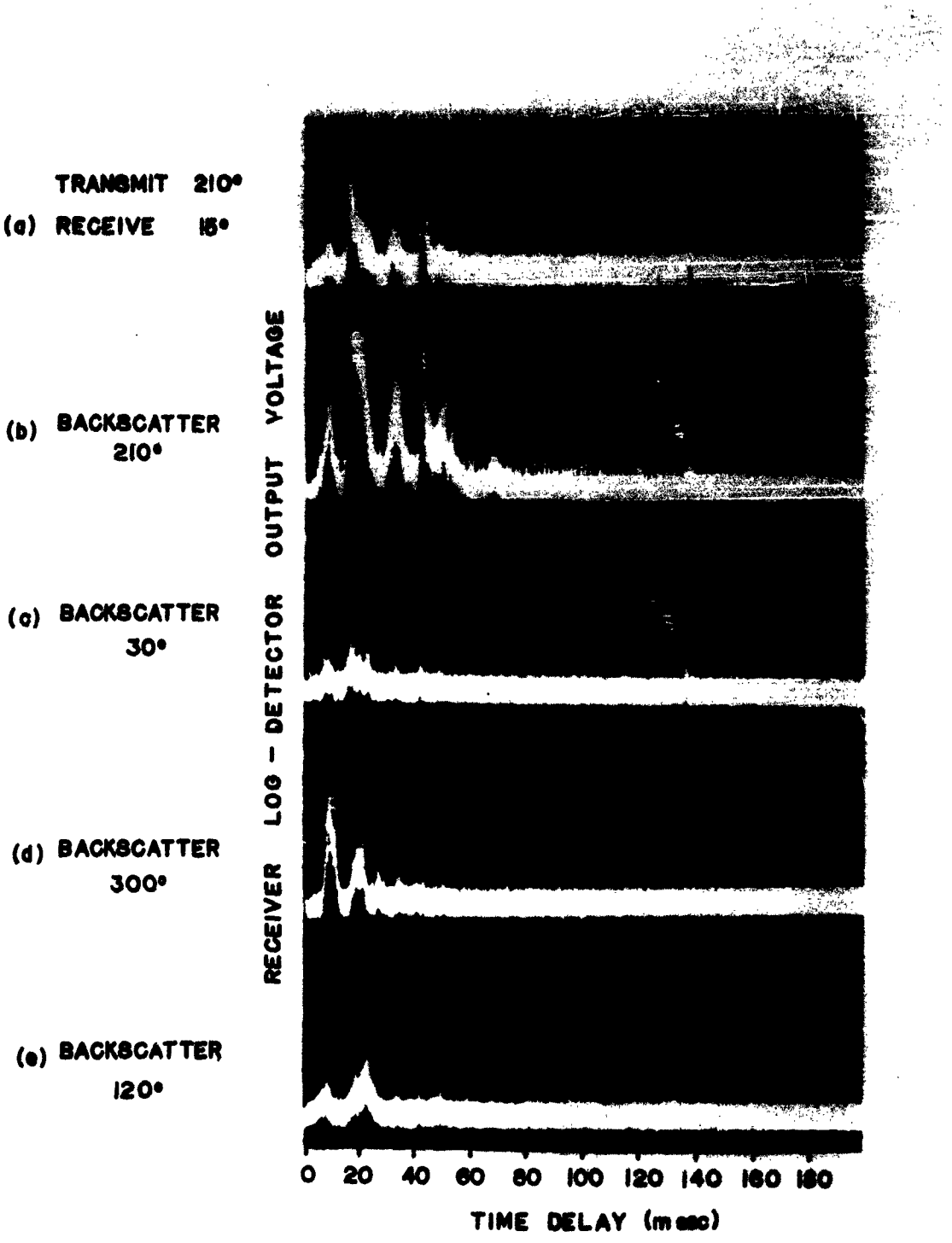

FIG. 52. A-SCOPE DISPLAY SHOWING PRESENCE OF RTW SIGNAL AT 25.0 Mc (2020 PST, 15 June 1961). The RTW pulse is indicated by arrows.

The existence of a tilt mode in the region northeast of Stanford in the summer evening has been further substantiated by Yeh [Ref. 27], who deduced from fading-rate studies on BBC stations that such a mode was dominant in the summer afternoon and evening between Stanford and London. (An estimate of the location of the separate modes is shown in Fig. 55c of Chapter V.)

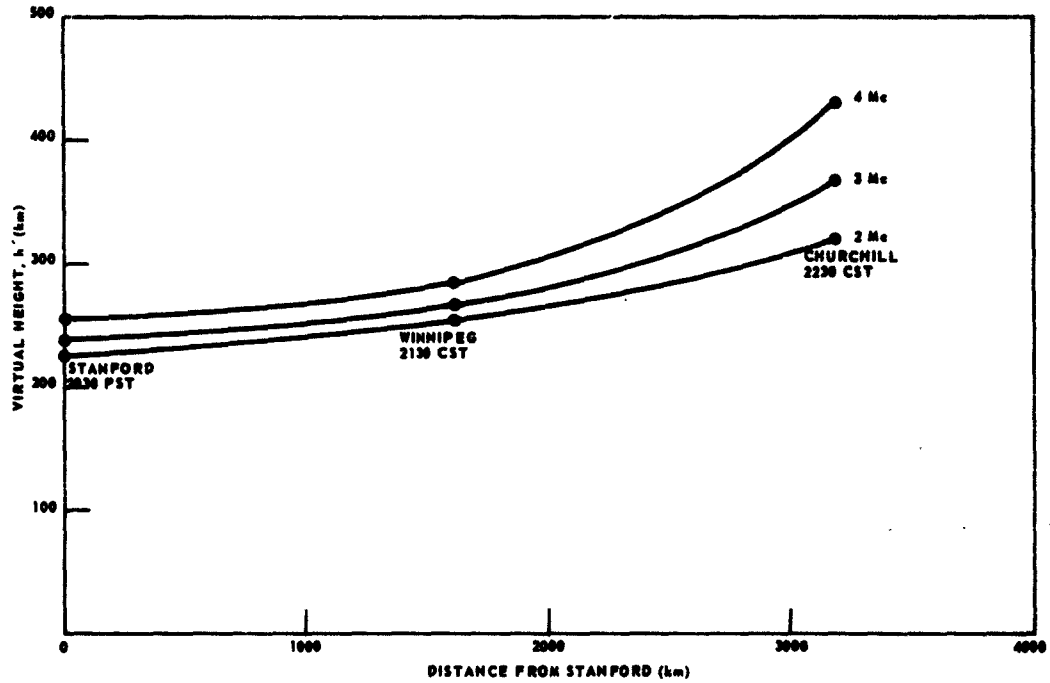

FIG. 53. CURVES OF VIRTUAL HEIGHT VS DISTANCE FROM STANFORD, 2030 PST DETERMINED FROM IONOGRAMS ON 15 JUNE 1961. Azimuth corresponds to theoretical and experimental optimum azimuth.

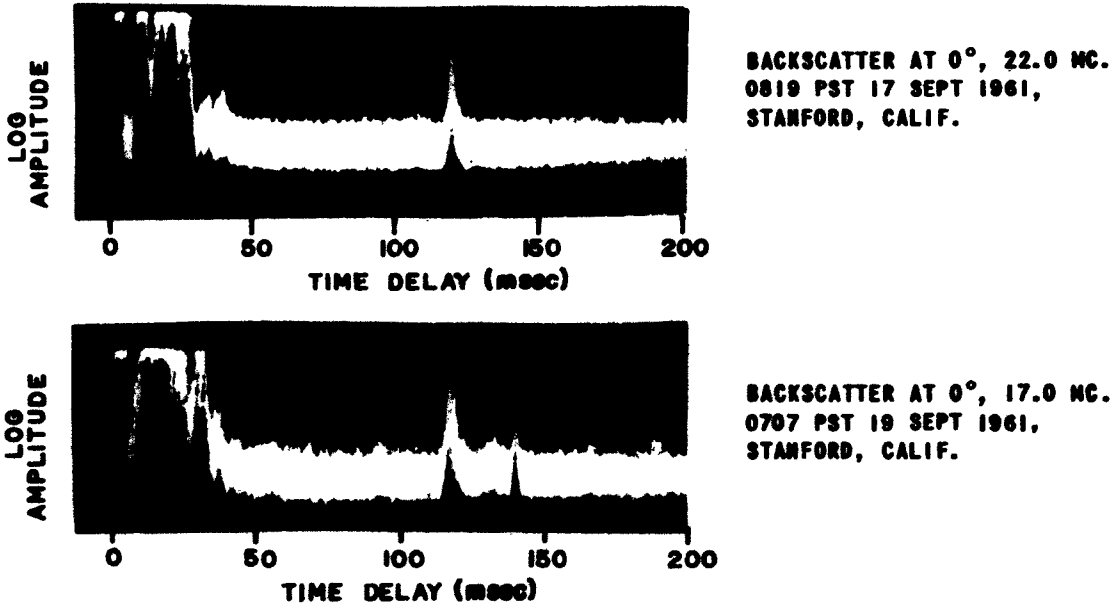

FIG. 54. LONG-RANGE BACKSCATTER OBSERVATIONS MADE AT TIMES AND IN AZIMUTHS OF RTW PROPAGATION.

V. DISCUSSION AND CONCLUSIONS

A. THE PROPAGATION MODES

The experimental measurements of the characteristics of hf round-the-world signals, conducted at Stanford during 1961 and 1962, together with the theoretical investigations undertaken concurrently, have provided new insight into the mechanism for the normally observed RTW propagation. This mechanism (for the dominant mode) is concluded to be the normal earth-ionosphere-earth hop mode over at least half of the path, particularly in any portion substantially in the daylight hemisphere, and an ionosphere-ionosphere tilt mode over the remainder of the path. The relative placement of the two types of mode structure appears to be discernible from NBS world maps of f_oF2. Figure 55 shows examples of six estimates of dominant mode placement for various times for RTW propagation at Stanford. The arrows indicate the directions of the stated azimuths.

In contrast to much previous work, the experimental measurements of pulse dispersion showed the RTW pulses to be significantly dispersed, the degree of dispersion varying inversely with frequency, as expected for normal hf propagation on shorter paths due to a superposition of modes. Minimum time delays varied directly with frequency, also as expected from theory.

A further substantiation of the mechanism described above was provided by the LUF measurements, which indicated clearly the effects of D-layer absorption, and hence the presence of earth-ionosphere-earth hop modes in the daylight hemisphere in normal RTW propagation. However, the MUF measurements showed that frequencies could often be propagated through regions (in the dark hemisphere) in which the normal hop mode should not be supported due to insufficient F2-layer critical frequencies. This phenomenon is explained on the basis of tilt modes which allow a more glancing incidence on the F2 layer, and hence permit higher frequencies to be propagated than would otherwise be possible. Backscatter measurements fully support this conclusion, as does theory if low-wave-angle propagation is assumed.

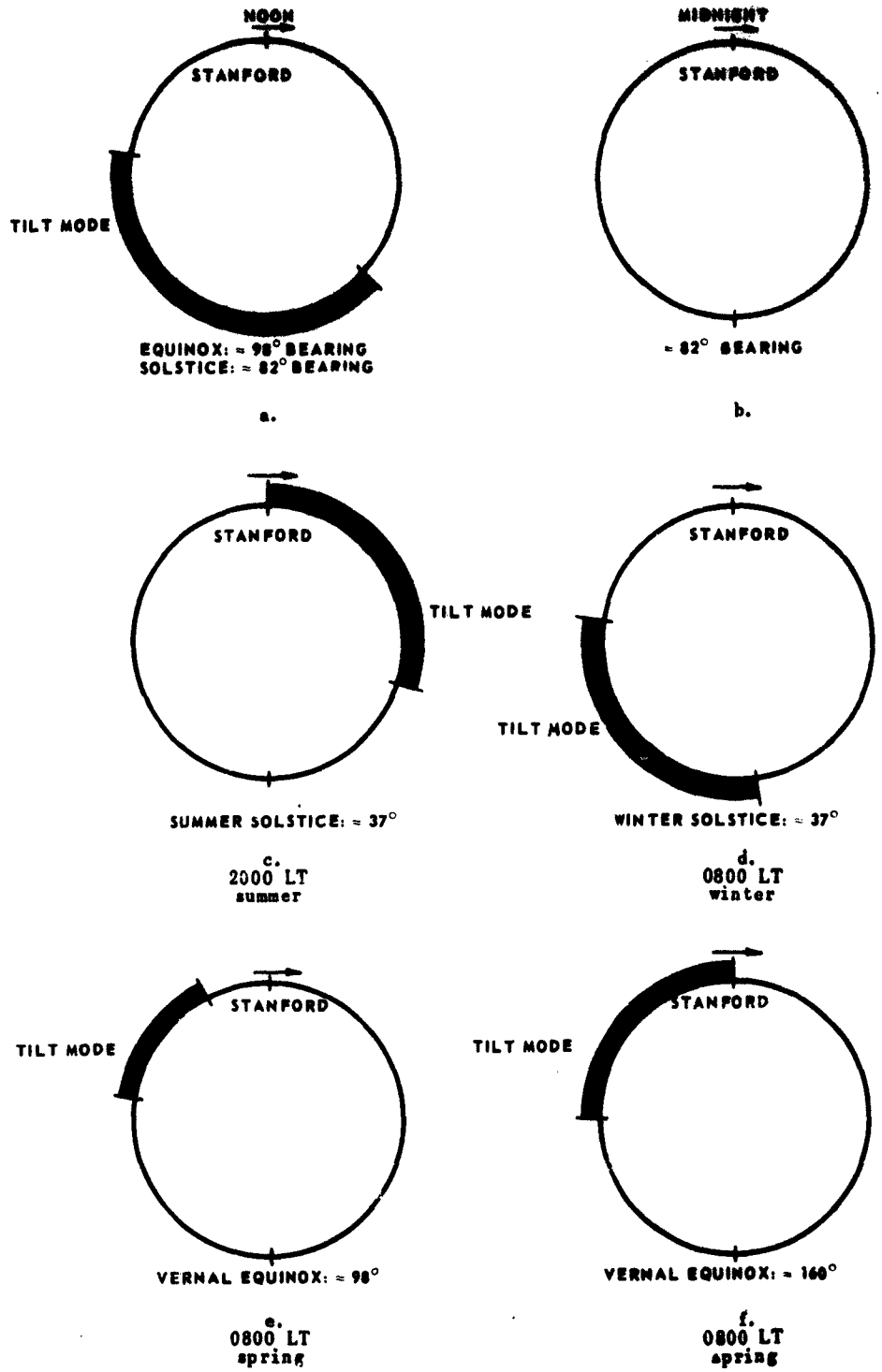

FIG. 55. ESTIMATES OF REGIONS IN WHICH TILT MODES WERE REQUIRED AT RTW-SIGNAL MUF FOR VARIOUS TIMES ON PATHS THROUGH STANFORD.

The optimum-azimuth measurements showed that the "twilight zone" was by no means the sole region in which RTW propagation was possible, but that this region was preferred at lower frequencies due to the lower absorption on such paths. These measurements also showed that RTW propagation was at times possible orthogonally to the twilight zone, at the higher frequencies, when F2-layer critical frequencies and effective tilts were appropriately disposed with respect to the transmission point. It was further shown by comparison of experimental results with theory that it is necessary to take into account absorption, disposition of F2-layer critical frequencies, and ionospheric tilt orientation and location if the optimum azimuth for RTW propagation is to be accurately predicted.

The maximum frequencies involved in normal RTW propagation are too high to be supported by the normal E-layer over any appreciable portion of the path. Further, the day-to-day consistency of the characteristics of RTW propagation greatly exceeds the consistency of the occurrence or characteristics of E_s. Hence, the role of the lower ionospheric layers, specifically E and E_s, in determining the mode structure in normal RTW propagation is concluded to be negligible.

Since the dominant RTW propagation mode appears to be low angle, the MUF obtainable should be very dependent on the precise mode geometry, since for very shallow angles of incidence on the ionosphere the frequency which can be "reflected" changes markedly for changes in angle of incidence of fractions of 1 deg. Hence, great accuracy in RTW-signal MUF prediction appears difficult to obtain if other than empirical means (based on previously measured MUF's on the path of interest) are to be used. In contrast, the qualitative LUF and normal field-strength variations appear nearly as predictable as for shorter paths, since, to first order, the effects of absorption are independent of mode and can be readily computed. The degree of energy focusing in RTW propagation is not yet clear, however, and may appreciably affect the realized field strength--and thus the LUF.

B. IMPLICATIONS FOR LONG DISTANCE HF PATHS

The conclusions regarding the propagation modes for RTW propagation have a bearing on propagation over shorter-distance hf paths as well. For instance, it follows that it is most likely for "long path"--as contrasted with "short path"--propagation to be possible (with moderate absorption loss) between two stations when both stations are in the daylight hemisphere (and particularly if they are near the twilight line). It might further be inferred that the long-path MUF will be highest if the two stations are fairly close together and on a line through the subsolar point (provided that this line does not pass too near to the auroral zones). It is also implied that long-path propagation may be exceedingly difficult for stations both of which are well into the dark hemisphere, or when one is in the dark hemisphere and the other is in the light hemisphere.

The MUF prediction problem for the long path between stations in the light hemisphere (or in the twilight zone) is seen to be nearly identical with that for RTW propagation--since an important consideration appears to be the existence and orientation of ionospheric tilts, which can cause "tilt modes." Long-path use appears attractive for communications (assuming that only tilt modes exist between stations), since interference from intervening stations should normally be nonexistent due to the tilt modes. (Albrecht [Ref. 28] has implied that tilt modes appear to be a normal part of all long-range propagation.) It appears reasonable to conclude, therefore, that greater attention should be paid in the future to the effect of ionospheric tilts in the prediction of MUF on long-distance hf paths, and that intentional utilization of these tilts could be quite beneficial in some communications systems.

C. RECOMMENDATIONS FOR FURTHER STUDY

Several of the conclusions drawn during this study of round-the-world propagation deserve further, and more direct, verification. In addition, there are features of RTW propagation which have been essentially unexplored. The role of "tilt modes" in RTW propagation, and in other long-distance hf propagation, needs to be further confirmed by means of

APPENDIX A. METHOD FOR CALCULATING IONOSPHERIC TILT EFFECTS

This appendix is intended to give a brief description of the method used by T. Croft [Ref. 19] for deriving the equations and subsequent computer program for calculation of ionospheric tilt effects. Program results are D, L, and M as shown in Figs. 15 through 17 f. It will be seen that the key to an easy solution lies in use of optimum shifting back and forth between cartesian and polar coordinates as illustrated in Fig. 56a.

Define three vectors, $\bar{a}$, $\bar{b}$, and $\bar{c}$ as shown in Fig. 56b. The mirror relationship (angle of incidence = angle of reflection) can be stated as $\bar{a} + \bar{b} + \bar{c} = 0$ provided $|\bar{a}| = |\bar{b}|$. In polar coordinates, let $\bar{a} = (\rho_a, \theta_a, \phi_a)$. In cartesian coordinates, let $\bar{a} = (x_a, y_a, z_a)$. Use similar notation for $\bar{b}$ and $\bar{c}$. Set $\rho_a = \rho_b = 1$. Then $|\bar{a}| = |\bar{b}|$. Now write $\bar{a} + \bar{b} + \bar{c} = 0$ in cartesian coordinates. This yields three equations of the form $x_a + x_b + x_c = 0$. Convert these equations to polar coordinates, giving three equations in nine parameters, six of which are known: $\rho_a = \rho_b = 1$; $\theta_a = -\pi/2$; ϕ_a is computed directly from the values of D_T and mirror height H (which are program inputs); ϕ_c is the ionospheric tilt; and θ_c is the tilt azimuth (these are program inputs). Solving the three equations yields ρ_c, θ_b, and ϕ_b. The value of ρ_c is not needed further.

Now let $\bar{b}$ be a ray path whose length, ρ_b, is measured from the mirror to the place where the ray strikes the ground. If the ray misses the earth, let ρ_b be the distance from mirror to perigee.

Case 1, The Reflected Ray Strikes the Earth

In cartesian coordinates write the equation of the earth centered on the origin: $x^2 + y^2 + z^2 = r^2$. Now shift the earth down the negative z axis a distance $h = r + H$, as shown on Fig. 56c. Convert this equation to polar coordinates and insert the values of θ_b and ϕ_b. This yields the value of ρ_b.

To find D, solve the oblique triangle shown in Fig. 56d. All three side lengths (h, r, and ρ_b) are now known. Find ψ and then $D = r\psi$.

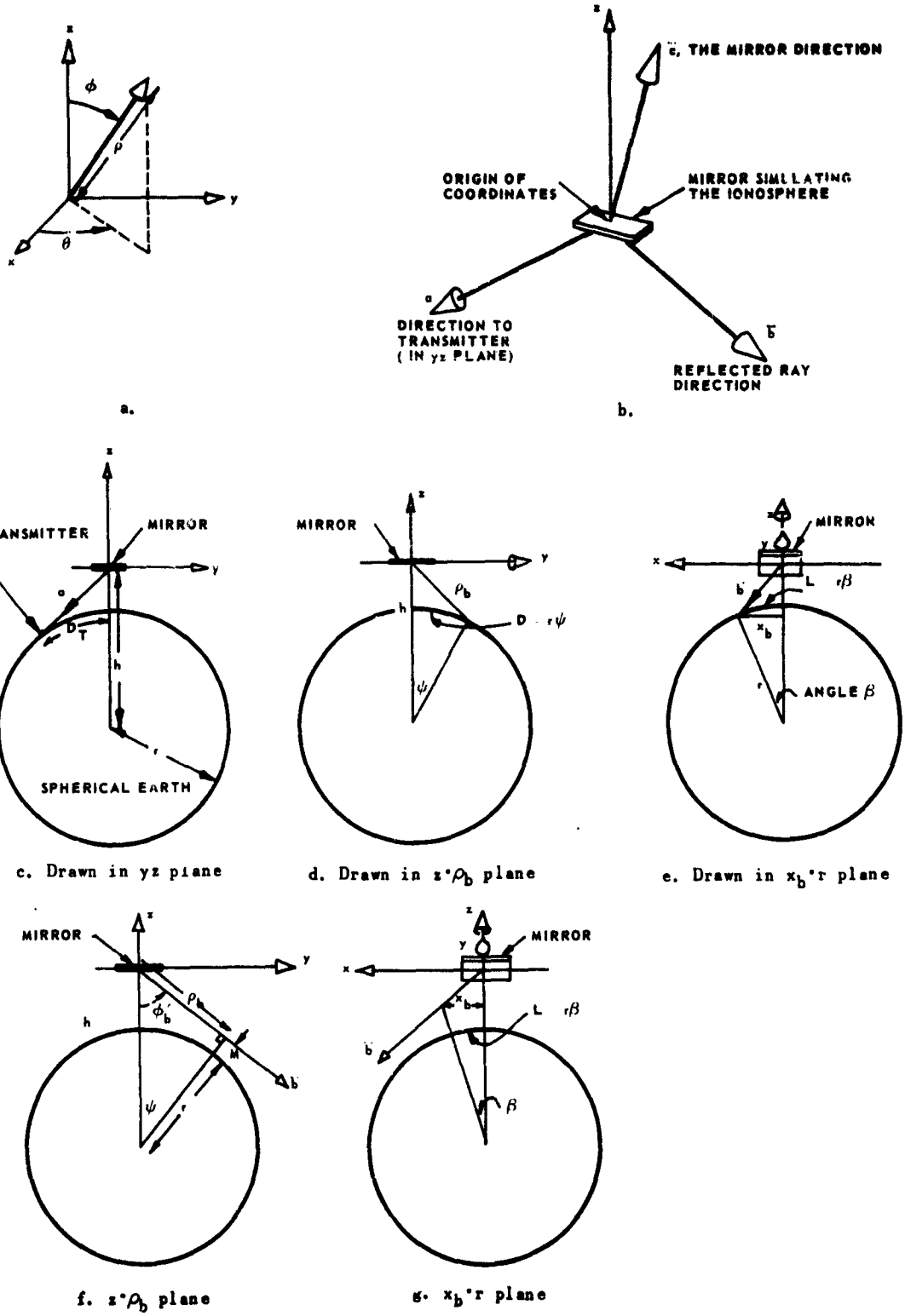

FIG. 56. STEPS IN DERIVATION OF IONOSPHERIC TILT PLOTS.

To find L, convert $(\rho_b, \theta_b, \phi_b)$ to cartesian coordinates and calculate x_b. Solve the right triangle of Fig. 56c which has hypotenuse r. This gives angle β and $L = r\beta$.

Case 2, The Reflected Ray Misses the Earth

In this case we find ρ_b by solving the right triangle shown in Fig. 56f. The hypotenuse is h and $\phi_b' = \pi - \phi_b$. Also solve for the other side length, which is r + M. The value of M is the height of ray perigee.

To find L, we again process $(\rho_b, \theta_b, \phi_b)$ to find x_b. As shown in Fig. 56g, we again have a right triangle but now the hypotenuse is r + M. Solve for β and then $L = r\beta$.

Now a computer program can be written. Inputs will be D_T, H, ϕ_c, and θ_c. Outputs will be D, L, and M. Results can be plotted as shown in Figs. 17a - f. The computer program for D_T = 1750 km follows. Running time was 22 min. In the computer program θ_c was measured from the transverse tilt condition, not from the "forward" longitudinal condition as shown in Fig. 15.

COMPUTER PROGRAM FOR D_T = 1750 km

```
BALGOL    22 MAR
  BURROUGHS ALGEBRAIC COMPILER - STANFORD VERSION   7/25/61$
 COMMENT IONOSPHERIC TILT PROGRAM$
 FORMAT F1(*HEIGHT*, B5, *PHI*, B5,*THETA*, B15, *DIST*, B23,
 *L*, W2)$
FORMAT F2(X6.2, B5, X4.2, B5, X5.1, B10, F16.8, B10, F16.8, W2)$
FORMAT F3(X6.2, B5, X4.2, B5, X5.1, B10, F16.8, B10, F15.8, B5,
 *RAY MISSES EARTH*, W2)$
 OUTPUT O1(HT, PHIC, THETAC, DIST, L)$
 OUTPUT O2(HT, PHIC, THETAC, HM, LM)$
 WRITE($$ F1)$
 PI=3.14159278$
 PI2=PI/2.0$   PI180=PI/180.0$
 RE=6367.65$  DT=1750.0$
 HT=250.0$
 L6..   H=HT+RE$
 DELTA =DT/RE$
 ETAPPHI2 =PI2-DELTA/2.0$
   ETAMPHI2    =ARCTAN((H-RE)/(H+RE)).TAN(ETAPPHI2)$
 PHIA=ETAPPHI2 - ETAMPHI2$
 PHIC=0.0$
 L4..   PHICR=PHIC.PI180$
        THETAC=-90.0$
 L3..   THETACR=THETAC.PI180$
        B=SIN(PHICR).SIN(THETACR)$
 C=SIN(PHIA)$
 D=COS(PHICR)$
 E=-COS(PHIA)$
 RHOC=-2(B.C+D.E)$
 A1=1.0-(D.RHOC+E)*2$
 PHIB=ARCSIN(SQRT(A1))$
 IF SIN(PHIB) GTR RE/H$
 GO TO L1$
 THETAB=ARCSIN((B.RHOC+C)/SIN(PHIB))$
 THETAB=PI-THETAB$
 PHIB=PI-PHIB$
 A2=(RE*2-(H.SIN(PHIB))*2)$
 RHO=-H.COS(PHIB)-SQRT(A2)$
       S=(RHO+RE+H)/2.0$
 R=SQRT(((S-RHO)(S-H)(S-RE))/S)$
 DIST=2RE.ARCTAN(R/(S-RHO))$
 XP=RHO.SIN(PHIB).COS(THETAB)$
 L=RE.ARCSIN(XP/RE)$
 WRITE($$ O1, F2)$
 GO TO L7$
 L1..   HM=H.SIN(PHIB)-RE$
 RHOM=H.COS(PHIB)$
 THETAB=ARCSIN((B.RHOC+C)/SIN(PHIB))$
 THETAB=PI-THETAB$
 PHIB=PI-PHIB$
 XPM=RHOM.SIN(PHIB).COS(THETAB)$
 LM=RE.ARCSIN(XPM/(RE+HM))$
 WRITE($$O2, F3)$
 L7..   THETAC=THETAC+ 5.0$
 EITHER IF THETAC GTR 90.0$  GO TO L2$
 OTHERWISE$   GO TO L3$
 L2..   IF PHIC GEQ 2.0$   GO TO L8$
 PHIC=PHIC+0.25$   GO TO L4$
 L8..   PHIC=PHIC+0.5$
 EITHER IF PHIC GTR 5.0$   GO TO L5$
 OTHERWISE$   GO TO L4$
 L5..   HT=HT+50.0$
 IF HT LEQ 350.0$   GO TO L6$
 FINISH$
```

REFERENCES

1. E. Quaeck, "Propagation of Short Waves Around the Earth," Proc. IRE, 15, 1927, pp. 341-345.

2. E. Quaeck, "Further Communication of the Propagation of Short-Waves," Proc. IRE, 15, 1927, pp. 1065-1068.

3. T. L. Eckersley, "Short-Wave Wireless Telegraphy," J. IEE., 65, 1927, pp. 600-644.

4. A. H. Taylor, and L. C. Young, "Studies of High-Frequency Radio Wave Propagation," Proc. IRE, 16, 1928, pp. 561-578.

5. E. Quaeck, and H. Moegel, "Double and Multiple Signals with Short Waves," Proc. IRE, 17, 1929, pp. 791-823.

6. H. A. Hess, "Investigations of High-Frequency Echoes," Proc. IRE, 36, 1948, pp. 981-992.

7. G. W. Luscombe, "Delayed Signals in Ionospheric Forward-Scatter Communication," Nature, 180, 1957, p. 138.

8. G. A. Isted, "Round-the-World Echoes," Marconi Rev., 21, 1958, pp. 173-183.

9. H. A. Hess, "Part III-Investigations of High-Frequency Echoes," Proc. IRE, 40, 1952, pp. 1065-1068.

10. A. H. de Voogt, "Les Echoes Radioelectriques Autour de la Terre," L'Onde Electrique, 30, 1950, pp. 433-437.

11. J. Ortner, "Around-the-World Echoes Observed on a Transpolar Transmission Path," J. Geophys. Res., 64, 1959, p. 2464.

12. H. A. Hess, "Part II--Investigations of High-Frequency Echoes," Proc. IRE, 37, 1949, pp. 986-989.

13. D. K. Bailey, "The Effect of Echo on the Operation of High-Frequency Communication Circuits," IRE Trans. on Antennas and Prop., Oct 1958, pp. 325-329.

14. National Bureau of Standards, "Ionospheric Radio Propagation," NBS Circular 462, 25 Jul 1948.

15. R. B. Fenwick, and O. G. Villard, Jr., "Time Variation of Optimum Azimuth for H-F Around-the-World Propagation," Rept. SEL-62-034 (TR 1004-2), Stanford Electronics Laboratories, Stanford, Calif., Mar 1962.

REFERENCES (Cont)

16. National Bureau of Standards, "World Maps of F2 Critical Frequencies and Maximum Usable Frequency Factors," NBS Tech. Note 2, Apr 1959.

17. National Bureau of Standards, "Supplementary World Maps of F2 Critical Frequencies and Maximum Usable Frequency Factors," NBS Tech. Note 2-2, Oct 1960.

18. S. Stein, "The Role of Ionospheric-Layer Tilts in Long-Range High-Frequency Radio Propagation," J. Geophys. Res., 63, 1958, pp. 217-241.

19. T. A. Croft, private communication, Dec 1962.

20. A. M. Peterson and O. G. Villard, Jr., private communication, 20 Nov 1960.

21. R. B. Fenwick, "Measurements of Around-the-World High-Frequency Propagation," Rept. SEL-62-011, TR 1004-1, Stanford Electronics Laboratories, Stanford, Calif., Jan 1962.

22. National Bureau of Standards, Solar-Geophysical Data, CRPL-F, Part B, Monthly Summary, Aug 1962.

23. H. Hoogasian, "Studies in Ionospheric Propagation," Rept. AFCRL 923, Raytheon Company, Waltham, Mass., 30 Jun 1961.

24. S. Matsushita, "A Study of the Morphology of Ionospheric Storms," J. Geophys. Res. 64, 1959, pp. 305-321.

25. F. de Mendonça, "Ionospheric Electron Content and Variations Measured by Doppler Shifts in Satellite Transmissions," J. Geophys. Res., 67, 1962, pp. 2315-2337.

26. K. M. Kosikov, "Oblique-Return Sounding and Problems of Radio Communication and Broadcasting over Long Distances," Electrosvyaz', 7, 1959, pp. 10-16.

27. K. C. Yeh and O. G. Villard, Jr., "Fading and Attenuation of High-Frequency Radio Waves Propagated over Long Paths Crossing the Auroral, Temperate and Equatorial Zones," J. Atmos. and Terr. Phys., 17, 1960, pp. 255-270.

28. H. J. Albrecht, "Applying the Chordal-Hop Theory of Ionospheric Long-Range Propagation to Echo-Signal Delay," Proc. IRE, 49, 1961, pp. 356-357.

29. D. P. Kanellakos, et al, "On the Altitude at Which Some Solar-Flare-Induced Ionization is Released," J. Geophys. Res., 67, 1962, pp. 1795-1804.

TEPEE DISTRIBUTION LIST

March 1963

Headquarters, Foreign Technology Div.
Wright-Patterson AFB, Ohio
1 Attn: ID-A3a
1 Attn: ID-E1B
1 Attn: TD-X1A

Headquarters, AF Cambridge Research Labs
Office of Aerospace Research
USAF, L.G. Hanscom Field
Bedford, Mass.
1 Attn: CRRK Dr. Philip Newman
1 Attn: CRRI Mr. Wm. F. Ring
1 Attn: Dr. G.J. Gassman

Comm. and AFCRL, OAR, USAF
L.G. Hanscom Field
Bedford, Mass.
1 Attn: T.P. Conley/CRRIP

Comm., Hq., Electr. Syst. Div.
L.G. Hanscom Field
Bedford, Mass.
1 Attn: Harry Byram/ESRUT

Hq., USAF, Office of Assist. Chief of Staff
Washington 25, D.C.
1 Attn: AFCIN-IC

Hq. U.S. Air Force
Washington 25, D.C.
1 Attn: AFTAC/TD-5

Hq., North American Air Defense Command
Ent Air Force Base
Colorado Springs, Colo.
1 Attn: NELC - Advanced Projects Group

Hq., Space Systems Division
Air Force Systems Command
USAF, Air Force Unit Post Office
Los Angeles 45, Calif.
1 Attn: Tech. Lib.

Hq., Rome Air Development Center
AF Systems Command
USAF, Griffiss Air Force Base, N.Y.
1 Attn: RALTT-2-Mr. F.C. Bradley
1 Attn: RAUEL-3-Mr. B. Cooper

Hq., Strategic Air Command
Offut Air Force Base, Neb.
1 Attn: DOCE

Comm., AFSC, RTH
Bolling Air Force Base, Md.
1 Attn: Lt./Col. Richard Cosel

Comm. Officer
U.S. Army Signal Radio Propagation Agency
Ft. Monmouth, N.J.
1 Attn: SIGRP-A

Comm. Officer
U.S. Army Signal Missile Support Agency
White Sands Missile Range, N.M.
1 Attn: SIGWS-PO

Hq., U.S. Army Material Command
Bldg., T-7
Washington 25, D.C.
1 Attn: AMCRD-DE-MI

Systems Branch
U.S. Army Scientific Liaison
and Advisory Group
Apex Station, Washington 4, D.C.
2 Attn: Mr. Arthur H. Frost

Chief, U.S. Army Security Agency
Arlington Hall Station
Arlington 12, Va.
1 Attn: LADEV-S

Comm. Officer
U.S. Army Signal Electronic
Research Unit
P.O. Box 205
1 Mountain View, Calif.

Comm. Officer
Picatinny Arsenal
Dover, N.J.
1 Attn: Technical Information
Lib.

Institute for Defense Analyses
1710 H St., N.W.
Washington 6, D.C.
1 Attn: Dr. Nils L. Muench

Comm. Officer
Army Rocket & Guided Missile
Agency
U.S. Army Ordnance Missile Comm.
Redstone Arsenal, Ala.
1 Attn: Mr. James E. Norman

Chief of Naval Operation
Dept. of the Navy
Washington 25, D.C.
1 Attn: Op-70
1 Attn: Op-92
1 Attn: Op-922B2
1 Attn: Op-723D
1 Attn: Op-07TE

Chief, Bureau of Ships
Dept. of the Navy
Washington 25, D.C.
1 Attn: Code 362A

Director, Special Projects
Dept. of the Navy
Washington 25, D.C.
1 Attn: SP-2041

Comm. Officer
U.S. Naval Ordnance Test Unit
Patrick Air Force Base, Fla.
1 Attn: N3

Comm., U.S. Naval Missile Center
Pt. Mugu, Calif.
1 Attn: Technical Library
Code N03022

Comm., Naval Air Test Center
Patuxent River, Md.
1 Attn: Weapons Systems Test Div.
(Code 424)

Director, U.S. Naval Research Laboratory
Washington 25, D.C.
1 Attn: Code 5320
1 Attn: Code 2027

Comm. Officer and Director
U.S. Navy Electronics Laboratory
San Diego 52, Calif.
1 Attn: Library

Chief of Naval Research
Dept. of the Navy
Washington 25, D.C.
1 Attn: Code 427
1 Attn: Code 463
1 Attn: Code 402C
5 Attn: Code 418

Commanding Officer
U.S. Naval Ordnance Laboratory
Corona, Calif.
1 Attn: Mr. V.E. Hildebrand
Code 453

Chief, Bureau of Naval Weapons
Dept. of the Navy
1 Washington 25, D.C.

*Armed Services Tech. Information
Agency
Arlington Hall Station
10 Arlington 12, Va.

Director, Weapons Systems
Evaluation Group
Rm. 1E875, The Pentagon
1 Washington 25, D.C.

Institute for Defense Analyses
Washington 6, D.C.
1 Attn: RESD - Dr. Paul von
Handel

Director, Advanced Research
Projects Agency
Washington 25, D.C.
1 Attn: LCDR D. Chandler
1 Attn: Mr. Jack Ruina
1 Attn: Dr. Cabell A. Pearse
1 Attn: Mr. A. Van Every

Director, National Security Agency
Ft. G.G. Meade, Md.
1 Attn: C3/TDL

Director, National Bureau of Standards
Boulder, Colo.
1 Attn: Mr. Richard C. Kirby
(Chf., Radio Systems Div.)
1 Attn: Mr. L.H. Tveten
(HF/VHF Research Section)

Office of the Secretary of Defense
The Pentagon
Washington 25, D.C.
1 Attn: Albert Weinstein/ODDRE
Rm. 3E-1030

ACF Electronics Division
ACF Industries, Inc.
3355 52nd Ave.
Hyattsville, Md.
1 Attn: Mr. Wm. T. Whelan (R & D)
**Inspector of Naval Material
401 Water St.
Baltimore 2, Md.

Aero Geo Astro Corp.
Edsall and Lincolnia Rds.
Box 1082, Alexandria Va.
1 Attn: Mr. D. Reiser
**Inspector of Naval Material
401 Water St.
Baltimore 2, Md.

Aero Geo Astro Corp.
13624 Magnolia Ave.
Corona, Calif.
1 Attn: Mr. A. Walters
**Inspector of Naval Material
401 Water St.
Baltimore 2, Md.

Radio Corp. of America
Aerospace Communications &
Control Div.
Burlington, Mass.
1 Attn: Mr. J. Rubinovitz
**Inspector of Naval Material
495 Summer St.
Boston 10, Mass.

Raytheon Company
Communications and Data Processing Ops.
1415 Boston-Providence Turnpike
Norwood, Mass.
1 Attn: L.C. Edwards
**Resident Naval Inspector of Material
Raytheon Manufacturing Co.
Waltham, Mass.

Stanford Research Institute
Communications & Prop., Lab.
Menlo Park, Calif.
1 Attn: Mr. R. Leadabrand
Communications & Prop. Lab.
1 Attn: Mr. L.T. Dolphin
**Commanding Officer
Office of Naval Research
Branch Office
1000 Geary St.
San Francisco, Calif.

Mass. Institute of Technology
Radio Physics Division
Lincoln Laboratory
P.O. Box 73
Lexington 73, Mass.
1 Attn: Dr. John V. Harrington
1 Attn: Dr. James H. Chisholm
(Radio Propagation Group)
1 Attn: Mr. Melvin L. Stone
(Radio Propagation Group)
**Inspector of Naval Material
495 Summer St.
Boston 10, Mass.

The University of Michigan
Research Security Office
P.O. Box 622
Ann Arbor, Mich.
1 Attn: Ralph E. Hiatt
Head, Rad. Lab.
**Office of Naval Research
Resident Repr.
Univ. of Mich.
820 E. Washington St.
Ann Arbor, Mich.

Westinghouse Electric Corp.
Defense Center-Baltimore
Tech. Info. Center
P.O. Box 1693
Baltimore 3, Md.
1 Attn: Mr. David Fales

The University of Michigan
Institute of Science & Technology
P.O. Box 618, Ann Arbor, Mich.
1 Attn: BAMIRAC-ad
**Office of Naval Research
Resident Repr.
University of Michigan
820 E. Washington St.
Ann Arbor, Mich.

RMS Engineering, Inc.
P.O. Box 6354, Station H
Atlanta 8, Ga.
1 Attn: Prof. William B. Wrigley
**Contract Administor
Southeastern Area
Office of Naval Research
2110 G. St., N.W.
Washington 7, D.C.

Rand Corporation
1700 Main St.
Santa Monica, Calif
1 Attn: Dr. Cullen M. Crain
**Inspector of Naval Material
929 S. Broadway
Los Angeles 15, Calif.

Pickard and Burns, Inc.
103 Fourth Ave.
Waltham 54, Mass.
(Subsidiary of Gorham Corp)
1 Attn: Dr. J.C. Williams
**Inspector of Naval [illegible]
495 Summer St.
Boston 10, Mass.

***Texas [illegible]
Electrical [illegible]
Lubbock, [illegible]
1 Attn: [illegible]

University of California
Berkeley 4, Calif.
1 Attn: Dr. E. Pinney
**Office of Naval Research
Branch Office
1000 Geary St.
San Francisco 9, Calif.

General Electric Corp.
Court St.
Syracuse, N.Y.
1 Attn: Dr. G.H. Millman

Battelle Memorial Institute
505 King Ave.
Columbus 1, Ohio
1 Attn: Battelle Defender

DASA Data Center
735 State St.
Santa Barbara, Calif.
1 Attn: Mgr., Warren W. Chen

*All requests
approved by [illegible]
(Code 418), [illegible]
**When document
of the receip
***Unclassified

General Electric Co.
Heavy Military Division
Court Street Plant
Syracuse, N. Y.
1 Attn: Dr. John Costas
Bldg. 9, Rom. 29

Diamond Ordnance Fuze Laboratories
Ordnance Corps
Washington 25, D.C.
1 Attn: Mr. Perry Griffen